NANOBUBBLE-ASSISTED ULTRASOUND THERAGNOSTICS IN CELLULAR IMMUNOTHERAPY FOR CANCERS

JIANG YIZHOU

PhD

The Hong Kong Polytechnic University

2024

The Hong Kong Polytechnic University
Department of Biomedical Engineering

Nanobubble-assisted Ultrasound Theragnostics in Cellular Immunotherapy for Cancers

JIANG Yizhou

A thesis submitted in partial fulfillment of the requirements for the degree of Doctor of Philosophy

December 2023

Certificate of Originality

I hereby declare that this thesis is my own work and that, to the best of my knowledge and belief, it reproduces no material previously published or written, nor material that has been accepted for the award of any other degree or diploma, except where due acknowledgment has been made in the text.

_____(Signed)

____JIANG Yizhou_____(Name of student)

Abstract

With the unprecedented success of cellular immunotherapies in cancer treatment, there has been a growing endeavor in developing noninvasive monitoring and manipulation strategies for therapeutic immune cells, for broader applications of these potent therapeutics in well-managed manners. Popular modalities of physical energy transmission have been explored for the imaging and modulation purposes , including ionizing radiation, magnetism and optics. Ultrasound, as a versatile mechanical energy transmission modality, has been extensively used in clinical practices, covering applications from imaging to noninvasive interventions. However, the potentials of this ubiquitous modality have yet to be uncovered in cellular immunotherapies.

The nanobubble (NB), gas-filled hollow nanostructures with various formulations, has recently brought substantial potentials into the field of ultrasound. With the assistance of NBs, the ultrasound modality, usually thought as macroscopic energy transmission modality, is now showing broadened potentials, especially on interacting with cellular targets with specificity. In this thesis, we describe strategies that, with the assistance of NBs, enable tracking and control of therapeutic immune cells by the ultrasound modality. We employ the novel biogenic NB, gas vesicles (GVs), as the acoustic tag and actuators for the implementation of cell tracking and mechanical switching strategies by ultrasound.

To achieve noninvasive tracking of adoptive immune cells by ultrasound imaging, GVs are employed for the acoustic labeling of the cells. The GV surface is functionalized by streptavidin coating, which enables stable attachment of GVs on biotinylated cell surface via biotin-streptavidin conjugation. We show that the labeling is well-tolerated by the cells, with essential functionalities unaffected after the labeling. We demonstrate that, after *ex vivo* labeling with GVs, it is feasible to detect labeled cells by nonlinear contrast-enhanced ultrasound imaging both *in vitro* and *in vivo*. In mouse models of subcutaneous hepatocellular carcinoma, we further demonstrate the

tracking of adoptive NK-92 cells by ultrasound imaging, showcasing a potential dynamic evaluation method for adoptive immune cells.

We then demonstrate a mechanical switching strategy for the ultrasound control of genetic expression in engineered immune cells, utilizing GVs as cell-attached actuators. We show that surface-attached GVs enable induction of calcium influx in cells upon ultrasound stimulation, which further elicited transcriptional activities in calcium-centered signaling pathways, laying grounds for mechanical switching of genetic expression. We show in engineered NK-92 cells that the expression of target genes could be induced by the GV-actuated ultrasound stimulation. This demonstrates the feasibility of controlling genetic expression through ultrasound stimulation, indicating potentials of on-demand induction of pre-programmed therapeutic potencies in engineered cells in cellular therapies.

Altogether, we demonstrate that, with the assistance of NBs, it is feasible to use the ultrasound modality for noninvasive tracking of adoptive immune cells, as well as for mechanical switching of genes. These establish a new role of the ultrasound modality in cellular therapies, with potentials in cost-effective post-treatment evaluation, therapy design and optimizations, as well as in implementing all-acoustic monitoring and manipulation on therapeutic cells. This also substantially expands the scope of ultrasound in theragnostic applications, paying the way for combining the ubiquitous ultrasound modality and the novel therapeutics.

Keywords: Ultrasound imaging, ultrasound stimulation, cellular immunotherapy, cell tracking, cell modulation

List of Publications and Awards

Journal Publications

1. **Jiang, Y.**, Hou, X., Zhao, X., Jing, J., & Sun, L. (2023). Tracking adoptive natural killer cells via ultrasound imaging assisted with nanobubbles. *Acta Biomaterialia*, 169, 542-555.
2. Xian, Q., Qiu, Z., ..., **Jiang, Y.**, …, & Sun, L. (2023). Modulation of deep neural circuits with sonogenetics. *Proceedings of the National Academy of Sciences*, 120(22), e2220575120.
3. Hou, X., Jing, J., **Jiang, Y.**, Huang, X., Xian, Q., Lei, T., ... & Sun, L. (2024). Nanobubble-actuated ultrasound neuromodulation for selectively shaping behavior in mice. *Nature Communications*, 15(1), 2253.

Conference Presentations

1. **Jiang, Y**., Hou, X., Zhao, X., Jing, J., & Sun, L. Ultrasound tracking of adoptive natural killer cells labeled with nanobubbles. World Molecular Imaging Congress 2023 (WMIC 2023), Prague, Czech Republic 2023/09/05-09. (Oral)
2. **Jiang, Y**., Hou, X., Zhao, X., Jing, J., & Sun, L. Applications of nanobubble-assisted ultrasound tracking of natural killer cells in adoptive cell therapy. The International Molecular Imaging Summit 2023 (IMIS 2023), Xiamen, China, 2023/10/20-22.
3. **Jiang, Y**., Hou, X., Zhao, X., Jing, J., & Sun, L. Tracking adoptive nature killer cells labeled with biogenic gas vesicles by ultrasound imaging. Biomedical Engineering Conference (BME2023), Hong Kong SAR, China, 2023/08/11-12.

Awards

1. **Best Presentation Award** in MINT Group of World Molecular Imaging Congress 2023, September 2023, Prague, Czech Republic

2. Student **Travel Support** of World Molecular Imaging Congress 2023, September 2023, Prague, Czech Republic

3. **Student Ambassador** of World Molecular Imaging Congress 2023, September 2023, Prague, Czech Republic

4. **Best Poster Award** of International Molecular Imaging Summit 2023, October 2023, Xiamen, China.

5. **Hong Kong Medical and Healthcare Device Industries Association Student Research Award**, February 2024, Hong Kong SAR, China

6. Champion of **Three Minute Thesis Competition** 2023 by Faculty of Engineering in Hong Kong Polytechnic University, June 2023, Hong Kong SAR, China

Acknowledgements

How time files.

From the day I started this journey in the lab, I have never really thought of this day, of how the viva would go, how I would be writing this acknowledgement in the thesis. At days after the viva, I finally woke up from the feeling of unreality, and came to realize that I have really made it this far. And now it's time complete this thesis with its most important part, time to cherish the moments we shared, and time to express all the gratitude to those who have been there by my side.

First of all, I would like thank Prof. SUN Lei and Dr. GUO Jinghui, who have guided me with their knowledge and vision, helped me grow from a student in the lab to one who might be called PhD. Yet, there is still so much more to learn along the path in front of me. But most importantly, thank you for helping me with my first step.

Then there's my deepest gratitude to Dr. XIAN Quanxiang, ZHAO Xinyi, WU Yong, JING Jianing, SU Min, Shashwati Kala, Kin Fung Wong, and Dr. HOU Xuandi. You guys have taught me so much in the lab and showed a rookie with all kinds of skills with so much patience. Hope you were not annoyed by all those rooky questions or any time I sought for help. I have been so lucky to have you guys, as good teachers, and also as good friends.

LIU Langzhou, ZHAO Dongshuai and GONG Zhiyong, the lab has never been such a joyful and lively place until you brought your humor. You guys came in just at the hardest time, and suddenly all those failed experiments became less exhausting. Hope you guys get rid of the belly, and we shall have another cup of beer.

Of course, I wouldn't have missed any of you guys, the lab mates, Dr. ZHU Ting, Dr. ZHU Jiejun, Dr. SONG Lin, Dr. CAO Fei, LI Danni, LEI Ting, SU Min, HUANG Xiaohui, CHEN Congmin, CHEN Zihao, QIANG Yu, SHI Zhuohan. Thank you for all the help, and for being there and making this team a better place.

Finally, here is the thanks to my beloved Baby Victoria. Bravery, joy, determination,

and the purest heart of love, there is no place to find them until I saw them in your eye. The world has become a colorful place, filled with laughter and surprise, a place to live a little, when you are there by my side. Thank you for running into my life. There is a life in front of us, there is more to live, and we shall see the world together.

Like a legend has once said, “the distinction between the past, present and future is only a stubbornly persistent illusion”. Indeed, for every moment we spent together, exploring the realm of science, eagerly searching for answers and solutions, backing each other like a family, they all became the eternity we shared at this glimpse of the universe.

Table of Contents

Chapter 1 Introduction

1.1 Cancers and cancer therapies

Cancer, one of the most devastating causes of death across the globe, has ranked the first or second leading cause of premature death in most countries around the world (**Figure 1.1**). With increasing ages in the global population, the death toll has been climbing up to nearly 10 million worldwide in 2020. The incident rate of cancer has also been expected to grow by almost 50% in year 2040, imposing great burden and challenges to the society [1]. Although dreadful, the mortality rate of cancers has been declining, thanks to the advances in the understandings of cancer biology, as well as in the theragnostic strategies.

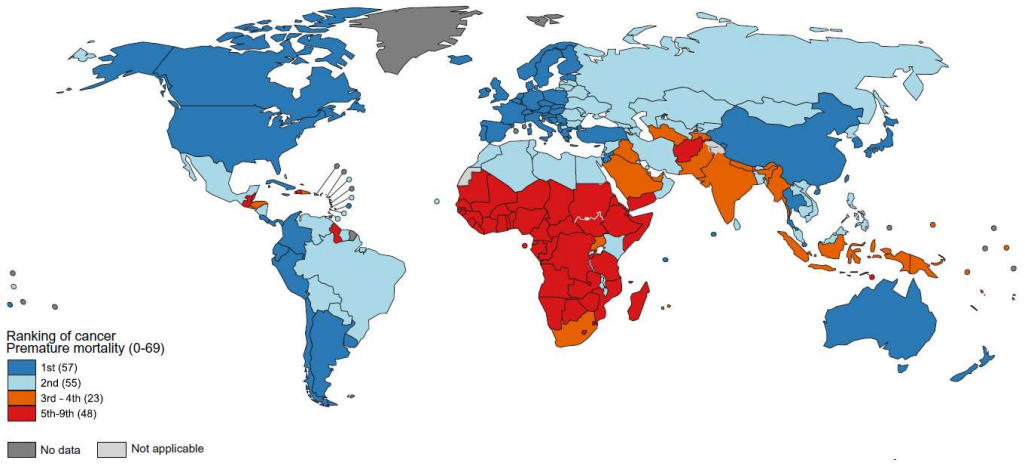

Figure 1.1. Global map of cancer as the leading cause of premature death. (Image adapted from [1]).

The dire of the cancer has been recognized and recorded throughout human history. Ancient Egyptian Imhotep wrote down, probably the first, description of breast cancers as bumps with irregular shapes and uncontrolled growth on his note of diagnosis and medicine, thousands of years ago. Unfortunately, the noted therapeutic approach was “There is none”. Over the past hundreds of years, several major therapeutic approaches nowadays for cancers have been explored by pioneers from various fields, driven by the evolution in the

understandings of the nature of cancers (**Figure 1.2)**.

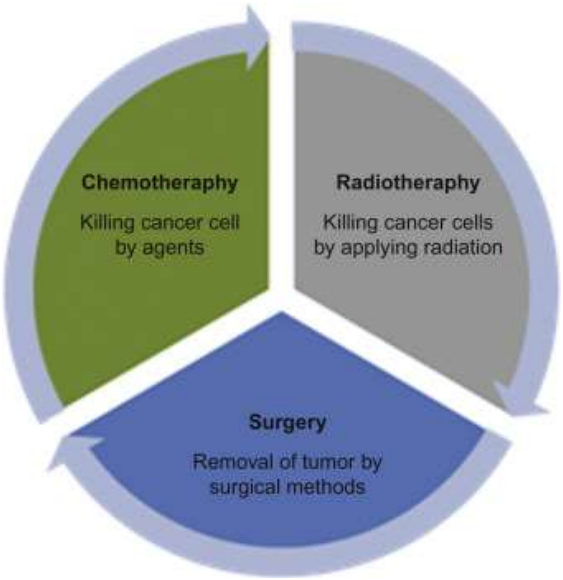

Figure 1.2 Traditional well-established treatment strategies for cancers. Image adapted from [2].

With the development of cellular pathology, the treatment strategy by surgical removal of tissues consisting of such uncontrolled cells was explored by William Halsted, known for his mastectomy in breast cancer treatment. Although with primary tumor removed, the surgical method usually provides limited efficacy. Most patients could suffer from recurrence due to the highly metastatic nature of cancers, one of the notorious cancer hallmarks that make it dreadful and difficult to treat (**Figure 1.3**) [3]. The therapy could sometimes be difficult to implement as well, since the primary tumor could be surgically un-removable due to the locations and/or the level of local and systematic progression.

With the discovery of radiation and in turns the prevalence of X-ray in imaging, the radiation has been explored for cancer treatment at no time. The ionizing radiation damages the DNA and causes cell death, which is exploited to neutralize malignant cells in the body. With the tissue-penetrating capability and advances in technology, it was further made possible to shape radiation beams to confined area of the body, decreasing burden of large-scale surgical interventions. By concept, the nature of radiotherapy is similar to surgical removal, while the blade and scissors were replaced by high-energy radiation that penetrate biological tissues to achieve non-invasive destruction of the malignant tissues. Therefore, a monotherapy by such

scheme could also suffer from tumor metastasis, since local destruction might not guarantee fully clearance of cancer cells that might have already been detached from the primary tumor. At the meantime, the radiation exposure itself is one of the risk factors for carcinogenesis, leading to concerns of secondary cancer malignancies [4].

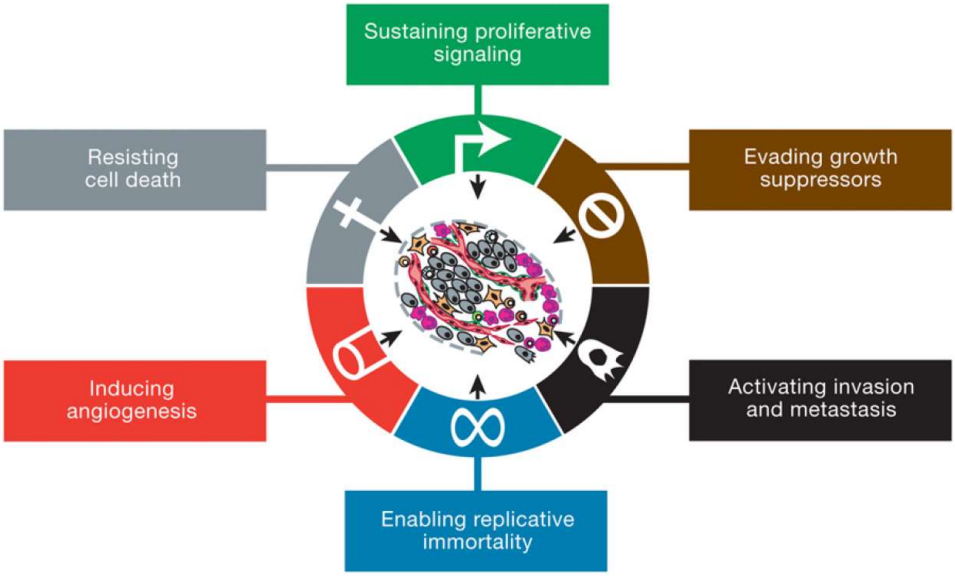

Figure 1.3. Hallmark capabilities of cancers. (Image adopted from [3])

Chemicals, biologicals, or pharmaceuticals in any sole or synergic forms, have long been pursued in human history of disease treatment, and the cancer makes no exception. The chemotherapy is often applied as adjuvant treatment following the surgical removal or radiotherapy. Based on the idea of inhibiting cancer cell growth by cytotoxic agents, chemotherapy has been introduced to slow or stop tumor growth, as well as preventing the spread of cancerous cells. Compared to local therapies like surgery or radiotherapy, the idea of administrating therapeutic agents into patients features a systematic therapeutic approach, with the potentials of controlling or even clearing metastatic cancerous cells. While the toxicity of the drug is usually not exclusive to the malignant cells, meaning that it could also greatly damage healthy tissues in the body, introducing significant burdens and severe side-effects on the patient [5].

The aforementioned surgical removal, radiotherapy, and the chemotherapy and often

combinations of these well-established strategies have all brought significant benefits to the treatment of cancers. The noted therapies against the cancer on our modern guidance of clinical practice is no longer the helpless “There is none” written in ancient Egyptian. However, the complete remission in long term is still a challenging goal, accompanied by numerous side effects that would be beard by patients undergoing the therapies. The deeper investigation into the cancer biology remains, and the search for novel therapeutic approaches with improved efficacy continues.

1.2 Immunotherapeutic approaches for cancer treatment

In recent decades, as the understanding in cancer-immune biology evolves, the researchers and practitioners have realized the importance of the active involvement of the immune system in therapeutics against cancers. The development and progression of cancers are found to associated with the changes in its local microenvironment, of which the immune cells have been revealed to make up a considerable portion. With the protracted and spiraling game between cancer cells and immune cells throughout the cancer development, as well as therapeutic interventions (**Figure 1.4**), the tumor immune microenvironment (TIME) has been revealed as one of the essential component to consider in the treatment of cancers [6, 7]. Effector immune cells, such as cytotoxic T lymphocytes (CTLs), are recruited to tumor initiation sites for the eradication of the cancerous cells, creating a pro-inflammatory environment. At the meantime, immune cells with suppressive functions like regulatory T cells (Tregs), are often recruited by the tumor during the progression, creating the immunosuppressive environment that neutralizes anti-tumor activities of the effectors [8]. Therefore, the “cold” and “hot” TIME landscapes are formed according to different tumor-immune interactions, presented at various stages of tumor progression with significant therapeutic and prognostic indications. The “cold” TIME is usually found with exclusion or absence of effectors, associated with tumor escape from immunological clearance and malignant progression, often found in patients with poor therapeutic outcomes. The “hot” TIME, on the other hand, with high level of resident effectors at non-exhausted status, is more

desired for thorough tumor eradication during therapeutic interventions [9]. The remodeling of the TIME, both on and before the cancer treatment, has been shown to closely related to the therapeutic outcomes. Therefore, ideas and strategies have been proposed, with the hope of maintaining and "hot" TIME accompanying other therapeutic interventions, as well as actively manipulating the immune landscape in tumor for therapeutic purposes.

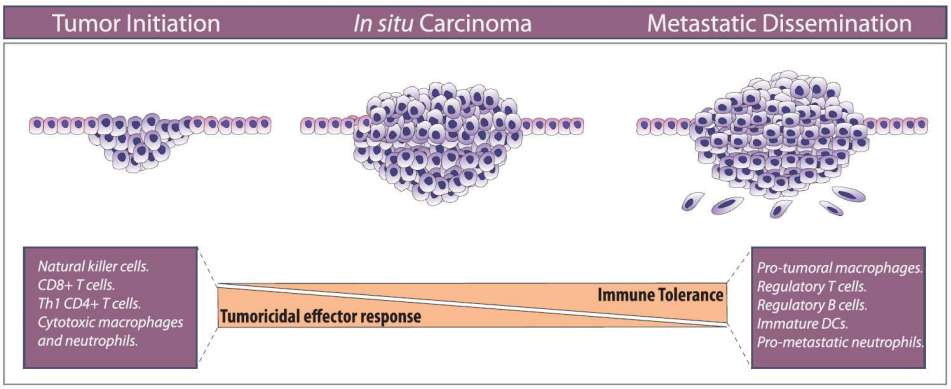

Figure 1.4 The changes in the balance between effector and suppressor immune cells through the tumor development. Image adapted from [6].

The awareness of association between immune system and cancer treatment has emerged as early as in the nineteenth century, as the skin infection was demonstrated with positive relation to better treatment outcomes in patients with sarcoma [10]. The idea of actively employing, enhancing and manipulating the patients' immune system in the cancer treatment has been gradually shaped throughout the years, while the advent of advanced technology in recent decades allowed identifications of axes and molecules related to immune regulation, which in turns enabled the effective and precise harnessing of immune activities as therapeutics against cancers.

Either by targeting immunity-regulating molecules and reshaping the TIME, or by actively transferring effector immune cells into patients, the immunotherapy aims at exploiting the tumor-specific killing effects of the immune system, as well as recruiting sustained waves of anti-tumor activities for systematic and thorough clearance of the cancer cells [12]. The past decade has witnessed the thriving development in the field of immunotherapies, which has brought us thrilling success in treating several types of cancers, like leukemia and non-small

cell lung cancer, etc., with several FDA approved forms [12, 13]. Based on different strategies of exploiting the powerful anti-tumor immunity, several forms of immunotherapeutic approaches have been explored for cancer treatment (**Figure 1.5**): immune checkpoint inhibitor (ICI) therapy that unleashes effector cell responses by targeted inhibition of immunosuppressive mechanisms; cancer vaccination that actively induces adaptive anti-tumor immunity in recipients by presenting tumor-associated antigens and initiating immune activation cascades, either with prophylactic or therapeutic purposes; and adoptive cell therapy (ACT) that exploits anti-tumor immunity by infusion of effector cells for cancer treatment.

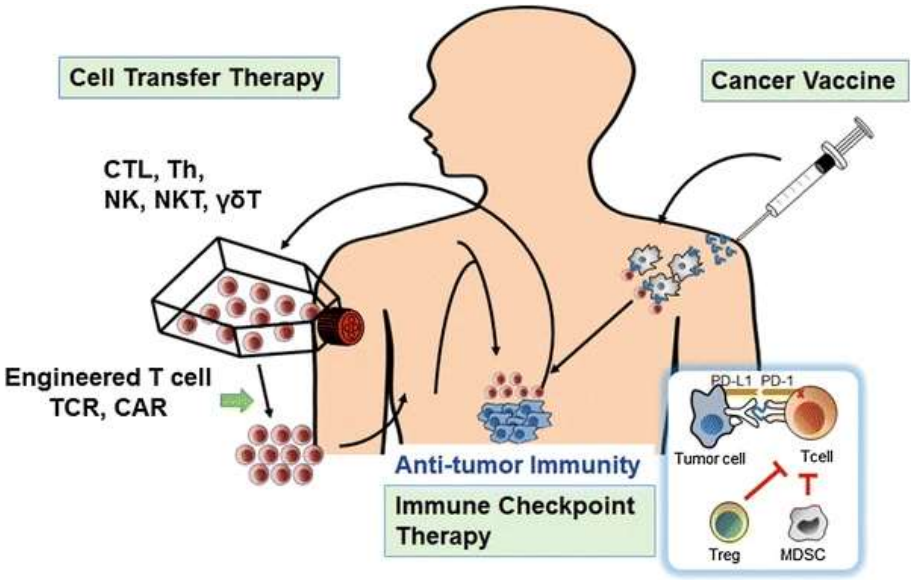

Figure 1.5. Three major categories of immunotherapeutic approaches. (Images adapted from [11]).

Adoptive cell therapies

The ICI therapies and cancer vaccination usually rely on the active involvement of patients' own immune system [12, 14, 15], which might often be comprised due to severe cancer progression and/or side effects of other prescribed therapies like chemotherapies. Under such circumstances, the patients' own effector immune cells could be exhausted or inadequate for systematic anti-tumor clearance, only limited benefits could be obtained even with the applications of checkpoint inhibitors or cancer vaccines. In ACT, the harnessing, expanding,

stimulating and re-deploying effector cells, either from autologous or allogeneic sources, provide better alternatives in such circumstances for improved efficacy based on potencies of the adoptive effector cells. Moreover, the ACT features opportunities for active manipulations on the therapeutic immune cells for higher anti-tumor potencies, as well as flexibility in designing either off-the-shelf or personalized therapeutic effectors, making the ACT a prospective therapeutic approach with potentials in a wider range of scenarios. As early as in 1960s, the adoptive cell transfer therapy was demonstrated by Southam et al., where half of the patients with advanced cancer showed tumor regression following adoptive transfer of leukocytes [16]. Similarly, the anti-leukemia effect of allogenic hematopoietic stem cell transfer was demonstrated to be mediated by T cell versus tumor responses [17]. The tumor-infiltrating effector cells could also be harvested from tumor biopsies, expanded *ex vivo* and re-infused for therapeutic purposes, with complete regression demonstrated in patients with metastatic melanoma when synergically used with lymphodepletion [18].

The effector cells could further be engineered for enhanced cytotoxicity against malignant cells before adoptive transfer, owing to advances in synthetic biology in recent decades. With the development of synthetic chimeric antigen receptors (CAR), the engineered effector cells could also bypass the downregulated MHC molecules on cancer cells, which further enhances their recognition and clearance ability against the tumor. By exploiting the active targeting and trafficking abilities of cells, the cell-based immunotherapy also provides potentials of lowering the systematic auto-immune responses associated with the use of whole-body checkpoint blockade. The cellular immunotherapy with engineered immune cells has been demonstrated with indispensable therapeutic benefits in various types of malignancies, with several FDA-approved forms as well as thousands of ongoing clinical trials [19-25].

Challenges on monitoring and control

Although the progresses and perspectives are encouraging, challenges remain for the adoptive cell therapy with largely heterogenous treatment outcomes across different patients. The transferred immune cells might not always accumulate in the tumor as desired, with frequent reports, often with significant delay, on insufficient intra-tumoral cell infiltration in

non-responders. The “on-target off-tumor” cytotoxicity is also a major concern when cell-based immunotherapy is applied, where the adoptive effector cells interact and attack on healthy cell population with target antigen expression. Meanwhile, the uncontrolled activation of the engineered effector cells has also been an issue, with chances of inducing adverse effects like cytokine release syndrome (CRS) as well, sometimes with severe graft-versus-host (GVH) toxicity in allogeneic transfer [26-28].

This calls for, urgently, strategies and tools for post-transfer monitoring and manipulation strategies for these “living therapeutics”. After the adoptive transfer, the tumor recruitment of the adoptive immune cells is one of the key factors related to the therapeutic efficacy, providing valuable information for timely post-treatment evaluations. At the meantime, the trafficking dynamics as well as cellular fate of the adoptive immune cells are also crucial in the understanding of the cell-based immunotherapies, indispensable in the development and optimization of cellular immunotherapies with adjuvant strategies [29]. Considering the adverse side effects associated with CAR-engineered immune cells, there seems to be a dilemma where the trade-off between potency and safety concerns is needed. Thankfully, with recent advances in nanotechnology and synthetic biology, the activation of the engineered immune cells could be tuned by external stimuli. The control of the anti-tumor cytotoxicity and/or the boosting of the immune cell responses, preferably localized in tumors, further enables overcoming immunosuppressive TIME with reduced concerns on eliciting systematic immune-related adverse effects. The control strategies offer opportunities for these “living therapeutic” to execute their strong effector functions in a well-orchestrated manner, featuring a better solution to fully exploiting high anti-tumor potencies in cellular immunotherapies with reduced safety concerns. As the prerequisite to timely and precise interventions, the noninvasive tracking of these adoptive immune cells is in turns also essential in the implementation of the on-demand activation of these potent effectors.

1.3 Monitoring and control strategies for therapeutic immune cells

1.3.1 Monitoring of the adoptive immune cells

The noninvasive cell tracking technology has enabled the monitoring of cellular fates and distribution in living organisms, not only contributing to study of basic cellular biology, but also playing crucial roles in understanding, managing and optimizing cell-based therapeutics. Several noninvasive imaging techniques, based on different forms of physical energy transmission, have been explored for the noninvasive cell tracking purpose.

Optical cell tracking methods

The optical imaging modality has been popular for observing dynamics of cells in preclinical studies, owing to its fine resolution in space and time and the maturity of fluorescence proteins. For the observation and tracking of cellular targets in living organisms, the cell population of interest are tethered with probes that direct or indirectly generate photons, often in specific wavelengths, either in forms of bioluminescence or fluorescence, for detection by optical device. The locations and trafficking of the cellular populations could be determined and followed by the changes of spots with concentrated photon emissions. Moreover, by tethering the expression of fluorescence proteins with certain cellular processes, the state of cellular activations functionalities and fate related to their homing locations could further be examined with optical imaging methods.

Among optical imaging methods, the intravital microscopy (IVM) has been widely applied in research to monitor the fine details on cellular activities in their domestic environment after infusion. The direct action of *in vitro*-activated adoptive T cells on tumor cells has been observed via IVM in an early study on a mouse model of solid tumor, which has been revealed as a primary mechanism behind adoptive T cell-mediated antitumor effects [30]. The slow killing rate in these adoptive T cells, however, was also reported with the observations via IVM, suggesting an intrinsic mechanism behind the limited efficacy observed sometimes in adoptive T cell therapies. The dampened cytotoxicity of adoptive T cells was shown to be associated with the presence of regulatory T cells (Treg), observed via IVM on lymph nodes [31]. A more

recent study further used IVM to monitor the cellular fates of adoptive T cells in response to synergic treatment with ICIs. The green fluorescence protein (GFP)-expressing cytotoxic T cells were adoptively transferred in a mouse model of melanoma, followed by checkpoint inhibitor administration. The microscopy revealed changes in T cell morphology, motility and trafficking patterns in response to checkpoint inhibitors, suggesting an enhanced tumor infiltration and target engagement on adoptive T cells synergically treated ICIs.

For a more wholistic view in small-animal imaging, bioluminescence imaging (BLI) and near-infrared imaging (NIR) were employed, exploiting the deeper penetration profile of photons at longer wavelengths. Such tool has been popular in following the traces and sometimes expansion of cancer cells administrated in experimental animals, with broad applications in preclinical studies for tumor progression profiling, tracking metastasis, etc. In an *ex vivo* direct labeling manner, the fluorophore with long wavelengths was employed for the labeling of natural killer (NK) cells. The *in vivo* tracking of these NK cells was then performed via optical imaging, with tumor accumulation profile compared between CAR-engineered NK cells with their parental cell lines [32]. Similarly, the near-infrared fluorophore was used to label activated T cells, and hence *in vivo* tracking following adoptive transfer was conducted via NIR imaging [33]. Using renilla luciferase-expressing T cells harvested from transgenic mice, the trafficking and expansion of activated T cells were followed by BLI after the adoptive transfer in mouse models of established tumors. Oscillating patterns were observed in proliferation of these adoptive T cells during tumor rejection process, as well as the long-term survival of these effectors in the recipient after the eradication of the tumor [34]. Similar BLI approach was applied for the monitoring the trafficking of adoptive NK-92MI cells in mouse model of anaplastic thyroid cancer pulmonary metastasis, with targeted inhibition of NK-92MI demonstrated on the metastatic tumors [35].

Although contributing to the elucidation of biological and modulatory mechanisms behind cellular therapies, the optical imaging methods are inherently with shallow penetration of light in biological tissues. Therefore, optical imaging methods are primarily serving as a powerful research tool in preclinical studies, widely employed for analyzing cellular distribution,

behaviors, and fate in small animals. However, their applications in large animals or even humans could be limited.

Nuclear Imaging methods

Nuclear imaging methods have long been applied in clinical practices for tracking radiolabeled white blood cells as probes for infection and inflammation. Either by directly labeling cells of interest with radioisotopes *ex vivo*, or by indirectly targeting them with radiolabeled probes *in vivo*, the nuclear imaging methods allow sensitive and specific detection of labeled cells after infusion with unlimited penetration, usually suited for whole-body distribution monitoring. The single-photon emission tomography (SPET) has been exploited for tracking *ex vivo* expanded NK cells in patients with renal cell carcinoma, where ^{111}In-oxine was used for labeling NK cells, with trafficking dynamics of these NK cells in major organs as well as tumor sites visualized via SPET [36]. Similarly, single-photon emission computed-tomography (SEPCT) has been explored for cytotoxic T cell tracking, with benefits of post-infusion lymphodepletion demonstrated [37]. While the sensitivity of SPECT is relatively limited compared to positron emission tomography (PET), the high dose of radioactivity is involved in ^{111}In-oxine labeling, raising concerns. Alternatively, the ^{89}Zr-oxine has been introduced for direct labeling of adoptive immune cells, including dendritic cells, cytotoxic T cells, CAR-T cell, etc., which provides higher sensitivity and a long half-life [38-40]. Apart from the direct labeling by radiotracers, reporter gene was introduced for nuclear imaging of adoptive immune cells, where the transduced cells selectively uptake the radioactive probe when positron-emitting substrates were administrated [41]. By reporter gene-assisted PET imaging, the homing and distribution of adoptive therapeutic cells like cytotoxic T cells and CAR-T cells were demonstrated, enabling the longitudinal monitoring of the trafficking and viability of these immune cells [42, 43].

The nuclear imaging has been popular in tracking therapeutic immune cells, owing to its deep penetration, high sensitivity and specificity. It has been widely employed for imaging adoptive cells, even those genetically engineered ones, in clinical practices. However, the

method provides relatively limited spatial resolution. Its intrinsic involvement of ionizing radiation has also been a concern, especially when repetitive imaging and monitoring are required, as radiation itself is a highly risky factor for carcinogenesis.

Magnetic resonance imaging methods

The magnetic resonance imaging (MRI) enjoys unlimited penetration and sub-organ level spatial resolution. It has received increasing interests as a radiation-free alternative to nuclear imaging methods for cell tracking in large animals and even humans. With superparamagnetic iron oxide (SPIO) as contrast agents for cell labeling, the MRI has been clinically used for visualizing the deposition of cells during adoptive injection [44, 45]. In cellular immunotherapy, early explorations have been made, using highly derivatized crosslinked iron oxide nanoparticle for *ex vivo* intracellular labeling of CD8+ cytotoxic T cells [46]. With the superior resolution of MRI, the spatial heterogenous tumor recruitment of immune cells was observed, and hence the serial administration regimen was suggested for its improved T cell coverage in tumor compared with bolus administration. Efforts have been seen in this field on improving the sensitivity and optimizing the labeling yield on non-phagocytic lymphocytes like NK cells [47, 48]. The Fluorine-19 MRI has been recognized with revolutionizing potentials in the field of MRI, as the ^{19}F tracers enables detection with negligible background signal [49]. It was exploited for the tracking of dendritic cells and CAR-T cells in recent studies, majorly based on *ex vivo* direct labeling methods. The sensitivity of MRI-based detection of cells, however, has been an issue. A large dose of magnetic contrast agents has to be applied for gaining sufficient signal from the target cell population, of which the safety raises concerns [49]. Moreover, the relatively long image acquisition time of MRI and also nuclear imaging methods limit their use in applications requiring real-time image-guided interventions.

By monitoring the post-infusion fate of the therapeutic cells, a deeper understanding of the living therapeutics could be gained for treatment scheme design and optimization. At the meantime, the timely post-treatment evaluation of therapeutic cell recruitment in the destination tissue could be made, which is regarded as the pre-requisite for them to execute their desired functions. By such evaluation, t the treatment-related decisions could be made

with first-hand information on trafficking and homing efficiency of the transferred therapeutics. Moreover, with the recent advances in biomaterials and synthetic biology, the monitored intra-tumoral accumulation of adoptive cells also informs practitioners with a window for well-orchestrated manipulation on the cellular activities.

1.3.2 Control strategies for immune cells

Apart from the post-infusion monitoring, the capability of fine-tuning the activities of the adoptive immune cells provides opportunities for addressing the side effects accompanying the cellular immunotherapies, improving the safety and manageability of these living therapeutics. At the meantime, the enhancement of the anti-tumor activity also offers chances for overcoming barriers presented in the immunosuppressive TIME. Indeed, the evolvement of cancer therapies, from surgical resection to immunotherapies, features more precise targeting and delicate control of the underlying biological processes in stronger association with the eradication of cancerous cells. With the hope of actively modulating therapeutic immune cells, tremendous efforts have been made in explorations of immunomodulatory molecules, as well as advanced nanocarriers for their delivery, along with the development of cellular immunotherapies [50-52]. Inevitably, these immunomodulatory molecules have been entangled with complications associated with their systematic redistribution, limiting the applicable dosage and achievable efficacy [53, 54].

With recent advances in nanotechnology and synthetic biology, the researcher has been gaining increasing control directly on the adoptive immune cells. As compared to the modulatory agent that caged in stimuli-responsive carriers, genetically engineered cells with responsive “switches” to external stimuli, sometimes combined with local actuators that amplify the stimulus. These engineered cells are then manipulated directly with spatiotemporal precisions via external energy transmission, free of concerns on the dissemination and redistribution of immunomodulatory agents in the system. In the cellular immunotherapy, these

approaches have been extensively explored for manipulating the activity and behavior of the cellular targets after adoptive transfer, so that the therapeutic functionalities could be initiated or enhanced locally at the tumor site.

Noninvasive genetic induction via physical energy transmission

With the broad success and application of optogenetics in neuroscience, it has naturally been explored in modulating and controlling therapeutic immune cells. In such schemes, the light-activatable proteins are introduced as "switches" that convert light stimulus into cellular responses, in forms of either specific genetic circuitry initiation, or assembly of functional components at protein level [55-57]. The light-controlled switches are extensively explored for the control of CAR-expression on effector cells, with the hope of exploiting their potent anti-tumor cytotoxicity while reducing concerns of serve immune-related side-effects associated with activations at off-tumor sites [58-61]. The blue-light inducible nuclear translocation and dimerization system was introduced in [59], optimized for expression efficiency of light-induced CAR expression in T cells and minimal background expression in the absence of light stimulation. Such stringent switching system offers opportunities for exploiting highly potent CAR designs, with reduced concerns on background activations of such effectors in undesired sites. In another design, the intracellular domain of CAR was designed to be expressed as two separate components, tethered with light-inducible dimerizers. Therefore, even with expression in the cell, the downstream signaling of these CAR components would be blocked in the absence of light, while the reversible assembly could be achieved by light switching with high spatiotemporal precision [60, 61].

Challenges, however, remain for the light switching control on therapeutic immune cells. The limited penetration depth has been haunting light-dependent mechanisms, especially when it comes to large animals and eventually patients. These systems rely on the blue light as switching signal, owing to the robustness of blue light-responsive components, while the light at such short wavelength has been known to have poor penetration in biological tissues. Even with NIR-responsive photosensors being explored, the requirement of expressing multiple exogenous proteins imposes extra burdens on engineered cells [62, 63]. At the meantime, the

non-specific background activation of the gene could also occur, imposing potential risks as well given the rapid and intensive anti-tumor activities of CAR-expressing effectors. Therefore, such blue light-based systems commonly require synergic implementations with upconversion nanoparticles (UCNPs), which convert photons from long wavelengths to short wavelengths. By the incorporation of UCNPs that convert NIR light into blue light, either through local injection or through conjugation with the cells, the penetration limitation of blue light-based switching systems could be partly overcome, exploiting both the penetration advantage of NIR light as well as the robustness of blue light switching systems [61].

Heat-responsive synthetic genetic circuitry is another popular switching strategy for controlling physiological processes. The heat shock factor (HSF), as naturally existing cellular machinery to sense thermal stress, activates heat shock promoter and hence initiates expression of downstream genetic circuitry upon hyperthermia [64]. It has been widely exploited for manipulating genetic expression in cellular structures, offering opportunities for transducing various forms of physical energy into biological signaling.

Several types of photothermal nanomaterials like gold nanoparticles converts light into heat, allowing initiation of heat-responsive genetic circuitry by NIR light at deeper tissues with spatial confinement [65-67]. Such photothermal switch has also been employed to preferentially manipulate gene expression in adoptive T cells in tumors. Gold nanorods were incorporated with T cells transfected with heat-responsive genetic circuits as local converters, transducing NIR light into heat for hyperthermia induction. The system has been explored for NIR-controlled CAR expression, as well as synergic expression of CAR and IL-15 superagonists, on adoptive T cells for enhanced tumor therapy and microenvironment remodeling [68].

Magnetic nanoparticles could serve as local transducers that convert alternating magnetic field into heat, allowing *in vivo* control of physiological processes with external magnetic field [69-71]. Intriguingly, with the deep penetration of magnetic energy in biological tissues, the nanoparticle-assisted magnetothermal effect could be exploited for initiating heat-responsive genetic circuitry, serving as another switching tool for the implementation of controlled cellular

therapy. Although there has not yet been any report on magnetic field-controlled CAR expression, the magnetothermal effect has been employed for controlling engineered probiotics in cancer treatment [72, 73]. The probiotics were engineered to express fluorescence reporters and NDH-2 enzyme upon hyperthermia, pre-loaded with magnetic nanoparticles before adoptive transfer. The alternating magnetic field was applied upon bacteria homing in the TME, initiating the heat-responsive genetic expression of reporters for location tracking and the NDH-2 enzyme for damaging tumor with reactive oxygen species (ROS) [73]. Similarly, the nanoparticle-loaded probiotics, engineered to express lysis proteins, were triggered intratumorally with external magnetic field for immunogenic bacterial lysis and release of immunotherapeutic drug payloads, implementing controlled immunotherapy with controlled cellular agents [72].

The high-intensity focused ultrasound has been clinically applied for local tumor ablation, owing to its deep penetration and fine spatial precision. The hyperthermia induced by focused ultrasound has also been exploited for *in vivo* gene expression manipulation [74-76]. It is, naturally, another prospective candidate for manipulating heat-responsive genetic circuitry in cellular immunotherapies. Indeed, the ultrasound has been employed for controlling the engineered microbe to express immunotherapeutic components like checkpoint inhibitors and interferon-γ in the tumor, through heat-shock protein tethered genetic circuitry [77, 78]. Recently, the focused ultrasound hyperthermia has also been employed to initiate CAR expression on adoptive T cells, featuring a spatiotemporally controlled activation of CAR-expression strategy by the ultrasound modality [79].

However, the heat dissipation through biological tissues imposes challenges on the spatial precision of the control strategy relying on hyperthermia. Some heat-responsive components have also been reported to be activated by mechanical stress or hypoxia [80-82], limiting the specificity of this such switching mechanism.

1.4 Ultrasound as a versatile tool for noninvasive energy transmission

The challenges faced by cellular immunotherapy, as well as the deepened understandings in cancer-immune biology, urge the development of strategies for noninvasive tracking and manipulation of therapeutic cells with spatial and temporal precision. The ultrasonic wave, the form in which mechanical energy travels through biological tissues at wavelengths on the order of hundreds of microns, has been extensively exploited for various applications in both preclinical research and clinical practices. Extensively used in clinical settings, the ultrasound imaging has been applied for a broad scope of examinations, including tissue morphology, fluid flow, mechanical properties, etc. [83]. The ultrasound imaging modality enjoys both deep tissue penetration and real-time compatibility, making it a popular tool of real-time imaging guidance for invasive interventions, such as image-guided biopsies and injection including therapeutic cells. With the assistance of targeted ultrasound contrast agents, the ultrasound imaging has also been introduced into the field of molecular imaging for noninvasive detection of molecular targets in living organisms [84]. When transmitted in a focused manner with high intensities, the ultrasonic energy is also capable of inducing temperature surge in the focal region. Such properties have been exploited for thermal ablation of biological tissues, tumors for example, for therapeutic purposes [85]. In recent years, the ultrasound has been further explored as a versatile tool for noninvasively modulating neuronal activities in a reversible manner [86, 87]. Such neuro-modulatory effects have been explored for the treatment of diseases related to neurological pathology directly, as well as indirectly modulating physiological processes linked to nervous systems [88-94].

By principle, the ultrasound enjoys both spatial and temporal precision with efficient energy transmission deep into biological tissues, which means a combination of advantages of other physical cues like light and magnetism together in one modality. This makes the ultrasound an attractive candidate for implementing noninvasive cell tracking in cellular immunotherapy, as well as serving as the triggering input in control strategy design for manipulating engineered immune cells. However, to date, the potentials of ultrasound modality

in cell tracking have yet to be fully explored, especially in cellular immunotherapies. At the meantime, although the hyperthermia-induced by high-intensity focused ultrasound has been applied for *in vivo* manipulation of cellular behaviors, such as CAR-T cells and engineered bacteria [77-79], the has not yet been a strategy that is exploiting the mechanical force generated by ultrasound to manipulate therapeutic cells with *in vivo* compatibility. While the heat dissipation limits the spatial precision of hyperthermia-based induction, the mechanical effect from ultrasonic waves in biological tissues comes with a deep-penetrating profile with fine spatial confinement. Moreover, comparing with the heat generated as secondary effect from interactions between high intensity mechanical waves and biological tissues, the direct mechanical force delivered by ultrasound features a potential multiplexing mechanism, offering opportunities to switch multiple genetic circuits by the same input stimulus at different parameters.

For the implementation of cell tracking with noninvasive imaging, the contrast agent is usually required for enhancing the characteristic signal from cells of interest, enabling specific detection of them from biological tissues in their resident environment. In ultrasound imaging, the microbubble (MB) has been the most commonly used contrast agent with several clinically approved formulation. The ultrasound contrast agent is usually gas-filled structures, providing gas-liquid interfaces with high acoustic impedance, such that the scattering of the ultrasonic wave could be significantly elevated in tissues with abundance of these agents. Moreover, the oscillation of these flexible gas-filled structures under ultrasonic wave also generates characteristic acoustic signal, which further enables specific detection of certain molecular targets under nonlinear contrast enhanced ultrasound (nCEUS) imaging with tissue signal suppressed. However, certain properties of MBs are inherently incompatible with the purpose of tracking immune cells. With sizes of serval microns, the MB usually stays within the intravascular space, while the migration and infiltration of immune cells through the tumor tissues are essential to the execution of their effector functions. Tagging immune cells with the micron-sized MBs should introduce physical burden on these cells, hamstringing their capability of tumor infiltration. In addition, the cellular dynamic of immune cells is usually at

time scales of hours and days, while the MB has a documented rapid breakdown at time scales of minutes at *in vivo* conditions [95-98].

For noninvasive manipulation of therapeutic immune cells via mechanical effects by ultrasound, such as CAR-expression initiation, the genetic circuitry of interest should be designed to tether with mechanosensitive components in the cell. Calcium is one of the most important mediators for cellular mechanoperception, whose ion homeostasis could change as a result of mechanoreceptor response to mechanical cues, e.g., opening of mechanosensitive channels. The change in intracellular calcium concentration further induces alterations transcriptional activities, transduced by calcium-dependent transcriptional factors such as nuclear factor of activated T cells (nFAT). A simple design is to tether gene of interest (GOI) downstream to nFAT-responsive promoters. In such simple insertion design, the mechanical force delivered by ultrasound pulses, under safety confinement or at intensities low enough to avoid unnecessary agitations on other resident cells, might not easily surpass the threshold of eliciting robust and sustained gene expression. A high intensity stimulation might also lead to nonspecific activation of other cell population, introducing undesired complications in the switching design. To achieve specific manipulation of the therapeutic immune cells, the key is thus to elicit such cell signaling selectively in target cells by introducing sensitization mechanisms. The immune cells, intrinsically with sensitivity to mechanical cues like shear stress or tissue stiffness [99, 100], also rely on calcium transients to modulate their own cellular processes [101, 102]. A simple sensitization design might suggest overexpression of mechanosensitive ion channels, either endogenous or exogeneous, to make target immune cells more responsive to mechanical ultrasound stimuli at low intensities. However, in such sensitization design, the presence of endogenous mechanical cues could easily lead to background expressions of the downstream gene circuits, limiting the specificity of the manipulation strategy. Therefore, it leads to a solution of incorporating localized actuators for amplifying the mechanical effects from ultrasound waves. The MB, with its flexible shell encapsulating gas core, could experience volumetric oscillation under the agitation of acoustic field, a mechanism addressed as stable cavitation. Such mechanism has been exploited for

mechanically perturbating the cellular membrane for intracellular delivery purposes [103, 104]. At the meantime, such mechanism inherently provides a means to locally amplify and exert the mechanical perturbation from ultrasound on cells, triggering mechanosensitive components for modulatory purposes. Although MBs have been explored as robust actuators for eliciting CAR expression *in vitro*, which is designed downstream to nFAT signaling [105], the short lifetime and large sizes of MBs still hinder the transition of such switching strategy to *in vivo* implementation.

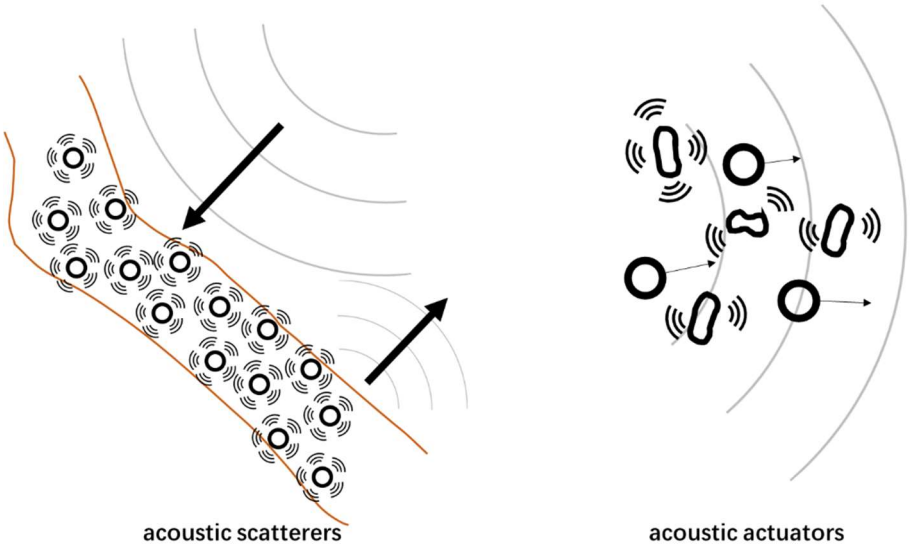

Figure 1.6. Different functional roles of gas-filled bubbles. The acoustic impedance in the gas-water interfaces of bubbles contribute to strong echogenicity, enabling imaging of certain structures with enhanced signal-to-noise ratio. At the meantime, the oscillations and movements of bubbles under ultrasound agitation exert mechanical perturbations to the surroundings, providing means of amplifying and focusing of mechanical force to structures tethered to these actuators.

The ultrasound contrast agent, with its gas-filled structure shell flexibility, plays a central role in implementing noninvasive tracking and mechanical manipulation by ultrasound, serving as transceivers of acoustic energy between microscopic cellular targets and the macroscopic ultrasound transducers. The strong scattering and nonlinear echogenicity of the contrast agent enables distinguishment of tagged cell population from their resident tissues in ultrasound imaging. At the meantime, the oscillation of these hollow structures further serves as a localized

actuator, which helps exert amplified mechanical perturbation on the cellular target. With the limitations in current formulation of MB contrast agents, it naturally suggests a desired gas-filled flexible structure at nanoscale sizes, with thermodynamical stability that endures long under *in vivo* conditions.

1.5 Gas vesicles and their applications in ultrasound technologies

The gas vesicles (GVs) are protein-shelled gas-filled structures, synthesized within species of prokaryotes for buoyancy adjustment in their aquatic environment. As intracellular organelles, GVs are usually cylinder-shaped with nanoscale sizes, a few tens nanometers in diameter and hundreds in length (**Figure 1.7**) [106, 107], demonstrating structures and properties of biogenic NBs. The protein shells of GVs consist of a series of hydrophobic proteins, which allow free exchange of gas from surrounding medium, enclosing an inner gas cavity without pressure gradient across the shell. By contrast, synthesized MBs or NBs rely on the shell to entrap preloaded gas within, which leads to high pressure gradient across the shell, resulting in a stability highly dependent on shell material strength. Rigid shell components are then inevitably reducing the flexibility of the bubbles, leading to trade-off between acoustic responsiveness and the stability. While as the nature proposes optimized solutions via evolution, GVs feature superior thermodynamical stability without the need of compromising shell flexibility, offering biogenic NB formulation with thrilling potentials in the field.

The GV, with their gas-encapsulating structure, has been explored in recent years as plausible ultrasound contrast agents, with their flexible shells shown to buckle under acoustic field, generating strong nonlinear responses [106, 108]. With the acoustic properties and surface functionalization methods demonstrated [109, 110], the GV has been popularly exploited in ultrasound imaging studies covering various applications. As biologically degradable protein structures, GVs have been employed for *in vivo* lysosomal function evaluation by dynamic changes of GV-based ultrasound signal in the liver [111]. The perfusion efficiency of GVs in the tumor has been compared with MBs, suggesting a higher perfusion rate and extravasation profile of GVs even in ischemic regions of tumors [112]. By tumor-

targeted and reticuloendothelial clearance-escaping surface modification, the GV has been demonstrated as plausible imaging probes for molecular ultrasound imaging, showing efficient extravasation in tumor tissues and persisted signal enhancement with specific target binding [113]. Specialized imaging strategies have also been proposed to increase the detection specificity and sensitivity of GVs, including plane-wave compounding method [114], burst-scheme combined with time-domain decomposition processing [115]. Other than imaging-oriented studies, GVs have also been exploited as ultrasound-responsive agents for the delivery of therapeutics, including therapeutic oxygen delivery, enhanced SDT therapy, and intracellular delivery of genes [116-118]. With their shell flexibility and buckling under acoustic field, GVs have been employed to locally amplify the mechanical effect of ultrasound wave, achieving modulation of deep-brain neuronal activities with spatial precision [119].

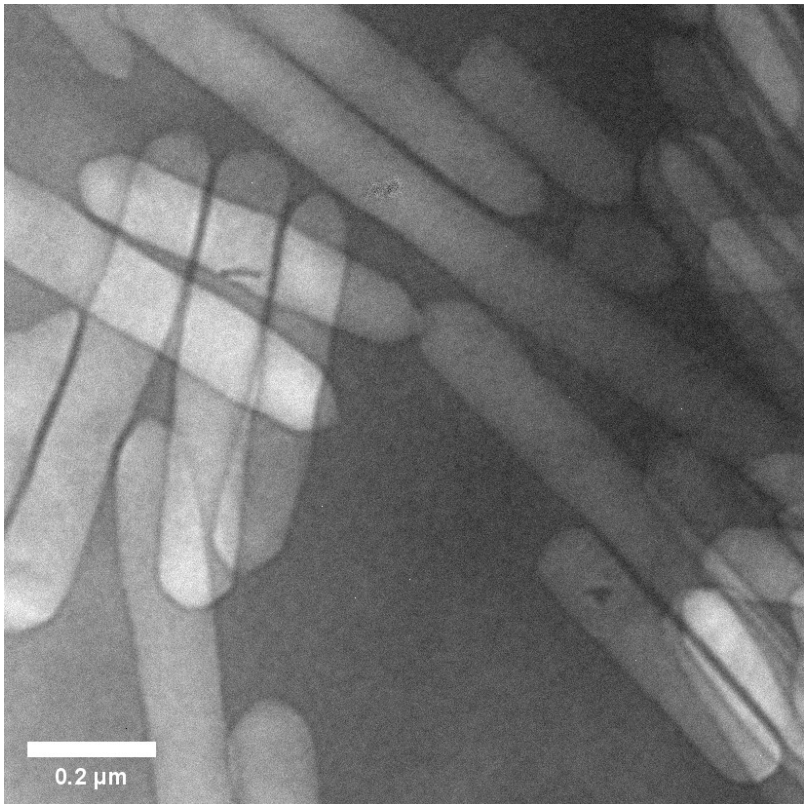

Figure 1.7. TEM image of GVs

With their biogenic nature and protein-only shell composition, GVs have also been explored as genetically encodable acoustic responsive structures. By mining the genetic

clusters with stable expression in mammalian cells, the acoustic reporter gene (ARG) has been shown as potent tool for ultrasound imaging of gene expressions *in vivo* [120, 121]. The bacterium expressing GVs have also been exploited for tumor treatment, where the intracellular GVs generate violet mechanical shock upon ultrasound-induced GV collapse, causing immunogenic cell death in tumors and enhancing the effect of checkpoint immunotherapy. The intracellular expressed GVs also enabled manipulations of bacterium movements by acoustic field [122, 123], with demonstration both *in vitro* and *in vivo*.

1.6 Employing GVs as probes and actuators in cellular immunotherapies.

The versatile GV has shown its tremendous potentials in various applications with ultrasound modality, including molecular imaging, therapeutic delivery, cellular modulation and manipulation, and malignancy destruction etc. With their nanoscale sizes and the demonstrated properties in response to ultrasound wave, it is reasonable to hypothesize that GVs shall serve as plausible tags for the ultrasound tracking of immune cells in cellular immunotherapy, and furtherly as the local actuators to exert modulatory mechanical force on engineered immune cells for switching purposes.

In this thesis, we shall first exploit GVs to label immune cells, by which we shall introduce an ultrasound cell tracking strategy with the application demonstrated in adoptive cell immunotherapy. This shall establish the compatibility of ultrasound imaging with the purpose of tracking immune cells *in vivo*, introducing the versatile ultrasound imaging tool into field of cellular immunotherapy. Moreover, the successful imaging of GV-tagged immune cells, after their infiltration into tumors, shall suggest intact GV structures and competence of their acoustic properties in the context of immune cell infiltration. This shall lay grounds for further GV-actuated ultrasound modulation on engineered cells, as these cell-tethered GVs should be responsive to ultrasound wave with their intact structures. The GV-actuated switching strategy on immune cells shall be then explored. The nFAT signaling pathway will be employed for designing genetic circuitry responsive to mechanical stimulus, with cellular responses to GV-enhanced ultrasound stimulation will be examined at stages along the pathway. Gene of interest

(GOI) expression shall be further demonstrated with the switching system, establishing the GV-actuated switching strategy that converts ultrasound mechanical stimulus into cellular behavioral responses for cell-based immunotherapy.

Chapter 2 Tracking adoptive NK cells with nonlinear contrast enhanced ultrasound imaging assisted with nanobubbles

With the versatile role of GVs in ultrasound-related applications, demonstrated in previous studies, GVs shall be exploited for labeling immune cells and hence tracking adoptive immune cells via ultrasound imaging in the context of cellular immunotherapy. Specifically, the cell line of natural killer (NK) cells, NK-92, shall be employed as the example platform. The labeling of NK cells by GVs shall be approached through *ex vivo* biomolecular conjugation, followed by functionality evaluations on the GV-tagged cells. Then the ultrasound imaging properties shall be examined *in vitro*, establishing the fundamentals for the feasibility of detecting GV-tagged NK cells under nonlinear ultrasound imaging. Then the labeled NK cells shall be infused into healthy mice, with the detectability by ultrasound imaging further determined *in vivo*. At the end, the tracking of acoustically labeled NK cells shall be demonstrated in the context of adoptive cell therapy, on animal models of subcutaneous hepatocellular carcinoma. The tumor recruitment of adoptive NK cells shall be examined, accompanying the dynamical analysis ultrasound contrast in the tumor following adoptive transfer, such that the efficacy of GVs on enabling ultrasound imaging detection of tumor-infiltrated adoptive NK cells will be evidenced. This will establish the ultrasound tracking of adoptive immune cells in cellular immunotherapies for cancers, validating the concept of employing stable and nanosized contrast agents for labeling cells without impairing their effector functions.

2.1 Backgrounds

The adoptive cell therapy (ACT) has received unprecedented success in cancer treatment in recent decades, with thrilling therapeutic benefits demonstrated especially in leukemia and lymphoma patients [12, 13, 124]. However, challenges remain for the ACT in many aspects. Some of the patients have been reported to have insufficient intra-tumoral recruitment of effector cells following the therapeutic cell transfer, accompanied by cases where on-target off-

tumor accumulation of the infused cells occurred. Poor responses to the therapy, as well as adverse side effects were often seen in these situations [28, 37, 125-127]. As the knowledge in cancer-immune biology evolves, it is gradually revealed that the trafficking, persistence and activation of the adoptive immune cells in the tumor microenvironment (TME) are tightly related to the therapeutic efficacy. This imposes the urgent needs for effective post-transfer monitoring of the therapeutic immune cells, by which crucial information could be assessed for both post-treatment evaluation, as well as exploration and desgin of co-treatment strategies that maximize the therapeutic benefits. [29, 128]. As the prerequisite to timely and precise interventions, keeping track of the adoptive immune cells also plays an important role in on-target activation strategies, by which higher anti-tumor potencies could be exploited with less safety concerns.

The traditional check-up methods like blood tests or biopsies often suffer from limited spatial precision, as well as delayed information on adoptive cell infiltration in the tumor, costing precious treatment window for cancer patients. The noninvasive imaging technologies, by contrast, have enabled the tracking of cells in living organisms with spatial precision. The trafficking, tumor infiltration, and even activation of adoptive immune cells could be evaluated with the imaging-based cell tracking techniques, allowing early-stage evaluation of the cellular therapies following adoptive transfer. These would also provide valuable information for practitioners to make treatment-related decisions [29, 37, 39, 42, 46, 129, 130]. Tremendous efforts have been made in recent decades in exploring cell tracking strategies, combining different imaging modalities with advanced materials to enable tracking of therapeutic immune cells. Various imaging modalities, popular both in preclinical research and clinical practices, have been explored for cell tracking purposes in cellular immunotherapies. Bioluminescence imaging (BLI) and near-infrared (NIR) imaging offer high imaging sensitivity of optical imaging methods, resolving *in vivo* biodistribution of targets with both spatial and temporal precision [32-35]. These techniques received great popularity in preclinical studies involving small animals, while their application in large animals and even humans are often limited due to the penetration depth of light. With the established use for tracking radiolabeled white blood

cells in clinical practices, the nuclear imaging methods naturally received intensive attentions in the exploration of immune cell tracking strategies. With superior sensitivity and unlimited tissue penetration, the nuclear imaging methods have enabled tracking of adoptive immune cells both in preclinical research and clinical settings [36-43, 131-133]. However, the ionizing radiation involved in nuclear imaging also raises concerns when repeated scanning and dynamic monitoring are required. The magnetic resonance imaging (MRI) has been pursued as a radiation-free alterative to nuclear imaging, as it also enjoys unlimited penetration with additional bonus of superior spatial resolution [46-49]. While the relatively long acquisition time limits the temporal resolution of MRI, safety concerns have been haunting MRI as well, since there is a requirement of large doses of magnetic contrast agents for sufficient signal from the target cell population.

Different imaging modalities have been contributing their unique advantages to the tracking of adoptive immune cells, there has yet to be gold-standard strategy for noninvasive tracking of these living therapeutics. The ultrasound imaging, as a widely accessible imaging modality in clinical practices, it enjoys both deep penetration and high temporal resolution at the same time. As a cost-effective and radiation-free imaging modality, the ultrasound imaging has been extensively used in clinical practices, covering applications from imaging examinations to image-guided procedures. It has also been adopted in cellular therapies for image-guided injection of cells, naturally appearing as an attractive candidate for tracking adoptive immune cells, showing unequivocal potentials in easy-to-access, early-phase and dynamic adoptive cell monitoring, with clinical relevance. However, to our knowledge, there has been limited results on ultrasound tracking of cells, especially in the context of cellular immunotherapy for cancers. To implement ultrasound tracking of cellular targets, ultrasound contrast agents (UCAs) are required for labeling cells of interests, generating signal for distinguishing these cells specifically from their surrounding tissues. The microbubble (MB) is the most common UCAs, which consists of either lipid or protein shells with gas core enclosed. [97, 134]. Unfortunately, properties of MBs like micron-scale sizes and *in vivo* lifespan of minutes have been hindering their application for the tracking of immune cells. The migration

and infiltration of the adoptive immune cells in the tumor are prerequisite of their effector functions. The MBs, usually with sizes of several microns, shall impose extra burden on the labeled cells during their tumor infiltration process, as particle passing limits in tumors are usually a few hundred nanometers [98]. At the meantime, the dynamics of immune cells in the context of cellular immunotherapy are usually at time scales of hours, days and even weeks. While the MBs are expected to experience quick decay within minutes at *in vivo* conditions due to their thermodynamical instability [95-97]. These limitations of existing UCAs have hamstrung the development of ultrasound-based tracking strategies for cellular immunotherapies.

To enable ultrasound tracking of adoptive immune cells, nanosized UCAs with longer *in vivo* persistence are desired. The gas vesicle (GV), a kind of protein-shelled gas-filled nanostructures, has been demonstrated as plausible ultrasound contrast agents in recent years. The GV has been receiving growing awareness, with versatile roles demonstrated in applications involving the ultrasound modality [106-108, 111, 113, 119, 122, 123]. Mechanistically, GVs enjoy superior stability as their shells exclude water while allowing free gas exchange, enclosing a hydrophobic core without pressure gradience across. The flexibility of GV shells has also been demonstrated capable of generating nonlinear echo, enabling specific detection for contrast-enhanced ultrasound imaging.

Herein, in this chapter, we propose to use GVs as nanosized UCAs to label immune cells, and further implement adoptive immune cell tracking with ultrasound imaging in the context of ACT for cancers. We chose the NK-92 cells, which have been shown with great clinical potentials in recent decades [135-139] , as the example platform. We bind GVs to the surface of NK-92 cells via the biotin-streptavidin conjugation, which allowed the detection of labeled NK cells by nonlinear ultrasound imaging both *in vitro* and *in vivo*. We showed that the labeling by GVs has no noticeable impact on cellular viability and functionalities, indicating competency in cellular therapies against cancers. In a mouse model of subcutaneous tumor xenografts, the tumor-infiltrating NK-92 cells were detected as early as 3h post-transfer by the proposed ultrasound tracking strategy, with significant increase in the nonlinear ultrasound

signal contrast. The dynamical monitoring of adoptive NK cell trafficking to tumors was further demonstrated, with the IL-2 bolus administrated i.p. showing drastic enhancement of NK-92 recruitment in the tumor. The presence of labeled NK-92 cells in the tumor was further co-validated by *ex vivo* examinations with optical imaging approaches. This suggests a successful tracking of NK-92 cells via ultrasound imaging modality with GVs as nanosized UCAs for acoustic labeling.

2.2 Materials and Methods

GV extraction

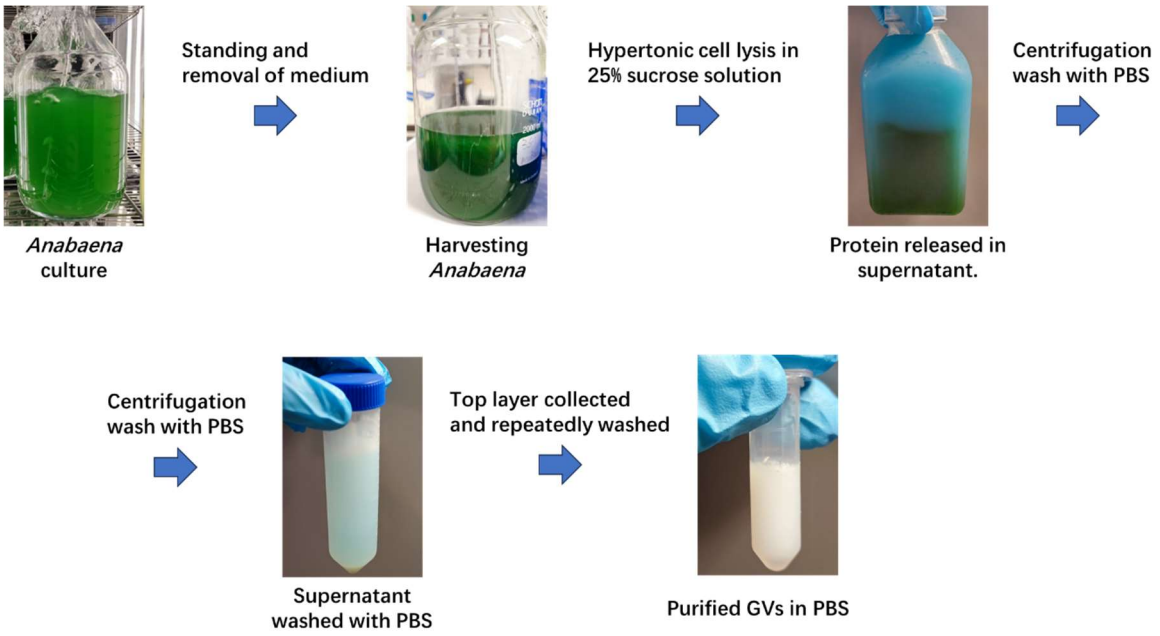

Figure 2.1. GV extraction procedures.

To extract GVs from *Anabaena flos-aquae*, the Walsby's method was used (**Figure 2.1**). The GVs were first isolated from *Ana* via the hypertonic cell lysis, where the cells were quickly suspended in the 25% sucrose solution to release in intracellular components upon lysis. The mixture was left standing in 4°C till the separation between blueish supernatant and the settling debris. The supernatant was collected and washed with PBS by centrifugation, during which the GVs formed a milky white layer at the top. The milky layer was collected while the blueish

solution was discarded, and such purification with PBS was repeated till the infranatant became transparent. Finally, the GVs were resuspended in PBS and stored at 4℃ for further use.

GV characterization

The size and zeta potentials of GVs were characterized using the Zetasizer Nano-Z (Malvern Instruments Ltd, Malvern, UK) according to the manufacturers' instructions. The GV suspension in DI water was balanced to 25℃ for the measurement. To determine GV concentration, the UV-Vis spectrometer (100 Pro, GE Healthcare, USA) was used as previously described [113, 116, 117, 119]. A documented conversion between OD_{500nm} readings, as $450pM/OD_{500nm,}$ was adopted for the calculation of prepared GVs.

GV functionalization

The biotin-streptavidin interaction was employed to attach GVs on the surfaces of NK-92 cells for the labeling purposes. To obtain a biotinylated surface on GVs, the EZ-link Sulfo-NHS-Biotin (ThermoFisher Scientific) was used for biotinylation reaction on surface lysine residuals according to manufacturer's instructions. Briefly, the GVs were incubated with the reagent for 20mins at room temperature, with a 10000-fold molar excess of the reagent over GVs. Afterwards, the residual biotinylation reagent was washed with PBS through centrifugation at least 3 times. The GVs were then mixed with the streptavidin, conjugated with fluorophore Dylight594, at a molar ratio of 1:10000 for avoiding formation of streptavidin-bridged aggregation. The mixture was incubated at room temperature for 30mins with gentle shaking, after which the streptavidin-coated GVs (SA-GVs) were formed for the attachment of biotinylated cell surfaces. The SA-GVs were purified with PBS through centrifugation for at least 3 times to remove residual streptavidin in the mixture. The prepared SA-GVs were then resuspended in PBS and balanced to desired concentrations, stored at 4℃ before further use.

NK cell culture

The NK-92 cell line was purchased from ATCC (Rockville, MD, USA). The NK-92 cells were cultured in MEM-α medium (12561056, ThermoFisher Scientific) at 37℃ with 5% CO_2.

To formulate the full medium for NK-92 cell growth, the following supplementations were included: 10% heat-inactivated FBS, 0.2mM inositol, 0.02mM folic acid, 100U/mL IL-2, 1% penicillin/streptomycin, and 0.1mM 2-Mercaptoethanol. To facilitate the observation of GV binding, as well as identification of tumor-homing of NK-92 cells, the cells were further transfected with EGFP and sorted before further experiments. The transfection of NK-92 cells will be conducted via the viral transfection system. Briefly, the reporter genes were incorporated into the lentivirus. Then 2×10^5 NK cells are transfected with lentivirus with MOI=40, supplemented with 8μg/ml polybrene. The mixture will be centrifuged at 800g for 40mins at room temperature and incubated for 24h afterwards. The medium will then be replaced by fresh medium and incubate for another 72h. Afterwards, 0.8μg/ml puromycin is added into culture to select the transfected cells. After one week of selection, the cells are collected for confirming the transfection and further experiments. The Hep-3B cell line was cultured in DMEM medium supplemented with 10% FBS and 1% penicillin/streptomycin.

Labeling NK-92 cells

The SA-GVs were attached to the surface of NK-92 cells via biotin-streptavidin conjugation. The surface of NK-92 cells were first biotinylated with EZ-Link Sulfo-NHS-Biotin according to manufacturers' instructions. The reagent was added to the cells and incubated at 4℃ to further avoid internalization of the biotin. Afterwards, the cells were then washed with PBS at least 3 times to remove the residual biotinylation reagents. Afterwards, the SA-GVs were added to the biotinylated NK cells for the binding, with an empirically determined dosage of 80μL (OD10 in PBS) GVs to 5×10^7 cells. The mixture was incubated at 4℃ for 30 minutes, with gentle shaking applied to avoid cell-cell binding due to pelleting during the incubation. The cells were then washed with PBS at least 3 times with centrifugation to remove free GVs from the suspension. The labeling rate was determined afterwards via trypan blue counting. In general, the empirically determined protocol yielded a roughly 100% labeling rate, with no obvious direct impact on the cell viability after the labeling procedure. No cell floatation was observed due to excessive GV binding, neither did the cell-cell binding

appear due to inadequate GV-cell ratio.

The MB was also included for the comparison of influences of different UCAs on cells. The MB was attached to cells with the same protocols. Biotin-coated MBs were first synthesized via the lipid film hydration protocol according to previously described formulation. The streptavidin was then added for coating, with a similar procedure to SA-GV preparation. The MB-labeled cells were then prepared according to protocol described above. The potential bioeffect of MB shell components was further excluded via an additional group with shattered MBs for labeling, where the SA-MBs were pretreated with sonication bath before labeling procedure.

MTS test

The viability and proliferation of labeled NK-92 cells was examined with MTS assay. The cells, after the labeling procedure, was balanced and seeded in 96-well plates at 5×10^3 cells/well for 0, 24, 48 and 72-h incubation. An additional group without any labeling agent (CTRL) was also included for comparison. After the incubation,10μL MTS was added, followed by another incubation of 3h. The optical absorbance of the mixture at 492 nm was then examined using a microplate reader (Ledetect 96, Labexim Products, Austria).

Migration Assay

The transwell assay was used to check the impact of labeling on the migratory ability of NK-92 cells. The labeled cells were suspended in FBS-free medium at a balanced density. The cells were then seeded in the transwell inserts of 24-well Transwell (5μm pore size, Corning Inc., Corning, NY) at 1×10^5 cells/well, with 600μL full medium was added to chambers at the bottom as the attractant to the labeled cells. After a 24h incubation, the medium at the bottom chamber was collected for quantification of migrated cells through the pores, by which the migration ability was evaluated.

***In vitro* ultrasound imaging of NK-92 cells with surface-attached GVs**

After labeling by GVs, the NK cells were first imaged *in vitro* to evaluate the feasibility of

detecting acoustically labeled cells via ultrasound imaging. The customized agarose phantom (3% w/v) was made for the *in vitro* imaging experiments, with a sample-loading well at sizes of pipette tips formed in the phantom. The imaging properties of the cell suspension was evaluated with the Vevo LAZR imaging system, equipped with transducer LZ250. The transducer was operating at Nonlinear Contrast Mode, with a center frequency of 18MHz and Transmit Power set to 4%. The images were collected with a Contrast Gain at 30dB with Dynamic Range set to 30dB and Standard Beamwidth. To further verify the source of the contrast signal, we further applied a fully-power ultrasound burst with 1s duration was used to collapse all GVs in the sample. The contrast signal before and after the burst was compared to confirm the presence of intact GVs.

To examine the sensitivity of the acoustic labeling by GVs, the labeled cells were further imaged at different cell densities. The cells were balanced to a gradient of densities from 10^3 to 10^6 cells/mL after labeling. *In vitro* ultrasound imaging was then conducted on cells at different densities for analysis of detection sensitivity. The signal persistence of the GVs was also evaluated, with the labeled cells cultured at 37℃ for 0, 3, 24, 48 and 72 hours before imaging. Th FBS-low (3%) medium was used for the culture to reduce cell proliferation to avoid confounding change in cell densities. After the incubation, the cells were collected by centrifugation, and resuspended to the same density of 10^6 cells/mL. For all *in vitro* imaging, the cells were imaged right after the processing procedures, with imaging phantom placed at room temperature.

Animal experiments

All experiments involving animals were pre-approved by Department of Health of Hong Kong SAR, with further authorization by the Hong Kong Polytechnic University Animal Subjects Ethics Sub-committee. The nude mice were provided by the Centralized Animal Facilities of Hong Kong Polytechnic University (male, 5-week-old, 20~25g weight).

The ultrasound imaging of mouse livers was conducted in healthy nude mice. The mice were randomly divided into 3 groups, receiving intravenous transfer of free GVs, NK-92 cells

(NK only) and labeled NK cells (GVNK). The nonlinear contrast signal in the liver was evaluated before and every 15mins after the i.v. injection. The major organs were collected right after the end of ultrasound imaging experiments, and the biodistribution of the infused NK-92 cells was evaluated via the IVIS imaging.

To establish the tumor xenograft, Hep-3B cells were collected at a total number of 2×10^7 cells for each group, suspended in a mixture of full medium and Matrigel (1:1 ratio). The mixture was injected subcutaneously to the right rear dorsum, with visible tumor established about 2 weeks after the transplant. The volume of tumors was closely monitored by B-mode ultrasound imaging. The experiments started when the average sizes of tumors reached 50~100mm^3. Five groups were included in the tumor imaging experiments, including (1) GV only, (2) Control, (3) NK only, (4) GVNK, and (5) GVNK+IL2, with corresponding i.v. infusion of 80μL free GVs in (1), 80μL PBS in (2), 80μL cell suspension of 5×10^6 NK cells in (3), 80μL cell suspension of 5×10^6 GV-labeled NK cells in (4) and (5). In addition to NK cell transfer, mice in (5) further received a bolus of recombinant IL-2 (50×10^3U), intraperitoneally at 1h following the cell transfer, to actively boost the recruitment of the adoptive NK cells to the tumor. The ultrasound imaging of the tumors was conducted before and 3, 24, 48, and 72 hours after the infusion, with all procedures conducted on day 0 and 14. The tumor growth was measured every other day after the infusion, and the animal conditions were also monitored by body weights, food consumption and activities on a daily basis. In groups receiving NK cell transfer, 3 mice from each group were sacrificed 24h after the infusion for the collection of tumors and major organs. The collected tissues were imaged with the IVIS imaging system to check the biodistribution of the transferred NK-92 cells. Afterwards, the tumors were fixed with 4% PFA, frozen for cryosection for microscopy examinations.

The *in vivo* ultrasound imaging experiments were conducted with the Vevo LAZR imaging system, equipped with transducer LZ250 operating under nonlinear contrast (NLC) mode. The center frequency was 18MHz, with a Transmit Power of 4%. The image collection was set with a Contrast Gain of 20dB and a Dynamic Range of 30d, with the Beamwidth set to Narrow. Anesthetization was applied during the experiment with isoflurane, with mouse body

temperature maintained with the heated pad and the vital signs were monitored. Considering the possible heterogenous distribution of adoptive immune cells in the tumor, the 3D ultrasound scanning was conducted with the motor-controlled moving platform at 0.05mm step size.

Image Analysis

The contrast intensities under NLC mode were analyzed by MATLAB (Mathworks) software. Manually defined regions of interest (ROIs) were applied to all images, covering intra-tumoral volume without incorporating the tissue boundaries. The contrast intensities were averaged within all ROIs throughout the tumor volume, with baseline normalization to reveal dynamical changes in the contrast signal. The distribution of the contrast signal The spatial pattern of contrast enhancement spots throughout the tumor volume was further shown in the 3D reconstruction images, generated with the Vevo LAB software.

Fluorescence microscopy

To observe and confirm the binding between SA-GVs and NK-92 cells, the confocal microscopy was used to image labeled cells after the labeling procedures. The cells were fixed with 4% PFA, and washed by centrifugation with PBS, stained with DAPI, followed by sealing with cover slips. Similarly, to examine the presence of adoptively transferred NK-92 cells in the tumor, the tumor slices were stained with DAPI and sealed with cover slips for fluorescence microscopy. The samples were observed with a laser-scanning confocal microscope, with the cells visualized by 488nm laser for their EGFP expression, and the GVs checked by 561nm laser for their surface conjugation of Dylight594. The nucleus of all cells was also observed with the 405nm laser for their DAPI staining.

Statistical Analysis

The statistical analysis was conducted with the MATLAB software, in triplicate data unless stated otherwise. The two-tailed Student's t-test was used to check significant differences between two groups, while the one-way analysis of variance (ANOVA) was used to conduct

comparisons among 3 or more groups with post-hoc correction by Fisher's least significant difference test. For all statistically significant differences (p<0.05), corresponding p-values were marked between the two groups to indicate the plausible differences.

2.3 Results

2.3.1 Labeling NK-92 cells by surface GV attachment via biotin-streptavidin conjugation

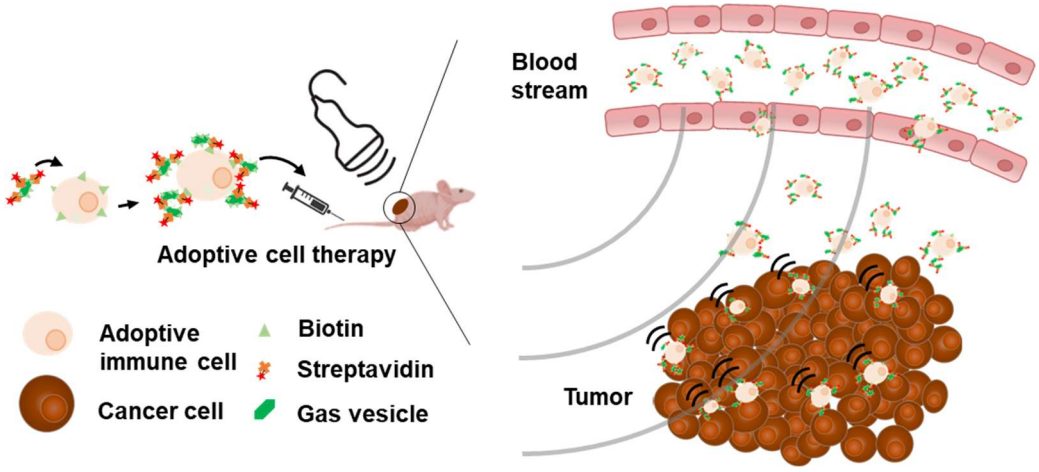

Figure 2.2. Graphical illustration of the GV-assisted tracking of adoptive immune cells by ultrasound imaging. The immune cells were labeled with the nanosized UCAs, GVs, via biotin-streptavidin interactions ex vivo, granting them nonlinear echogenicity for detection by ultrasound imaging after systematic transfer.

To grant adoptive immune cells with nonlinear echogenicity for detection by ultrasound imaging modality, we proposed to use GVs for the *ex vivo* labeling via biotin-streptavidin conjugation. Upon systematic infusion into tumor-bearing animals, the labeled immune cells infiltrate tumors while the nanosized UCAs impose negligible burden. Upon accumulation of the adoptive immune cells in the tumor, the cell-tethered GVs generate nonlinear echo upon nonlinear contrast ultrasound imaging, enabling specific detection of these adoptive cells in the tumor tissue (**Figure 2.2**). As the GVs have been extensively characterized for their imaging properties as well as their surface chemical components in previous studies [113, 116, 117, 140], we do not provide detailed characterizations in this chapter while those who are interested in these vesicles could refer to the aforementioned materials. As we adopted the established

extraction and surface modification protocols, we do not expect alterations on GV imaging properties.

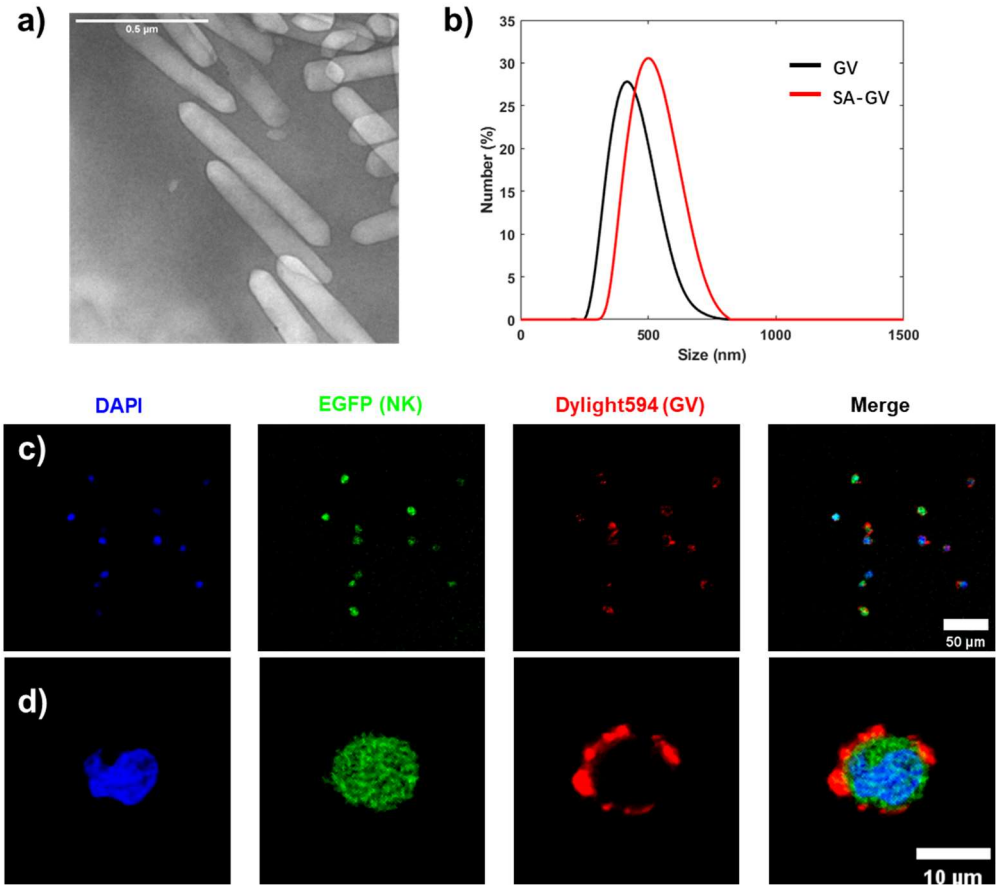

Figure 2.3. Labeling of NK-92 cells with surface-functionalized GVs. **a)** TEM image of GVs. **b)** Size distribution of GVs characterized by DLS before and after the surface functionalization. **c)** Fluorescence microscopy of EGFP-expressing NK-92 cells (green) after labeling with GVs (red). The cell nucleus was stained with DAPI (blue). **d)** A zoomed-in fluorescence microscopy of representative NK-92 cells after labeling with GVs.

Indeed, the GVs prepared for the labeling showed a cylindrical shape, with sizes of around 80nm in diameter and 600nm in length (**Figure 2.3a**). The size of GVs was examined by DLS before and after the functionalization, with no significant change of the size observed for surface coating by streptavidin (**Figure 2.3b**). Although a slight shift of the peak size was seen in SA-GVs, the sizes were still within the nanometer ranges desirable for the application in cell labeling and tracking purposes. The SA-GVs were then attached to the biotinylated surface of

NK-92 cells, which was observed with the fluorescence microscopy (**Figure 2.3c&d**). The position and morphology of NK-92 cells were determined by their EGFP expression as well as the DAPI staining of the nucleus. Red spots indicating positive Dylight594 signal was observed surrounding NK cells, with all cells in the field of view showing certain level of GV signal (**Figure 2.3c**). No noticeable binding between cells was observed, as excessive SA-GV dosage was introduced to avoid GV-bridged cell-cell binding and ensure high labeling rate. Images at higher magnifications further confirmed the presence of GVs at the vicinity of NK-92 cells, with a clustered distribution pattern at the periphery of the cytoplasm (**Figure 2.3d**). No noticeable entry of the GVs into the cytoplasm after the labeling procedure. This indicated that the labeling was achieved, with SA-GVs attached to NK-92 cell surfaces. To ensure higher labeling rate and to avoid GV-bridged binding between cells, the high dosage of SA-GVs was introduced. The overdose might, however, lead to cell flotation when excessive GVs might make labeled cells buoyant. To facilitate separation of GV-labeled cells from free GVs, as well as efficient collection of labeled cells, the empirically determined GV dose was used in all experiments, with gentle shaking applied during the binding process.

The fluorescence microscopy was used to observe and confirm the attachment of GVs on NK-92 cells. However, the intensities should be partially related to the amount of GVs loaded on individual cells, considering the variations in the sizes of GVs. The surface-attached shell fragments of GVs, if any, could also contribute partly to the fluorescence intensities, making it undesired for the estimation of GV loading capacity on individual cells. Therefore, regarding the loading capacity of intact GVs, a rough estimation was made via the measurement of initial GV and residual GV concentrations. To estimate the loading capacity of GVs on the cells, we measured the dosage of GVs before adding to the labeling mixture, as well as the residual GVs collected at the end of the labeling protocol. The difference two dosages should provide a rough estimation on the number of GVs loaded on each cell. In current study, we estimated an average of 895 ± 526 GVs loaded on each cell. However, it should be noted that such estimation shall be overestimate, as the method should also be prone to presence of fragmentation, as well as loss of residual GVs during centrifugation.

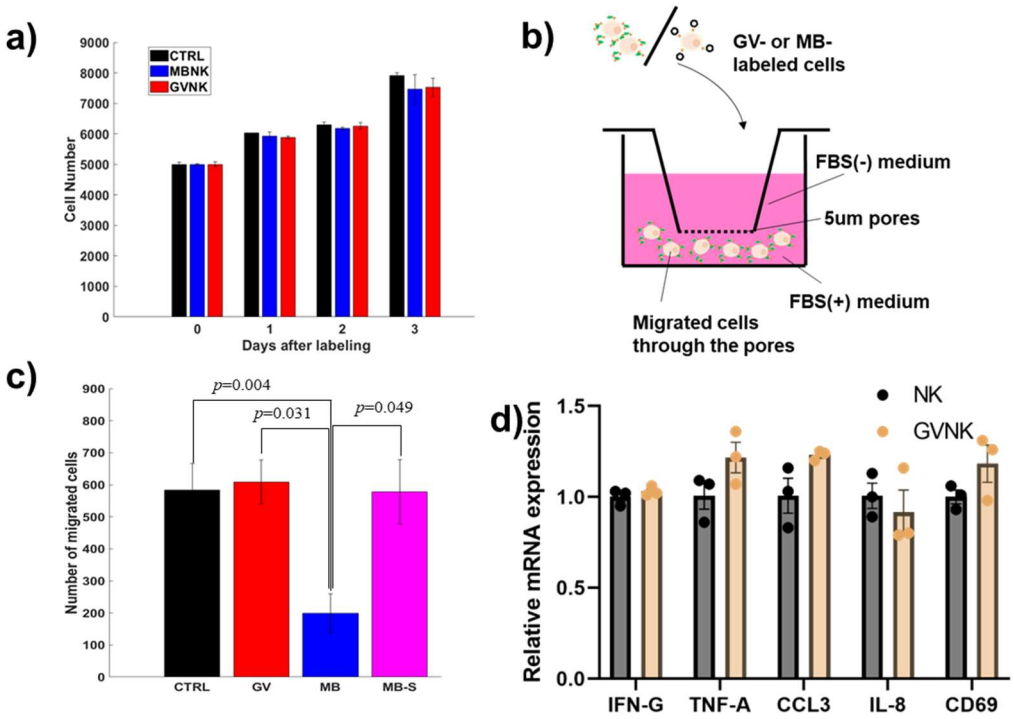

Figure 2.4 Viability and functionality examinations of labeled NK-92 cells. **a)** Cell viability quantified in MTS assay, on cells with no labeling (CTRL), MB labeling (MBNK) and GV labeling (GVNK). **b)** Illustration of the migration test design. NK-92 cells, after surface attachment of different agents, were loaded into the inserts with FBS-free medium. The lower chamber contained full medium to attract the infiltration and migration through pores of 5μm. **c)** Quantification of the migrated cells in lower chambers, collected from groups with no labeling (CTRL), GV labeling (GV), MB labeling (MB) and shattered-MB labeling (MB-S). All significant differences were marked with the corresponding *p*-values. **d)** NK-92 cell functionality characterization by qPCR. Data collected from 3 independent experiments and presented in mean ± SD.

After validating the labeling strategy, we then examine its impact on the labeled cells. We first confirmed the viability after all labeling procedures by trypan-blue counting, by which the viability could be determined at over 90%. The following experiments were then conducted according to the balanced densities of viable cells after labeling. The proliferation of labeled NK-92 cells was examined with MTS assay. Indeed, for either MB or GV labeling, no noticeable impact was observed (**Figure 2.4a**). The number of cells determined at days

following the labeling with either of the agents showed no significant difference from the control group, indicating that the procedures and the agents were safe for the labeled cells. We then moved on to examine the migratory ability of labeled cells, using the FBS as the attractant in the transwell assay with 5μm pores (**Figure 2.4b**). The migrated cells through the pores were then collected and quantified for evaluations of the migratory capabilities (**Figure 2.4c**). In both GV group and shattered MB groups, no difference was observed in the number of migrated cells compared to the control group, suggesting no impact on the cellular infiltration and migration through the pores. By contrast, there was a significant reduction in the migration of the MB-labeled cells, indicating a compromised ability of MB-bound NK-92 cells in migration and infiltration. Indeed, no viability change was observed within the span of the transwell assay, nor was any bioeffect from MB shell components observed in MB-S group upon the migratory ability. These suggested that, as we expected, the physical properties of MBs, most probably their large sizes, were behind the compromised NK cell infiltration through the pores. Carrying intact MBs with micron-scale sizes, the NK-92 cells were hamstrung during the infiltration, as these large bubbles might increase impedance or even lodge the pathway. Effective infiltration and migratory abilities are pre-requisite for the adoptive immune cells to execute their effector functions in cancer immunotherapies. Considering the previously demonstrated stability and entry capability of GVs into tumor [113], we demonstrated here that the use of nanosized GVs for the labeling purposes shall preserve these capabilities of labeled NK cells. We further evaluated other functionalities of NK-92 cells via qPCR (**Figuer 2.4d**). Indeed, we observed no noticeable impact on the GV-labeled NK -92 cells on the mRNA level. These results suggested good biocompatibility of GVs with the labeled NK-92 cells, with no impact cell viability and functionalities, desirable for the implementation of cell tracking in the context of cellular immunotherapy.

2.3.2 *In vitro* ultrasound imaging of NK-92 cells after GV labeling

After confirming the labeling protocol, we then proceeded to evaluate the feasibility of detecting labeled NK cells by nonlinear contrast ultrasound imaging *in vitro*. The experiments

were conducted in agarose phantoms made with sample-loading wells to hold the cell suspension. Ultrasound images were collected under nonlinear contrast mode (NLC mode) with the Vevo LAZR system, with B-mode images collected for comparison as well (**Figure 2.5a**).

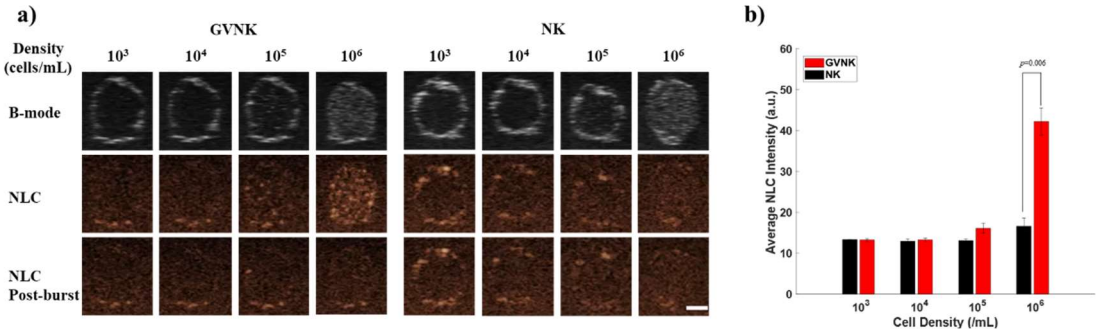

Figure 2.5 *In vitro* ultrasound imaging of NK cells against cell densities. **a)** B-mode and nonlinear ultrasound images of labeled (GVNK) and control (NK) NK-92 cells. Cells were balanced to various densities. Scale bars, 2mm. **b)** Average nonlinear contrast intensities in **a**. Contrast intensities were averaged in manually defined ROIs within the phantom well cavity. Data collected from 3 independent experiments with results presented in mean ± SD. All significant differences were labeled with the *p*-values.

Although without any labeling by contrast agent, some speckles started to appear in B-mode images of the NK cells when the density reached 10^5 cells/mL. The signal surged when the density further increased from 10^5 cells/mL to 10^6 cells/mL, as the dense cell population in the suspension significantly altered the acoustic property. By contrast, there was no observable signal in the non-labeled NK cells under NLC mode even in the densest sample, since no source of nonlinear echo was presented naturally in NK-92 cells (**Figure 2.5a**). The B-mode images of GV-labeled cells showed a similar change in intensities across densities, with no noticeable difference from the NK group. In NLC mode images of GV-labeled cells, speckles could be seen starting at the density 10^5 cells/mL, indicating presence of detectable nonlinear echo in the labeled cell population. The signal then became considerably bright when the density increased to 10^6 cells/mL. The high-power ultrasound burst was applied to collapse the contrast agents presented in the suspension, which led to the loss of contrast in GVNK group, indicating GVs as the signal source. The average contrast intensity was quantified in ROIs covering the

sample-loading well (**Figure 2.5b**). As expected, no change in NLC intensities was seen in the NK group as cell density increased, as cellular structures of NK-92 cells should not contribute to nonlinear echogenicity. By contrast, in GVNK group, the contrast intensity dramatically increased at 10^6 cells/mL, with a significant 2.6-fold enhancement from the nonlabelled counterpart. This suggested a detection threshold in current GV-based labeling scheme, where the labeled cells were detected by nonlinear ultrasound imaging, with clear distinguishment from non-labeled counterparts at densities around 10^6 cells/mL. Essentially, the biological tissue is predominantly echogenic in fundamental frequency, similar to the non-labeled NK-92 cells at high density. This imposes substantial difficulties in identifying of specific cell population in tissues, such as tumors, using B-mode ultrasound imaging. By attaching GVs to target cells, echo at harmonic frequencies could be generated from cell populations of interests, enabling specific detection of these labeled cells under nonlinear ultrasound imaging while the background signal from surrounding tissues could be suppressed. Therefore, these suggested that the labeling by GVs shall enable specific detection of the adoptive NK-92 cells, with distinguishment from the surrounding biological tissues.

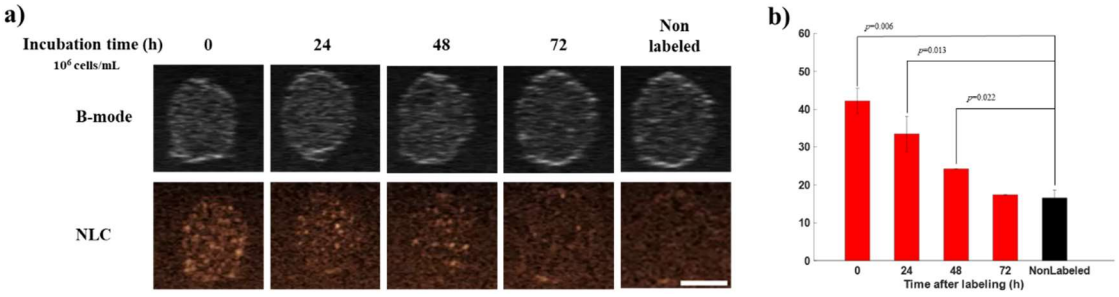

Figure 2.6 Ultrasound imaging of labeled NK-92 cells at different time points after labeling. **a)** Ultrasound images of NK-92 cells labeled by GVs, 0, 24, 48, 72h after labeling procedures. Images were collected under both B-mode and NLC mode. Scale bars, 2mm. **b)** Average contrast intensities in **a**. Contrast intensities were averaged in manually defined ROIs within the phantom well cavity. Data collected from 3 independent experiments with results presented in mean ± SD. All significant differences were marked with the *p*-values.

We then evaluated the persistence of the GVs after attaching on the NK-92 cell. After

attaching GVs to the cells, the labeled cells were cultured for different periods of time and imaged afterwards with density balanced (**Figure 2.6a&b**). FBS-low medium was used for cell culture at 37℃ to reduce cell proliferation, and the contrast signal dropped with increasing post-labeling incubation time (**Figure 2.6a**). Nonetheless, distinguishably bright spots were still observable in labeled cells after 48h incubation as compared to the non-labeled control, suggesting presence of labeled cells with intact GVs in the sample. The intensity quantification showed significant contrast enhancement up to 48h post-labeling in labeled cells compared to their non-labeled counterparts, which returned to the baseline at 72h (**Figure 2.6b**). In previous ultrasound imaging study, the GVs were shown to have longer signal persistence and such signal decay was not observed [113]. Two possible mechanisms were speculated to underlie the signal decay observed in current *in vitro* experiments. One possible mechanism was the cell proliferation and the reduction in labeling rate. Since the cells were collected for density balancing after the incubation, which was meant to exclude possible confounders by the changes in cell numbers. Even with FBS-low medium used, however, the proliferation might still occur, which would lead to a decreased labeling rate after the density rebalancing procedures. Once with free GVs washed from the labeling mixture, the amount of GVs remained unchanged in the system even when the cell number increased during proliferation. Therefore, the rebalancing procedure might lower the total amount of labeled cells in the samples, lowering the signal contrast. Secondly, the collapse and breakdown of GVs during potential cell-GV interactions could also be a reason behind the signal decay during post-labeling incubation.

The clustering of NK-92 cells during cell culture could increase possibilities of cell-GV contact and hence interactions, even with the cushioning spatial arms introduced in the biotin molecules used in current study. In certain cases, the tight clustering between cells might also introduce chances of direct rupture of GVs during cell-cell interactions, while potential interactions between cells and GVs could also lead to GV breakdown. Considering the previously reported post-transfer dynamics of NK-92 cells [129], nonetheless, a signal persistence up to 48h should also be adequate for detection and monitoring of these labeled

cells at early phases following the adoptive transfer. As we focus on verifying the feasibility of implementing adoptive immune cell tracking by ultrasound imaging during their tumor infiltration, answering the question whether NBs were plausible agents for acoustic labeling of adoptive immune cells, we shall proceed with the currently employed contrast agents and labeling schemes.

2.3.3 Ultrasound imaging of acoustically labeled NK-92 cells after intravenous transfer *in vivo*

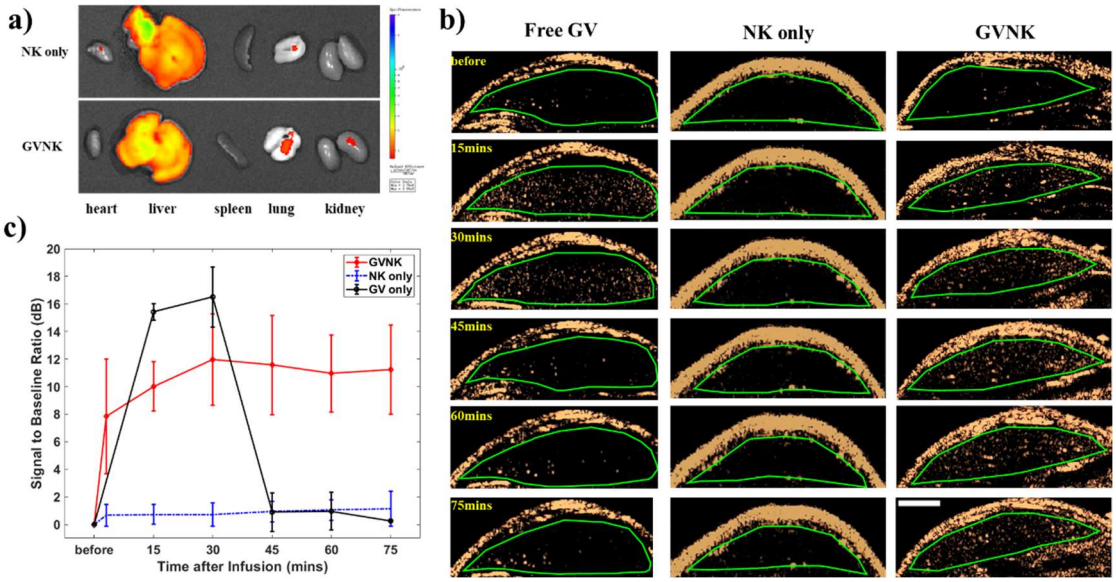

Figure 2.7 Ultrasound imaging of acoustically labeled NK-92 cells *in vivo*. **a)** Representative fluorescence imaging of major organs harvested from mice. The organs were collected at one hour after receiving transfer of either acoustically labeled (GVNK) or control (NK only) NK-92 cells through tail vein. **b)** Representative NLC mode ultrasound images of mouse livers, collected before and at 15, 30, 45, 60, 75mins post-transfer of GVs (Free GV), acoustically labeled (GVNK) or control (NK only) NK-92 cells. The liver tissues are circulated in by manually drawn ROIs (green solid lines) according to B-mode image features. Scale bars, 2mm. **c)** Average contrast signal in **b**. Contrast intensities were averaged within manually defined ROIs within liver tissues, with baseline normalization to reveal dynamic changes in the contrast signal. Data presented as mean ± SD, n=3 for each group.

After establishing the detectability of acoustically labeled NK cells by ultrasound imaging *in vivo*, we then proceeded to verify the feasibility of tracking these labeled cells in living organisms by nonlinear ultrasound imaging. Since the liver has been reported as one of the tissues that adoptive NK-92 cells accumulate in after intravenous infusion [129], we chose it as the example homing environment for imaging and detecting labeled NK-92 cells. We first validated the reported accumulation of NK-92 cells in livers by *ex vivo* IVIS fluorescence imaging on organs collected from mice after one hour post-transfer. Indeed, in mice receiving intravenous transfer of either labeled or non-labeled NK cells, the EGFP signal suggested livers as the major distribution site of transferred NK-92 cells at 60min post-infusion (**Figure 2.7a**), which was consistent with previous studies [32, 35, 129, 141]. As expected, in GVNK group, the acoustic labeling by GVs didn't alter the biodistribution of adoptive NK-92 cells, with the labeled cells majorly found in liver. Hence, we proceeded to image mouse livers *in vivo* with nonlinear ultrasound imaging, at various time points, including pre-transfer baseline, and every 15mins after the infusion of either free GVs, non-labeled and labeled NK-92 cells (**Figure 2.7b**). Before the infusion, livers in all groups showed minimal contrast signal as expected, as the tissue background was greatly suppressed under the nCEUS imaging. After the intravenous infusion of NK-92 cells, no change in the contrast could be seen in NK only group, while clear bright spots started to show at 15min post-infusion (**Figure 2.7b**). Quantification of the contrast intensities showed that the signal in GVNK group reached a plateau of about 10dB at 15mins, which persisted till the end of the imaging session at 75mins post-infusion (**Figure 2.7c**). In NK only group, the signal remained unchanged compared to the baseline throughout the imaging session, consistent with the observations in the NLC images. The EGFP distribution shown in *ex vivo* IVIS images suggested liver accumulation of NK-92 cells in both groups, while only the GVNK group was seen with contrast enhancement. These suggested that the NK-92 cells tethered with GVs in GVNK group were detected by the nCEUS imaging, with distinguishment from the liver tissue. The signal in Free GV group showed a quick rise similar to GVNK group, with high contrast intensities at 15mins and 30mins post-infusion. While the contrast in Free GV group quickly diminished after 30min, returning to baseline at 45mins

(**Figure 2.7c**). Indeed, the free GV has been reported to undergo lysosomal degradation, mainly through phagocytosis by liver resident macrophages. This clearance mechanism led to quick accumulation of free GVs in liver, followed by a rapid contrast decay within one hour [111]., which was consistent with the observations in current study. By contrast, the contrast dynamics observed in GVNK group were different from the reported free GV decay, which plateaued between 15 and 30 minutes, persisted up to the 75mins. These further verified that the source of contrast signal was indeed cell-tethered GVs instead of free GVs. The GVs attached on the NK-92 cell surfaces might have undergone a different *in vivo* degradation mechanism from free GVs, contributing to the longer persistence observed in current study. Without being internalized and degraded by the resident macrophages, intact GVs preserved their echogenicity on labeled cells. This allowed *in vivo* detection and distinguishment of labeled cells by nCEUS imaging in the liver, and more importantly, prospectively in destination tissues of their further migration.

2.3.4 Tracking acoustically labeled adoptive NK-92 cells by ultrasound imaging in cellular immunotherapy

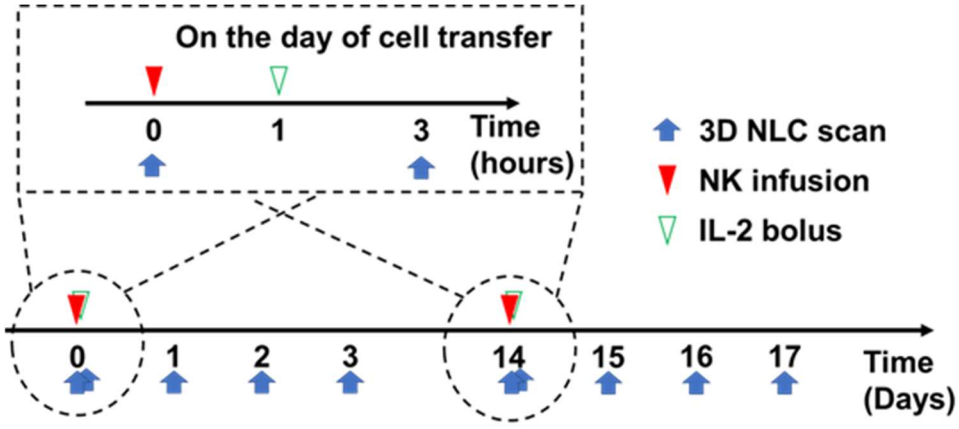

Figure 2.8. Illustration of the experiment procedures. The experiment started when the tumor sizes reached 50~100mm^3 (day0). Two doses of transfer were applied at day0 and day14, respectively. 3D scans under the NLC mode imaging wer conducted on the tumor, before and at 3h, 24h, 48h and 72h post-transfer. In one group of mice, a single bolus of IL-2 was administrated intraperitoneally for the boosting of the NK-92 trafficking to tumors.

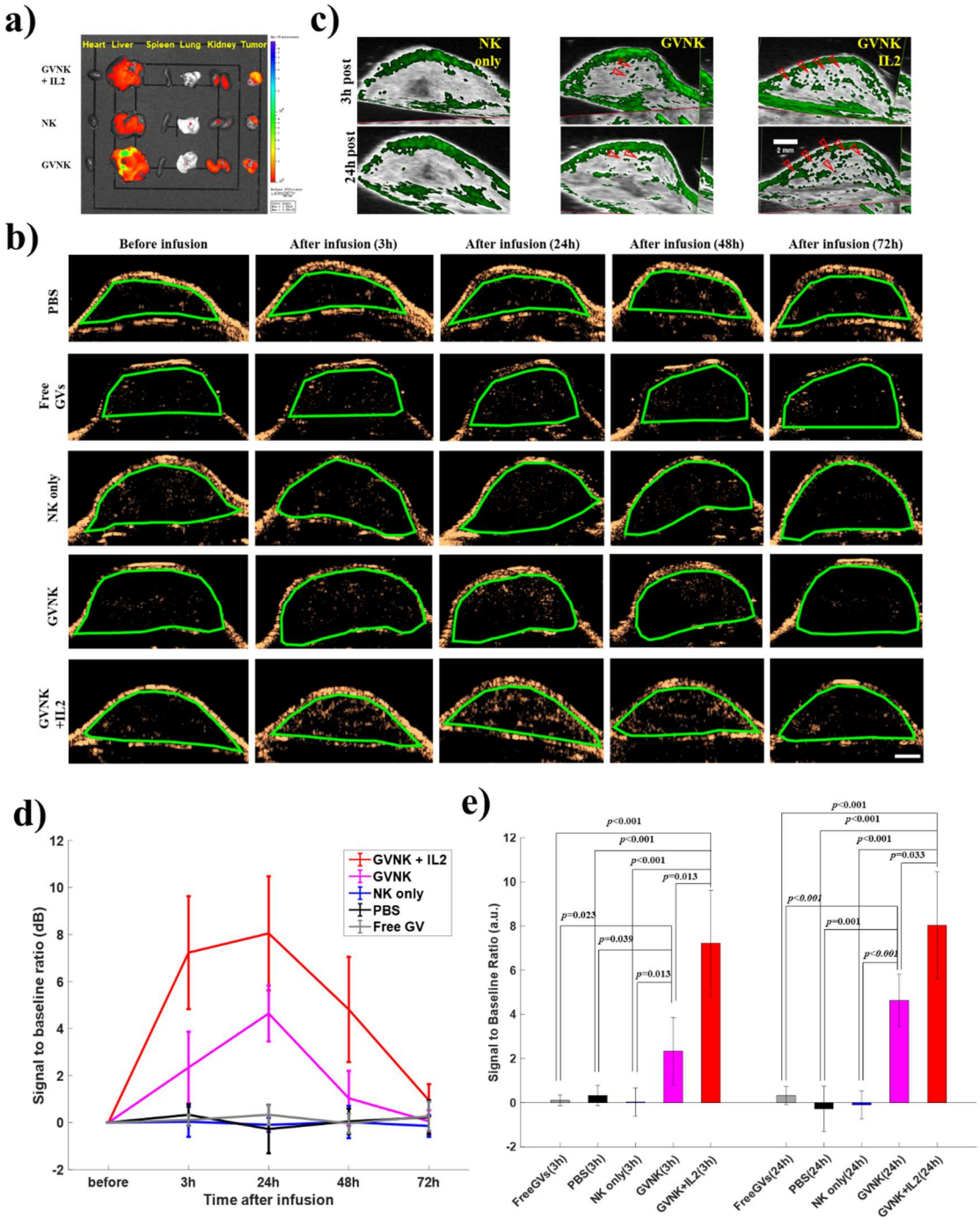

Figure 2.9. Tracking acoustically labeled NK-92 cells in tumor-bearing mice by ultrasound imaging. **a)** Representative IVIS images of major organs and tumors. Samples were collected at 24h post-transfer of NK-92 cells through tail vein. Samples were imaged for EGFP fluorescence for the localization of NK-92 cells. **b)** Representative NLC mode ultrasound images of tumors taken at various points before and after the cell transfer. The tumor tissue was circled within manually determined ROIs (green lines). Scale bars, 2mm. **c)** Representative 3D-reconstructed tumor ultrasound images at 3 and 24h post-transfer of adoptive NK-92 cells.

Red arrows indicate areas with increased contrast signal compared to baseline. Scale bars, 2mm. **d)** Average contrast intensities in **b**. The contrast intensities were averaged within manually defined ROIs in intra-tumoral tissues. All slices through the 3D scans were quantified and averaged throughout the volume, normalized to the baseline NLC intensity obtained before the infusion (Data collected from three animals for each group, two imaging experiments were conducted on each animal. Data presented as mean ± SD). **e)** Average intra-tumoral contrast intensities at 3h and 24h post-transfer. Statistical differences are labeled with the *p*-values.

After confirming the feasibility of tracking acoustically labeled NK-92 cells in livers, we then proceeded to perform cell tracking in adoptive NK-92 therapy for subcutaneous tumor treatment. In mice with established tumors, two doses of intravenous infusion were applied at day0 and day14 during the experiment, with corresponding ultrasound imaging collected at various time points of interest (**Figure 2.8**). Vehicle (PBS), free GVs (GV only), control NK-92 cells (NK only), and acoustically labeled NK-92 cells with GVs (GVNK) were included in the experiment. An additional group of mice receiving both GV-labeled cells and an intraperitoneal bolus of IL-2 (GVNK+IL2) was introduced, with the IL-2 used for actively enhancing the NK-92 cell trafficking to tumors. Ultrasound scanning under NLC mode was conducted, with 3D scans collected before and at 3, 24, 48 and 72 hours after the transfer.

We first evaluated the distribution of adoptive NK-92 cells by IVIS imaging, which shall lay grounds for ultrasound tracking of these adoptive cells. Major organs and tumors were collected from groups with NK-92 cell transfer at 24h post-transfer, and IVIS imaging was performed to assess EGFP fluorescence in the samples for localizing adoptive NK-92 cells (**Figure 2.9a**). As expected, the tumor collected from all groups showed positive EGFP fluorescence signal, with distribution through major organs similar to previous studies [32, 35]. The NK-92 cells have been reported to target and accumulate in tumors at 24h post-transfer, consistent with our observations on the *ex vivo* samples. By validating the homing of adoptive NK-92 cells in tumors, we then proceeded to verify the feasibility of tracking their accumulation in tumors by ultrasound imaging. NLC images of tumors were collected before

and at several time points after the infusion, where tumor tissues in all groups showed only low levels of contrast signal before the infusion (**Figure 2.9b**). In tumor tissues, some low level of NLC signal shall be reasonable due to presence of heterogeneity and high vascularization level, while the background could still be greatly suppressed under nonlinear ultrasound imaging as compared to traditional B-mode. This shall facilitate the specific detection and distinguishment of labeled cells from their homing environment, as the contrast agents are expected to show high level of nonlinear contrast under such imaging mode.

As expected, no noticeable change could be seen in the contrast of NK only group at all time points after the adoptive transfer, similarly to those observed in PBS group and Free GV groups (**Figure 2.9b**, top 3 rows). Since no contrast agents were included in NK only group and PBS group, the reason behind the absence of NLC signal change was straight-forward. The free GVs have been known to experience rapid degradation by liver macrophages, if no surface modification of protection had been introduced, after intravenous infusion [111, 113]. With their small sizes, one may also expect certain level of GV leakage into tumor parenchyma shortly after the infusion. Indeed, our team have previously examined the dynamics of GV accumulation in tumors. Without surface protection by PEG, or active targeting modifications, free GVs were quickly cleared out in the tumor even with certain level of early-phase accumulation, which shall be negligible considering the low dosage applied in current study. By contrast, clear bright spots could be seen in both groups with acoustical labeling by GVs (GVNK & GNVK+IL2) (**Figure 2.9b**, bottom 2 rows). Starting from 3h post-infusion, clear contrast enhancement was identified in acoustically labeled groups, which continued to increase to 24h. A slight signal decrease in the contrast was seen at 48h, which returned to the baseline around 72h. Combining with the biodistribution observed in *ex vivo* IVIS imaging, the acoustic labeling by GVs indeed contributed to nonlinear contrast signal generation on tumor-homing NK-92 cells, enabling the tracking of these adoptive cells by ultrasound imaging.

Previously, the tumor recruitment of adoptive NK-92 cells was also reported in optical imaging studies, while such early-phase detection was achieved via ultrasound modality in our study. With 3D ultrasound scans, the reconstructed contrast mappings were obtained, by which

the sub-organ distribution of the contrast enhanced spots could be assessed (**Figure 2.9c**). The enhancement could be seen with clustered distribution, with a localized pattern in separated regions in the tumor, instead of any homogenous spreading pattern. Such clustering pattern was consistent with the widely reported spatial heterogeneity in tumor cell recruitment of adoptive immune cells [46]. With the increasing number of tumor-homing NK-92 cells, the number and sizes of regions with enhanced contrast both increased at 24h. A 2.3dB intra-tumoral contrast enhancement was quantified at 3h post-transfer in GVNK group, with a sustained increase to 4.6dB at 24h (**Figure 2.9d**), indicating a process of gradual tumor recruitment of adoptive NK-92 cells within this period. The surface attached GVs on these tumor-infiltrating cells, in turns, contributed to the increase in ultrasound contrast.

The IL-2 has been widely used in adoptive cell therapies for enhancing the anti-tumor activities and supporting the persistence of transferred cells, including NK-92 cells [51]. Therefore, we introduced a single intraperitoneal IL-2 bolus in GVNK+IL2 group at 1h post NK-92 transfer, which shall actively boost the infiltration of NK-92 cells in the tumors. By such, we shall be able to evaluate the capability of proposed tracking strategy in capturing dynamic changes when adoptive immune cells are recruited to tumor sites at different efficiency. As we expected, with the enhanced trafficking, stronger ultrasound contrast was seen in both single-slice and 3D-reconstructed images of GVNK+IL2 group (**Figure 2.9b&c**), with contrast enhanced regions becoming considerably brighter. The IL-2 bolus led to a wider-spreading pattern of contrast-enhanced regions in the tumor tissue, with 7dB enhancement in the average contrast at 3h and 8dB at 24h (**Figure 2.9d**). Considering the whole-tumor NLC intensities at 3h post-infusion, a significantly higher enhancement was seen in GVNK+IL2 compared to that seen in GVNK group (**Figure 2.9e**). With GVs as the signal source of nonlinear echo, such increase suggested a significant increase in the tumor-infiltrating NK cells upon IL-2 boost, carrying GVs as acoustic labels. With the well characterized half-life of IL-2 in the serum after intraperitoneal bolus injection, the booster effect of IL-2 dose adopted in current study shall last only within the few hours following the NK transfer [142]. Therefore, a slower increase rate was seen between 3 and 24h in GVNK+IL2 group, and an 8dB peak was observed at 24h.

Nonetheless, with increased number of tumor-infiltrating NK-92 cells, the peak in IL-2 boosted group was still significantly higher as compared to GVNK group, suggesting a robustly enhanced trafficking detected by the proposed ultrasound tracking strategy. After the early-phase increases, the NLC intensities started to decline at 48h and returned to baseline around 72h, with similar decay rates in both groups with labeled cell transfer.

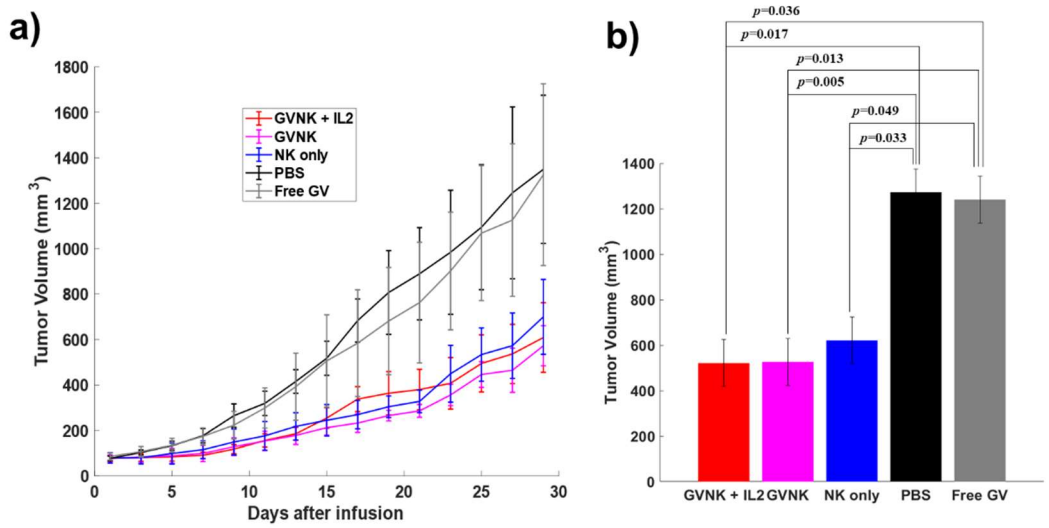

Figure 2.10. Tumor growth profile in the adoptive NK-92 therapy for subcutaneous tumors. **a)** Relative tumor growth, with respect to initial volume, monitored every other day throughout the experiment period. **b)** Relative tumor volume at the end of the experiment. Data collected from 3 animals in each group, presented as mean ± SD. Statistically significant differences were labeled with *p*-values.

In all groups receiving treatment, the tumor volume was recorded for 4 weeks to for the evaluation of therapeutic effect of adoptive NK-92 therapy (**Figure 2.10a**). As expected, either the free GVs or the vehicle showed no noticeable treatment effect as compared to the groups with NK-92 cell transfer. While in those mice receiving NK cells, either labeled or unlabeled, certain level of the tumor growth inhibition was observed after the treatment with significantly smaller tumor volume (**Figure 2.10b**).

Indeed, the biotin-streptavidin interaction rarely imposes impact on the molecules being labeled, with which the bridging between NK-92 cells and GVs should be minimally impactful on the cell functionality. As demonstrated in our *in vitro* data, the nanosized GVs showed no

influence on the migration ability of labeled NK cells either, allowing the infiltration of labeled NK cells in the tumor and further execution of their effector functions. However, no significant difference was found in the tumor volume from all three groups receiving NK-92 cell transfer. Indeed, the long-term survival of the NK-92 cell *in vivo* depends on continuous supplementation of IL-2 following adoptive transfer, while in our experiments, we only applied single-bolus IL-2 in one group to promote trafficking shortly after the transfer. Such single dose should indeed be insufficient for the long-term supplementation on NK-92 cells, while we employed such design to avoid confounding changes in NK cell recruitment to tumors, such that we were able to compare the ultrasound contrast with direct link to boosted or non-boosted trafficking dynamics. In this regard, it is not surprising to expect tumor inhibition effects to a similar extent in all NK-infused groups. While the current tumor growth results were still able to provide information on the effector functionalities *in vivo*, where the NK-92 cells with GV labeling led to suppressed tumor growth in a similar manner compared to their non-labeled counterparts.

2.3.5 Tumor slice fluorescence microscopy

To further validate the infiltration of adoptive NK-92 cells in the tumor, as well as the tethering between GVs and the cells to be tracked, tumors were harvested from all groups at 24h post-infusion, the time point at which we observed strongest ultrasound contrast enhancement. The tumor slices were collected via cryosection, stained with DAPI and examined via fluorescence microscopy. In groups receiving adoptive NK-92 transfer, positive EGFP fluorescence was observed on the slices (**Figure 2.11a**), while the Dylight594 fluorescence indicating presence of GVs were only seen in those groups with labeled cell transfer. Moreover, colocalization between EGFP and the Dylight594 signal was seen in both groups with GVs for the acoustic labeling (GVNK & GVNK+IL2), which could be further confirmed in the zoom-in images (**Figure 2.11c**). Considering the ultrasound contrast enhancement observed in these two groups, as well as the colocalization profile of GV and NK-92 fluorescence signal, these results suggested that the adoptive NK-92 cells are successfully

detected with ultrasound imaging, where the cells were acoustically labeled by GVs attaching to their surfaces throughout the process of tumor trafficking and infiltration.

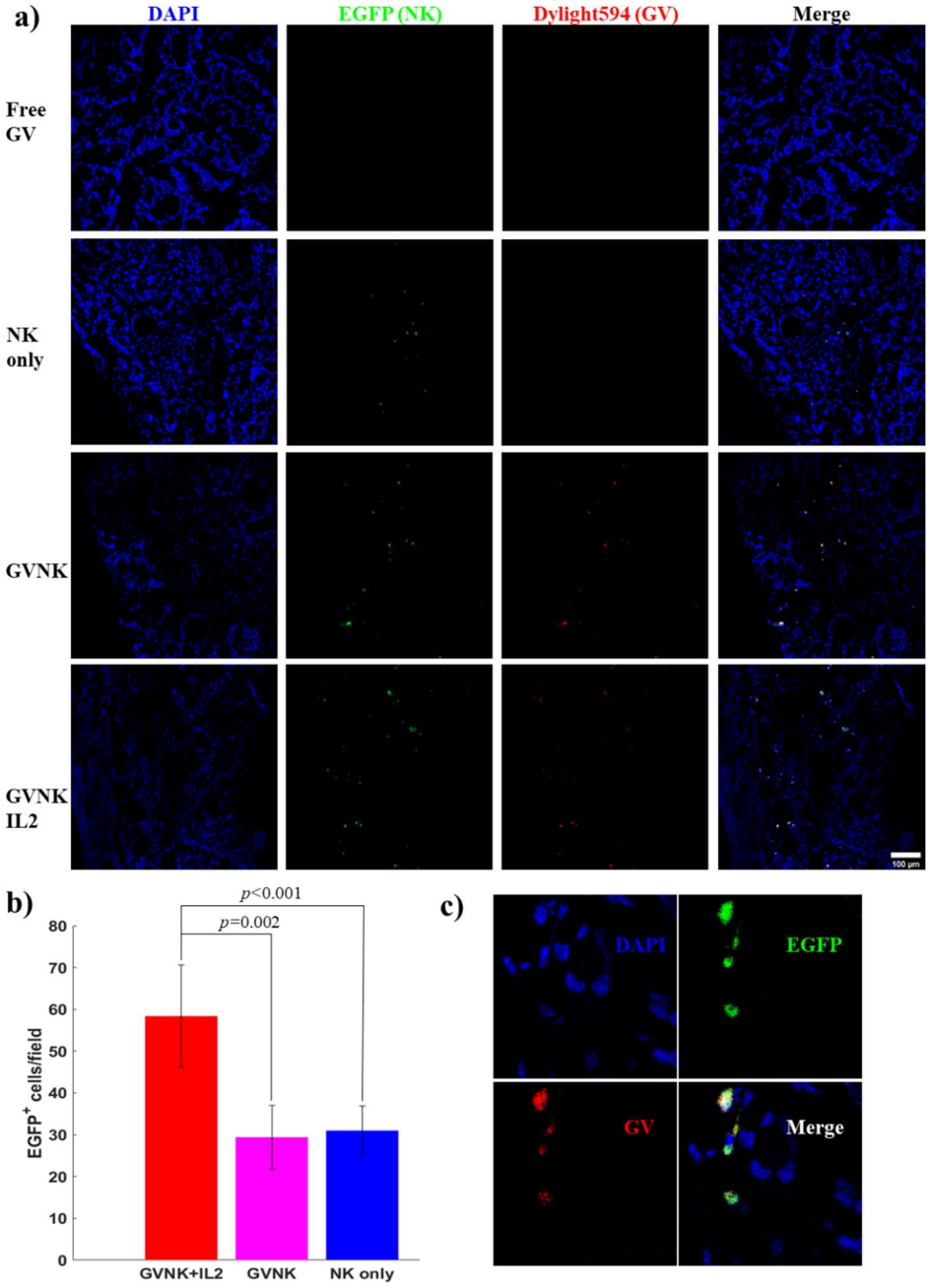

Figure 2.11. Confocal microscopy images of tumor slices. **a)** Representative fluorescence images of tumor slices at 24h post-transfer. **b)** Quantification of $EGFP^+$ cells per field in the tumor slices in groups receiving NK-92 cell transfer. Data collected from 3 animal for each group, presented as mean ± SD.. All statistically significant differences labeled with the *p*-values **c)** Zoom-in fluorescence microscopy image of tumor slice mice receiving GV-labeled NK-92 cells.

Indeed, no GV fluorescence could be seen in Free GV group, which is consistent with observations in our previous study [113]. In our previous study with surface-modified GVs and molecular imaging of tumors, we examined the signal decay and clearance of plain GVs. With the reported rapid clearance of free GVs from blood stream [143], extravasation of non-targeted GVs showed minimal level of extravasation into tumors. Those with tumor-targeted modifications, without PEG protection, also have been shown to be cleared out within 12h, with no observable GV in the tumor slices collected at this point [113]. Indeed, in current study, we introduced SA coating with the purpose of attaching to biotinylated cells, by which we expect minimally affinity to tumors. Hence, in Free GV group, it should be reasonable to expect absence of GV fluorescence in slices collected at 24h. This shall ease complications in distinguishing false positive due to signal arising from free GVs and tumor-infiltrating effector cells carrying acoustic labels.

In the quantification of $EGFP^+$ cells, no significant difference was seen between the tumor-infiltrating control NK-92 cells and the acoustically labeled NK-92 cells (**Figure 2.11b**). This suggested that the labeled and non-labeled cells showed similar trafficking and infiltration capabilities, in consistence with migration assay results. The nanosized GVs are expected to impose minimal burden on those labeled cells, with sizes below the tumor vasculature passing limits.

With the IL-2 boosting, the number of NK-92 cells presented in the tumor was significantly higher in GVNK+IL2 group than other two groups without synergic IL-2 administration. As the cells were derived from the same labeling mixture at all rounds of experiments, the increase in the contrast intensities shall be attributed to the increase in number of GVs in the tumor, carried by a larger number of labeled cells infiltrating the tumor. Taken together, the results suggested a successful assessment of recruitment efficiency of adoptive NK-92 cells in the tumors, via the proposed tracking strategy, under either cell transfer monotherapy or synergic strategies with supplementation combined.

2.4 Discussions

Owing to the advent development in advanced biomaterials, imaging technologies and synthetic biology, noninvasive cell tracking techniques have enabled monitoring of cellular fates in living organisms, contributing to study of basic cellular biology, as well as understanding and development of cellular therapies. There have been tremendous efforts in recent decades on exploring cell tracking strategies for the cellular immunotherapies, by which the living therapeutics could be closely monitored following adoptive transfer, contributing to both post-treatment evaluation in real-world applications, as well as understanding and optimizing the cellular therapeutic approaches. Here, we described, for the first time, a tracking strategy for adoptive immune cells with ultrasound imaging, in the context of systematic infusion for cancer immunotherapy.

In this study, we chose NK-92 cells as the example to demonstrate the proposed strategies, as the NK cell has emerged as an up-rising candidate in cellular immunotherapies. These innate effectors feature several advantages, e.g., the ease in accessing and preparing off-the-shelf product, better safety concerns regarding graft-versus-host disease, and efficient anti-tumor cytotoxicity at scenarios with antigen loss, etc. [135-139]. Hence, we chose one of the popularly applied strands of NK cells, the NK-92 cell line as the model platform to demonstrate our implementation with ultrasound, by which we also expected to show the compatibility of the ubiquitous and cost-effective ultrasound modality with this candidate therapeutic with broad application prospectives.

We demonstrated that, by employing nanosized ultrasound contrast agents, GVs, the NK-92 cells could be acoustically labeled by surface attachment, with no noticeable impact on cellular viability or functionalities. The labeled NK-92 cells were shown to be echogenic under nCEUS imaging, with specific and sensitive distinguishment from the non-labeled counterparts, allowing detection of labeled cells *in vitro* and *in vivo* by ultrasound imaging. We then showed that, in subcutaneous tumor model, the adoptive NK-92 cells could be tracked via ultrasound imaging for post-transfer evaluation. By multiple nCEUS imaging scans after the adoptive

transfer, we showed that the early-phase recruitment of NK-92 cells to tumors could be captured by ultrasound imaging, with significant contrast enhancement observed as early as 3h post-transfer. The homing of adoptive NK-92 cells in tumors was also validated via optical approaches, with consistency to previously reported NK-92 trafficking dynamics. With the synergic treatment of IL-2 bolus following transfer, the intra-tumoral recruitment of NK-92 cells was significantly boosted, which was captured by the contrast changes in ultrasound images, demonstrating the capability of dynamic post-infusion monitoring by the proposed ultrasound tracking strategy.

In current study, the signal decay in GV-labeled NK-92 cells was observed between 24 and 48h both *in vitro* and *in vivo*. We speculated possible cell-GV interactions that might have led to GV structural breakdown, which in turns resulted in the loss of contrast signal overtime. Indeed, in our previous study, the tumor-targeted GVs showed a similar decay dynamic in the TME [113], indicating a presence of GV interactions with components in the TME that could also lead to GV structural breakdown. The exact mechanisms underlying the loss of GV integrity in the TME is yet to be investigated, which shall contribute to development of proper surface modification schemes that enable longer-term labeling and tracking.

In this study, we employed an experiment design centering the assessment of whether ultrasound imaging was feasible in tracking adoptive immune cells, and whether the introduction of nanosized ultrasound contrast agents could be the solution to limitations of traditional MB contrast agents. Although a signal loss was seen after 48h, we were able to focus on the early-phase recruitment of adoptive immune cells to tumors, applying the proposed strategies for acoustic labeling and ultrasound tracking. As expected, the intra-tumoral ultrasound contrast reflected the trace of tumor-infiltrating NK cells, with an early increase identified 3h post-transfer and a sustained recruitment revealed up to 24h. With the synergic administration of IL-2, the significant elevation of ultrasound contrast was seen in the observation time window, suggesting a boosting of NK-92 cell recruitment to tumors by IL-2 captured via the ultrasound tracking. Such trafficking and recruitment dynamics at early post-transfer window captured by the proposed strategy shall provide valuable information for the

evaluation and optimization of adoptive cell therapies, with indications on adjuvant strategy design for maximizing the therapeutic outcomes.

In current study, we applied the single bolus of IL-2 in GVNK+IL group, while the other groups with NK-92 transfer were not supported with the IL-2 supplementation. Although the NK-92 cells rely on exogenous IL-2 supplementation [144], which shall maintain their anti-tumor activities and survival after adoptive transfer, we employed the current paradigm to set baseline trafficking status in GVNK and NK only groups. By such design, we were able to compare the ultrasound contrast dynamics under different trafficking conditions, facilitating the demonstration of the tracking strategy on dynamic evaluations. Therefore, we did not use any further IL-2 either within the imaging period or afterwards, avoiding the introduction of potential confounders. Therefore, the withdrawal of IL-2 should compromise the viability of adoptive NK-92 cells afterwards. As a result, the GVs, as well as the cell debris, might experience clearance by resident cells in the TME, as another possible reason behind signal loss *in vivo*. At the meantime, it should be reasonable to expect only moderate tumor growth inhibition in all groups, with the intraperitoneal IL-2 bolus insufficient to alter long-term therapeutic outcomes either. Nonetheless, with the characterized functionalities and viability in our *in vitro* experiments, one shall expect full competency of the NK-92 cells in delivering promising therapeutic effects when supported, while the GVs could be applied for acoustic labeling and ultrasound tracking. The in-depth evaluation and improvement of therapeutic effects will be pursued in future studies, as well as relating the trafficking dynamics captured by ultrasound to therapeutic outcomes.

Indeed, ultrasound imaging has been explored for imaging cellular targets in some previous studies, yet the effective tracking strategy for systematically infused immune cells in ACT has not been available. In an early study, ultrasound tracking of neural progenitor cells has been demonstrated with cationic MBs employed for acoustical labeling, which indeed granted labeled cells with high echogenicity under nCEUS imaging. The labeled cells were detected after intravenous infusion and accumulation in mouse livers by nCEUS imaging, establishing the feasibility of detecting cellular targets by ultrasound imaging [145]. However,

the MB-based labeling was incompatible with cell tracking in ACT, as the large sizes of these contrast agents would compromise the tumor-infiltrating ability of the effector immune cells. In a more recent study, the sonazoid MBs were employed for the acoustic labeling of NK cells, which were then observed via ultrasound imaging during and after the intra-tumoral injection. Although this has provided a demonstration on detecting acoustically labeled immune cells in the tumor tissues, the underlying incompatibility between MBs and the tumor-infiltrating immune cells was left unaddressed [146]. At the meantime, we also observed a quick decay of the acoustic signal in MB-labeled cells within a few hours under the incubation conditions at 37℃, imposing additional difficulty when tracking the adoptive immune cells with dynamics at time scale of days. The mesoporous silica nanoparticles were employed recently for drug encapsulating, along with the phase-changeable perfluorocarbon. These ultrasound-responsive nanoparticles were loaded into macrophages, which were exploited as tumor-seeking drug carriers, allowing temporary detection of these carrier macrophages because of the partial vaporization of the perfluorocarbon. The high intensity ultrasound bursts were used to trigger violate vaporization, allowing position detection and destruction of the carrier cells for payload release [147]. Such destruction-dependent detection was not suitable for ACT, as full cell viability and functionalities were essential to the therapeutic effects. While the declining rate at partial vaporization state of theses nanoparticles was also similar to traditional microbubbles, undesirable for tracking in ACT either.

We have demonstrated the feasibility of implementing post-treatment evaluations for adoptive immune cells recruitment in tumors by ultrasound imaging. The broad application of the ultrasound modality with the real-time image guidance further suggests opportunities to implement image-guided interventions on these living therapeutics. In recent years, the ultrasound has been shown as the versatile cell stimulation tool, allowing modulation on cellular activities including immune cells through noninvasive delivery of mechanical energy [79, 105]. With the ultrasound-based tracking strategy demonstrated in this study, we foresee great prospectives of the ultrasound modality in the image-guided control of the engineered immune cells. The real-world applications and safety management of cell-based therapies shall

benefit from this versatile and already-on-board tool. The in-depth investigation on the relation between labeling capacity and the contrast intensities, an optimization on the labeling protocol and the exploration alternative nanobubble formulations, as well as the demonstration of ultrasound tracking in orthotopic tumor models shall all accelerate the translation and implementation of the proposed tracking strategies.

For the acoustic labeling of the immune cells, the biogenic nanosized ultrasound contrast agents, GVs, were employed in current study. With an *ex vivo* direct labeling scheme, we attached GVs on cell surfaces via biotin-streptavidin conjugation, which should be applicable for the labeling of a wide range of non-phagocytic immune cells. Indeed, the proposed labeling and tracking strategy shall be compatible with a variety of immune cell types like cytotoxic T cells and CAR-T cells, showing broad prospectives in the cellular immunotherapy. As we hypothesized, the acoustic labeling by nanosized contrast agents showed no impact on the migration and infiltration of the labeled immune cells, with the compatibility to tumor infiltration further demonstrated in the *in vivo* experiments. Such direct labeling method is cost effective and easy to implement, it is, however, also suffering from the limited labeling timespan and scope of imaging. The cell-GV interactions, as well as cell-cell interactions could both lead to signal decay, limiting the span of the tracking time window. Another potential concern associated with the direct labeling method would be the steric hindrance. This means the interactions between labeled cells and their targets might be obstructed if the nanobubbles were presented in bulk on the cell surface. The position of the adoptive immune cells could be reflected by the echo signal generated from the cell-bound contrast agents, while the activation status or the cellular viability would be difficult to assess with such surface-attached contrast agents. Therefore, an intracellular labeling scheme shall be a plausible alternative to pursue, preferentially by genetically encodable mechanisms that could further be related to cell fate. As biogenic protein structures, the GVs are naturally associated with potentials in the development of genetical approaches for acoustic labeling. Indeed, in recent years, the gene clusters encoding GVs have been mined for expression in eukaryotic cells, allowing the labeling of cellular targets via acoustic reporters [115, 121]. However, the stable expression of

GV gene clusters remains a substantial challenge. Moreover, with the complex intracellular environment and functionalities of immune cells, the introduction of acoustic reporter gene into immune cell tracking requires optimizations of GV gene clusters for stable assembly of functional GVs. Efforts have also been made recently on improving acoustic reporter genes, as well as sensitive detection methods for improved image qualities [114, 115, 120]. With the feasibility of ultrasound immune cell tracking with GVs for acoustic labeling established, we see tremendous potentials on the immune cell tracking based on acoustic reporter genes, where a broader spectrum of biological processes associated with the immune cells could be accessed with ultrasound, along with the survival monitoring to a longer term, providing more information with prognostic relevance [29]. The compatibility of ultrasound imaging with real-time image guided procedures would further allow image-guided biopsies, which shall allow more in-depth examinations of adoptive immune cells in the TME with improved sampling precision.

In noninvasive cell tracking, the leakage of the markers could be a major concern especially when direct labeling method was applied, as the efflux of the marker could lead to false negative and misinterpretation of the imaging results. Nonetheless, it should be less of a concern when GVs were employed for the acoustic labeling. As protein structures, the free GVs, if were to be released from labeled cells, are known to experience quick clearance in the blood stream by liver resident macrophages [111]. Moreover, the biotin-streptavidin conjugation was employed for the labeling purposes, known as one of the most stable non-covalent bonds in nature. Once formed, the binding remains stable even at extremes. The biotinylation also features great compatibility with the molecules to be decorated, whose functionalities are rarely influenced by biotin decorations. These make the biotin-streptavidin interaction popular in the functionalization of molecules and particles at various size ranges [72]. In cell tracking, the interaction has been explored for the labeling of cytotoxic T lymphocytes, with demonstrated compatibility to optical, magnetic and radioactive markers. The labeling was shown to be stable, with no observed impact on the cell functionalities [148]. Therefore, we also expect stable binding between GVs and NK-92 cells when infused into the

living organisms. Indeed, no free GV was observed in the tumor samples harvested after the transfer of labeled NK cells. Even if the shell components could detach from the labeled cells, which might be a result of GV collapse, the shell components will not lead to contrast enhancement in other organs, as the intact structure of GVs is central to their echogenicity. Indeed, such collapse could limit the highest signal-to-noise ratio reachable in cell tracking, as well as shortening the observation time window. Therefore, we encourage the exploration of alternative nanosized contrast agent formulations, as well as the modification and functionalization that improve the stability of the acoustic tracers, such that the unwanted premature collapse could be avoided *in vivo*.

2.5 Conclusions

In conclusion, this study demonstrated a noninvasive immune cell tracking strategy based on ultrasound imaging. The biogenic nanobubble has been employed for the acoustic labeling of NK-92 cells, and the tumor recruitment of adoptive NK-92 cells was captured and monitored with the nonlinear contrast-enhanced ultrasound imaging. We were able to characterize the tumor recruitment of adoptive NK-92 cells when the IL-2 bolus was applied for the enhanced NK cell trafficking, suggesting strategies for the treatment evaluations and strategy designs in adoptive NK cell therapies. The ubiquitous ultrasound imaging tool has been shown compatible with the tracking of adoptive immune cells, indicating potentials of implementing cost-effective and widely accessible post-treatment evaluations, allowing acquisition of information for treatment-related decision making. With the temporal resolution of ultrasound imaging, the proposed strategy will also enable the real-time image-guided interventions following the cell transfer. Furtherly, the echogenicity of GVs following the tumor infiltration of GV-carrying immune cells suggested a functional competency of these structures, indicating their potentials as local amplifiers of the mechanical effects from ultrasound. Such potentials shall be explored and exploited in the next chapter for initiating genetic circuitry, which is designed to be responsive to external mechanical stimulus in engineered immune cells.

Chapter 3 Nanobubbles as local actuators for mechanical stimulation and gene expression control on immune cells by ultrasound

In the last chapter, the ultrasound tracking of GV-labeled NK-92 cells has been demonstrated. These cell-tethered GVs have been shown to exhibit nonlinear echogenicity and enable ultrasound imaging of these tagged cells within 3 days following the transfer. This suggests the structural integrity and functional competency of GVs during the tumor infiltration of the tethered immune cells, which is unaffected by these nanosized tags, and that they are durable within a certain time window. Therefore, the GVs should naturally be considered as potential sonosensitizers on these immune cells after tumor infiltration, amplifying the mechanical stimulus from ultrasound waves for modulatory and switching purposes.

In this chapter, the rationale and design of the GV-actuated ultrasound switching system on engineered immune cells will be demonstrated, with the NK cell as example platform. The endogenous mechanosensitivity of NK-92 cells will be examined, laying grounds for modulating their cellular behaviors through mechanical stimulus. Then the calcium responses to mechanical stimulation by ultrasound on GV-tethered NK-92 cells will be examined, serving as fundamentals for initiating nFAT signaling and hence the expression of nFAT-promoted genetic circuitry. The translocation of nFAT shall be demonstrated as well, as a key step connecting calcium responses and genetic expression. Afterwards, the expression of downstream reporter genes to nFAT promoters will be examined, validating the efficacy of the GV-actuated mechanical switching system and its potentials in controlling the engineered immune cells.

3.1 Backgrounds

Modulation and control in cellular immunotherapies

The recent years have witnessed encouraging success of cellular immunotherapeutic

approaches in cancer treatment, with thriving research interests in the development, optimization and translation of CAR-engineered cells [22-24, 27, 138, 139]. With generations of CAR modifications, now the CAR-expressing immune cells come with high potency and improved specificity. However, the challenge remain, as the immune-related side-effect raises concerns on the safety and management of these therapeutic cells, as well as the unsatisfying efficacy in solid tumor treatment [125, 127]. On one hand, in pursuit of higher efficacy, there is a demand to further enhance the effector functions of these therapeutic cells. On the other hand, the overactivation and off-tumor targeting of these engineered cells are associated with the immune-related toxicity, e.g., the cytokine release syndrome, sometimes severe enough to be life-threatening. This seemingly leads to a dilemma where the trade-off between potency and safety concerns is needed. Alternatively, the on-demand modulation and control of the therapeutic immune cells provides solutions to exploiting powerful anti-tumor potencies, while preserving the manageability and safety of the treatment. The concept of manipulating cellular behaviors has long been brought up and pursued throughout the development of modern cellular biology. It offers means of probing fundamental biological processes related to life and pathology, as well as ways of directing the living organisms to execute certain functions for therapeutic purposes.

Immunomodulatory molecules

Traditionally, the cellular activity and behavior are widely manipulated through biochemical agents, e.g., drugs and cytokines, owing to their well-characterized effects in *ex vivo* basic cellular biology studies. It naturally leads to explorations on applying these agents for the supplementation and potentiation of immune cells *in vivo*, either resident or adoptive, for therapeutic benefits [50-52]. The idea of boosting and supporting the adoptive immune cells by synergic adjuvant administration has been explored as early as in the 80s. For example, the immune adjuvant, interleukin 2 (IL-2), was administered following the adoptive transfer of activated T cells to induce T cell growth *in vivo*, with the efficacy evaluated against the injection route and timing in mouse models [142]. Similarly, the IL-2 effect has been studied in clinical trials on patients with malignant brain tumors, injected intratumorally with lymphokine-

activated killer cells [149]. Despite the well-appreciated supporting effects on persistence and cytotoxicity of therapeutic cells, pitfalls have been reported, including systematic toxicity, non-specifically activating immunosuppressive cells like Treg, and limited responses, etc. [50]. Similar issues have been haunting other immunotherapeutic strategies relying on drugs, cytokines and even ICIs that directly exert modulatory effects on cellular targets. The system-wide distribution of the regulatory molecules naturally introduces hazards of stimulating resident effector cells in healthy tissues, breaking the balance of endogenous immune tolerance, leading to systematic toxicity often resembling severe infection. Even with local administration in tumor tissues, the rapid leakage into bloodstream has also been reported, still raising concerns on systematic toxicity [53, 54]. Such concerns limit the doses applicable in patients, trading-off between the systematic immune-related side-effects and the level of boosting effects on effector cells of interests, compromising efficacy for safety issues [150]. The non-specific stimulation of other undesired cell types also imposes a dilemma, as suppressors often have endogenous activation mechanisms similar to effectors as a natural mechanism to maintain balances [151].

Nanocarriers for improved localization

With the hope of overcoming the limitations and improving safety of immunomodulatory agents, efforts have been made to improve the spatial precision by introducing control strategies for the on-demand release of these molecules. By incorporating nanomaterials, the explored solutions include capsuling and on-site uncaging strategies, agonist engineering for improved specificity, and targeted modification strategies, etc. The proper capsuling of the active components prevents them from exerting effects on other tissues passed by during circulation. At the meantime, either through external interventions via physical energy transmission, or with caging designs reactive to certain features in tumor microenvironment (e.g., acidity, hypoxia) [152], the on-site drug release mechanism enables exertion of bioeffects localized to malignant tissues. By such controlled release, the systematic toxicity of the active component could be alleviated, with increased and extended drug exposure locally on immune cells in the tumor.

These modulatory methods relying on administration of modulatory agents are inevitably entangled with the pharmacokinetics and systematic effects of these agents. The dissemination and whole-system redistribution of these agents limit the spatiotemporal precision of such modulatory schemes, while the specificity also imposes challenges on biochemical engineering on these modulatory molecules. Improvements could be made, to some level, with the incorporation of nanomaterials that allow controlled release of these therapeutic agents. However, once triggered, the dissemination of these immunomodulatory agents in the treated tissues still impose uncertainty on the exposure both in space and time. The leakage of the released components into circulation could also impose hazards of systematic side-effects, challenging the use of agents with high potency.

Switching of genetic expression by noninvasive energy transmission

Thankfully, with the advances in synthetic biology and nanomaterials, the controllable activation of these engineered immune cells by external triggers has been made possible. External stimulus from physical energy transmission enables the on-demand activation of engineered immune cells, often in a manner of CAR expression initiation, unleashing the powerful cytotoxicity of these potent effectors at sites of therapeutic interests. The control strategy for therapeutic cells offers a better solution, where the high potency could be exploited in a controllable manner with confinement to tumor sites, instead of being traded off for safety concerns or relying on systematically administered modulatory molecules.

To achieve switching of cellular activities by external stimuli, the key is to introduce transduction mechanisms, of certain sorts, that specifically converts external stimuli into biological signaling in cell population of interests, preferentially with spatiotemporal precision. To date, various cell-manipulating tools relying on different forms of physical energy transmission, some in combination with advanced nanomaterials, have been introduced to the field of cellular therapies for the control of “living therapeutics”. Among all physical energy forms, the light must be one of the most popular tools owing to the maturity and broad success

of optogenetic technology, granting researchers with unprecedented capabilities to modulate cellular activities. In the design of light-controllable therapeutic cells, the light-responsive proteins are incorporated into cells as “switches” that convert light stimulus into biological processes that direct cellular fates, in forms of either genetic circuitry initiation or assembly of functional components at protein level [55-57]. Such light-activatable tools are exploited for manipulating engineered immune cells, which localizes the expression of genes with potent effector functions like CAR and/or cytokines with spatiotemporal precision [58-61], often implemented with assistance of nanomaterials for improved light stimulus delivery *in vivo*. The heat shock factor (HSF), with the heat-responsive circuitry, has also enabled the transduction of various physical energy into biological signaling [64]. With the help of photothermal nanomaterials, the NIR light with deeper tissue penetration could be transduced into heat that activate heat-responsive genetic circuitry [65-68]. Similarly, the magnetic nanoparticles could also serve as local antenna to convert energy from alternating magnetic field into heat for the activation of heat-responsive genes *in vivo* [69-71]. Such switching system has been explored for the control of engineered probiotics, implementing on-site release of immunotherapeutic biologics in tumors [72, 73]. The mechanical energy, transmitted in forms of ultrasonic waves, could also be exploited for initiation of heat-responsive components when transmitted in high intensities and focused manners. This has been exploited for *in vivo* gene expression manipulation [74-76], and has also been explored in recent years for activation of engineered microbes and CAR-T cells for cancer therapies [77-79].

However, challenges remain for the switching systems explored for remote control in cellular immunotherapies. The penetration depth has long been hamstringing the application of optical switching systems in large animals, accompanied by issues of immunogenicity and certain-level background activation. Similarly, the HSF has also been known to be non-specifically activated by other cues like mechanical stress and hypoxia [80-82], which limits the specificity of such switching machinery. At the meantime, the heat dissipation in biological tissues imposes uncertainties upon the exact margins of the hyperthermia induction, and the effective heating could also be limited due to the heat sink effect. These lead to the

compromised predictability and spatiotemporal precision in hyperthermia switching system.

The mechanical force as a potential switching mechanism

Among several forms of physical energy explored, the mechanical effect from ultrasound waves, without the transduction into heat, has been a potent candidate for precise manipulation in deep tissues by principle. The mechanical effect from ultrasound waves comes with a deep-penetrating profile with fine spatiotemporal confinement in biological tissues. By applying high-intensity ultrasound in a highly focused manner, with fine-controlled duration down to microseconds, the mechanical force could be applied noninvasively to destroy tissues with sharp margins [153]. Featuring such controllability in spatial and temporal domains, the mechanical ultrasound stands out as an attractive candidate for implementing switching system with improved precision. Moreover, exploiting the direct mechanical force delivered by ultrasound also offers a potential solution to multiplexed switching strategies, considering the existing genetic switching strategy with ultrasound hyperthermia. By controlling the input ultrasound stimuli at different parameters, the thermal and non-thermal effects could be preferentially elicited according to demands. This would allow noninvasive switching of multiple genetic circuits in desired orders and/or at distinct sites in deep tissues, with potentials of implementing logic gates with multiple switching circuits. This will further contribute to more sophisticated control strategy designs, exploiting highly potent cellular therapies with stringent safety management.

Indeed, there is a growing body of evidence showing that the ultrasound is capable of mechanically modulating cellular activities in recent years [86, 87]. With the superior precision both in spatial and temporal domains, the ultrasound has been demonstrated effective in elevating neuronal activities in a reversible manner, showing thrilling potentials in therapeutic neuromodulation [88-93]. The transduction of the mechanical effects from ultrasound wave is widely believed to rely on the mechano-sensing components in the cells, as mechanosensitive ion channels have been widely reported to underly the neuronal activities elicited by ultrasound stimulation [154-157]. As endogenous mechanical cue sensing components, mechanosensitive

ion channels open upon mechanical agitation, which causes changes in intracellular ion homeostasis, transducing the mechanical stimuli into biological signaling like electrophysiological activities, transcription induction, etc. Sensitizers have also been introduced to enable finer control of the modulatory effects on designated regions or even cell types [86, 89, 94, 119, 158, 159]. By either exogenous expression of mechanosensitive ion channels on specific cellular targets, or by applying local actuators that amplify mechanical effects from ultrasound waves, the cellular response threshold to mechanical ultrasound could be lowered, enabling modulation of cellular activities with regional or even cell-type specificity by low-intensity ultrasound.

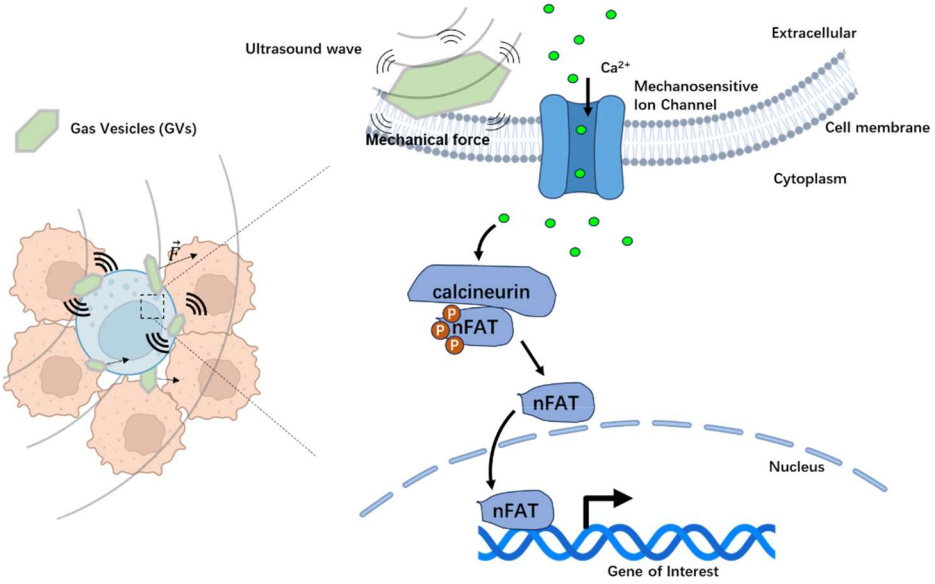

Figure 3.1. Schematic illustration of the GV-based sensitization scheme. The gas-filled GVs oscillate and/or move under the ultrasound mechanical agitation, which generates mechanical force localized to the cell surface to which they attach. The force then disturbs the cell membrane, opening the endogenous mechanosensitive ion channels on the immune cells, resulting in the calcium ion influx. The calcium then induces the genetic circuitry designed downstream to the nFAT responding elements.

Similarly, to implement precise and specific mechanical modulation of therapeutic immune cells by ultrasound stimulus, the key is to bring localized sensitization to these cellular targets of interests. The traditional ultrasound contrast agents, microbubbles (MBs), with their flexible shell encapsulating gas core, could experience stable cavitation under acoustic field,

generating cell membrane-perturbating mechanical force. Such mechanism has been exploited for mechanical perturbation for intracellular delivery purposes, as well as amplifying mechanical ultrasound stimuli for implementing controlled CAR expression *in vitro* through nFAT signaling [103-105]. However, the short lifetime and large sizes of MBs still hinder the application of such switching strategy for *in vivo* implementation. The therapeutic immune cells are expected to infiltrate and migrate into tumors, involving dynamical trafficking and extravasation at timescale of hours and even days, while the MB has been widely documented with *in vivo* lifespan at timescale of minutes. The micron-scale size of MBs may also impose extra burden on therapeutic cells during tumor infiltration, given their usually confined presence in the intravascular space [95-98].

In this regard, we propose to introduce GVs as the localized actuators, tethered to immune cells, to amplify the ultrasound wave for sensitization purposes. The GV has been recently shown as gas-filled nanostructures with superior thermodynamical stability, and has been demonstrated with buckling under acoustic agitation [106, 108]. These properties have granted GVs popularity in various applications involving the ultrasound modality, including molecular ultrasound imaging, tumor therapies and deep-brain neuromodulation [94, 113, 116-119]. Given the demonstrated ultrasound-responding capabilities of GVs, as well as their nanoscale sizes and superior stability, we hypothesize that GVs shall serve as plausible local actuators to amplify and exert modulatory mechanical force on engineered immune cells for switching purposes (**Figure 3.1**) . The sensitization by GVs shall initiate the transduction mechanism that converts mechanical ultrasound stimuli to changes in intracellular calcium ion homeostasis, as the opening of the endogenous mechanosensitive ion channels would lead to calcium influx in respond to GV-amplified mechanical agitation. Downstream to the calcium influx, we shall further employ the nFAT response components as the calcium responding element to initiate the expression of gene of interest (GOI). The calcium-sensitive phosphatase, calcineurin, is activated upon the influx of calcium ions upon channel opening, dephosphorylating the transcription factor nFAT in the cytoplasm. The dephosphorylated nFAT then translocates into the nucleus, engaging with the nFAT responding element and initiating the expression of GOI.

The nFAT response element has been shown as a central calcium-responsive transcription factor in various immune cells [160, 161]. Therefore, employing nFAT as the responding element shall provide stable GOI expression, once calcium events could be robustly induced by mechanical ultrasound with proposed sensitization schemes [162].

In this chapter, we employed NK cells as example platforms for demonstrating the sensitization and switching scheme, given their uprising roles in cellular immunotherapies in recent years. Specifically, we chose NK-92 cells, a cell line of human NK cells that has been receiving growing success throughout decades of explorations in cellular immunotherapies [138], as example effector cells for engineering and mechanical switching. We first evaluated the functional expression of endogenous mechanosensitive ion channels on NK-92 cells, serving as the fundamentals for transducing mechanical agitation into biological signaling. Afterwards, we validated the capability of GV-sensitized mechanical ultrasound switching system in eliciting cellular responses upon low-intensity ultrasound stimulation *in vitro*, at several nodes along the nFAT signaling pathway we had chosen for GOI initiation, i.e., the calcium responses, nFAT nuclear translocation, and the reporter gene expression in GV-tethered NK-92 cells. We showed robust calcium responses upon low-intensity ultrasound stimulation in those NK-92 cells sensitized by surface-bound GVs, following which the nucleus translocation of nFAT was also observed. Negative control by mechanosensitive ion channel blockers was also introduced, such that the mechanical switching system could be validated against other potential confounding effects. The successful induction of reporter gene, luciferase, expression further suggested the validity of the GV-sensitized mechanical ultrasound switching system. In a model platform of nFAT-promoted INF-γ NK-92 cells, we showed that the proposed switching strategy has the capability of activating INF-γ secretion in transfected cells, featuring a potent therapeutic with enhanced anti-tumor cytotoxicity as well as TME remodeling capability. The ultrasound-activated INF-γ secretion was further demonstrated to promote anti-tumor immunity in an *in vitro* model, featuring a potent therapeutic strategy for cancer treatment with engineered NK cells controlled via mechanical ultrasound switching system.

3.2 Materials and Methods

Calcium imaging of NK-92 cells

Calcium signaling is central to the activation of nFAT transcription factors, whose ion homeostasis changes upon opening of mechanosensitive ion channels that causes influx of calcium ions. To verify the presence of functional mechanosensitive ion channels on NK-92 cells, as well as to evaluate the efficacy of proposed sensitization scheme in eliciting calcium signaling upon ultrasound stimulus, we conducted the calcium imaging *in vitro*. In brief, the NK cells to be tested were seeded onto the glass-bottom culture dish, pre-coated with PDL to facilitate the attachment of the suspension cells. After seeding, the medium was replaced with the imaging buffer solution (a buffer solution with 130 mM NaCl, 2mM $MgCl_2$, 4.5 mM KCl, 10 mM Glucose, 20 mM HEPES, and 2 mM $CaCl_2$, pH 7.4.). Then the cells were then incubated with the calcium indicator, Rhod-2 AM (ThermoFisher, R1244), according to the manufacturers' instructions. After the 30-min incubation, the cells were washed with imaging buffer to remove residual indicators at least three times. The cells were then balanced for 30mins according to the manufacturers' instruction, after which the fluorescence was checked before further experiments.

The imaging was conducted using a customized microscopy system compatible with simultaneous ultrasound stimulation on the cells. The upright epifluorescence microscope was equipped with a dual-color LED for the generation of the excitation light, which was filtered according to the excitation spectrum of the calcium indicator. The fluorescence signal was collected by an objective, with filters adjusted according to the emission spectrum, and captured by a sCMOS camera. The excitation LED was triggered at 0.5Hz to minimize the phototoxicity, synchronized with sCMOS for time-lapse imaging. To deliver ultrasound stimulation, the plane transducer operating at 0.5MHz was equipped with a customized cone-shaped waveguide, of which the front was just merged in the imaging buffer. The transducer was placed in alignment to the microscopy system, generating acoustic field homogenously covering a circular area with a diameter of ~4mm. The parameters stimulation is generated with

the following empirically determined parameters: 10ms pulse width, 5Hz pulse repetition rate, and 1s duration for each stimulus.

During the stimulation experiment, the broad-spectrum mechanosensitive ion channel blocker, gadolinium (Gd), was introduced as the negative control to verify the role of mechanical transduction in the calcium responses against potential confounding effects. The blocker will be prepared in form of 20mM GdCl3 solution in DI water, diluted in the imaging buffer to result in a final ion concentration of 100μM for Gd^{3+}. At the end of the calcium imaging experiment, the viability of the cell was further checked with the Propidium Iodide (PI) staining, so that the biosafety of the stimulation system could be evaluated.

To prepare NK-92 cells with GV as surface-tethered actuators, the cells are biotinylated with the EZ-Link Sulfo-NHS-Biotin reagent for 15mins at room temperature. Afterwards, the reagent was removed, and the cells are further washed with imaging buffer 3 times. After removing the imaging buffer, a drop of 5μL SA-GVs at OD10 was added on the cells, with the dish flipped upside down for improved contact between the cells and GVs. After 5mins of the binding reaction, the imaging buffer was added to wash free GVs away, and the GV binding was checked with the fluorescence imaging, with cells ready for calcium imaging with ultrasound stimulation.

Nuclear translocation of nFAT in stimulated NK-92 cells

To verify the transduction of calcium influx into transcriptional activities, the translocation of the nFAT was examined with the immunofluorescence staining. The cells to be tested were seeded at 5×10^5 cells/well in 96-well plate. The plane transducer operating a 0.5MHz was used to deliver ultrasound stimulation from the bottom of the plate, equipped with a customized cone-shaped waveguide with coupling gel in between the plate and the waveguide front. The setting was used for generating acoustic field homogenously within a circular area with a diameter of ~4mm, covering the volume of cell suspension in the wells. The stimulation was generated with the following empirically determined parameters: 10ms pulse width, 5Hz pulse

repetition rate, and 15mins duration for each well. Some slight shaking will be used to ensure the coverage of all cells during the stimulation period. After the 15-min ultrasound stimulation, the medium was replaced with PBS through centrifugation, and the cells were fixed with 4% paraformaldehyde (PFA). After fixing, the cells were blocked using a blocking solution containing 10% normal goat serum, 1% bovine serum albumin, and 0.3% Triton X-100, for 60 mins. The primary antibody was then diluted in the blocking solution, and the cells were incubated with the primary antibody overnight at 4℃. The primary antibody was then washed away with the blocking solution through centrifugation, and the secondary antibody, diluted in blocking solution as well, was added for another incubation of 60mins. The cells were washed with PBS, and a small drop of the stained cells was mounted on glass slides with DAPI. Primary antibody to nFAT (dilution 1:100) was used to stain the intracellular distribution of nFAT, and the secondary antibody of goat anti-rabbit Alexa Fluor 555 (A-21428, Invitrogen, dilution1:1,000) was used. The cells were then observed with a laser-scanning confocal microscope (Leica TCS SPE, Germany) with 40X objective. The 561nm laser excitation was used for visualizing the distribution of nFAT, while the nucleus was observed by the 405nm laser excitation for DAPI staining. Morphology and colocalization of the nFAT staining and DAPI staining were observed and compared to analyze the translocation profile.

Luciferase expression in engineered NK cells

For the evaluation of GOI expression initiation *in vitro*, we chose luciferase protein as reporter gene, whose activation efficiency was characterized by bioluminescence reading, as well as immunofluorescence staining. For the switching experiment *in vitro*, an ultrasound stimulation setup similar to nFAT translocation experiment was used, except for a prolonged stimulation period of 25mins. After the stimulation, the cells were incubated for another 4h to allow expression of the reporter gene and synthesis of the proteins. For the bioluminescence examination, D-luciferin was then added to the medium with an incubation of 10mins before reading. The bioluminescence signal was read using the IVIS imaging system (Perkin Elmer, Waltham, MA). The reporter gene expression was also checked with the positive control treated

with the cell stimulation cocktail (PMA/Ionomycin, ThermoFisher, 00-4970-93). For the immunofluorescence staining, the similar procedure of fixing and staining was applied as in nFAT translocation analysis. The primary antibody against a tag peptide on the expressed luciferase was used (1:100 dilution), such that the induction of luciferase expression could be determined by positive staining. The luciferase staining was further analyzed by microscopy and flow cytometry to evaluate the efficiency of induction in the stimulated cell population.

In vitro ultrasound stimulation system

The plane transducer (0.5MHz, Panametrics) was equipped with the customized cone-shaped waveguide, designated to generate an acoustic field with homogenous pressure distribution covering an area ~4mm in diameter, within 10mm away from its surface. The transducer was driven by a radio frequency amplifier (A075, Electronics & Innovation Ltd.), with the control input generated by a function generator (AFG251, Tektronix). The sinusoidal signal at 0.5MHz was generated in pulse trains with 10ms width and 5Hz repetition rate. Different stimulation durations were programed according to the paradigms set for different experiments.

3.3 Mechanical switching of GOI in NK cells with ultrasound

3.3.1 Functional mechanosensitive ion channel expression on NK-92 cells

We first examined the presence of endogenous mechano-sensing components, laying down the basis for implementing GV-based sensitization for the mechanical switching design. The functional expression of endogenous mechanosensitive ion channels on NK-92 cells were examined with *in vitro* calcium imaging experiments using a customized microscopy system for time-lapse imaging of live cells (**Figure 3.2a**). We used the Yoda1 agonist to induce the probe the presence and function of mechanosensitive ion channel Piezo1. Upon addition of 10μM Yoda1 to the imaging buffer, the calcium responses were quickly elicited in most NK-92 cells observed in the experiment (**Figure 3.2b**). The fold changes in calcium indicator

fluorescence intensities were quantified with the recorded baseline signal from each cell, within 30s before the stimulation. The addition of Yoda1 elicited robust calcium responses within most cells observed in the imaging experiment, with similar latencies observed across the field of view (**Figure 3.2b**). By such, we have verified the functionality of Piezo1 on NK-92 cells, given the well-known specificity of agonist Yoda1 to Piezo1. The mechanosensitive ion channel Piezo1 has been previously shown to mediate robust calcium responses in various cell types to low-intensity ultrasound stimulation [86, 94, 105, 154, 155].

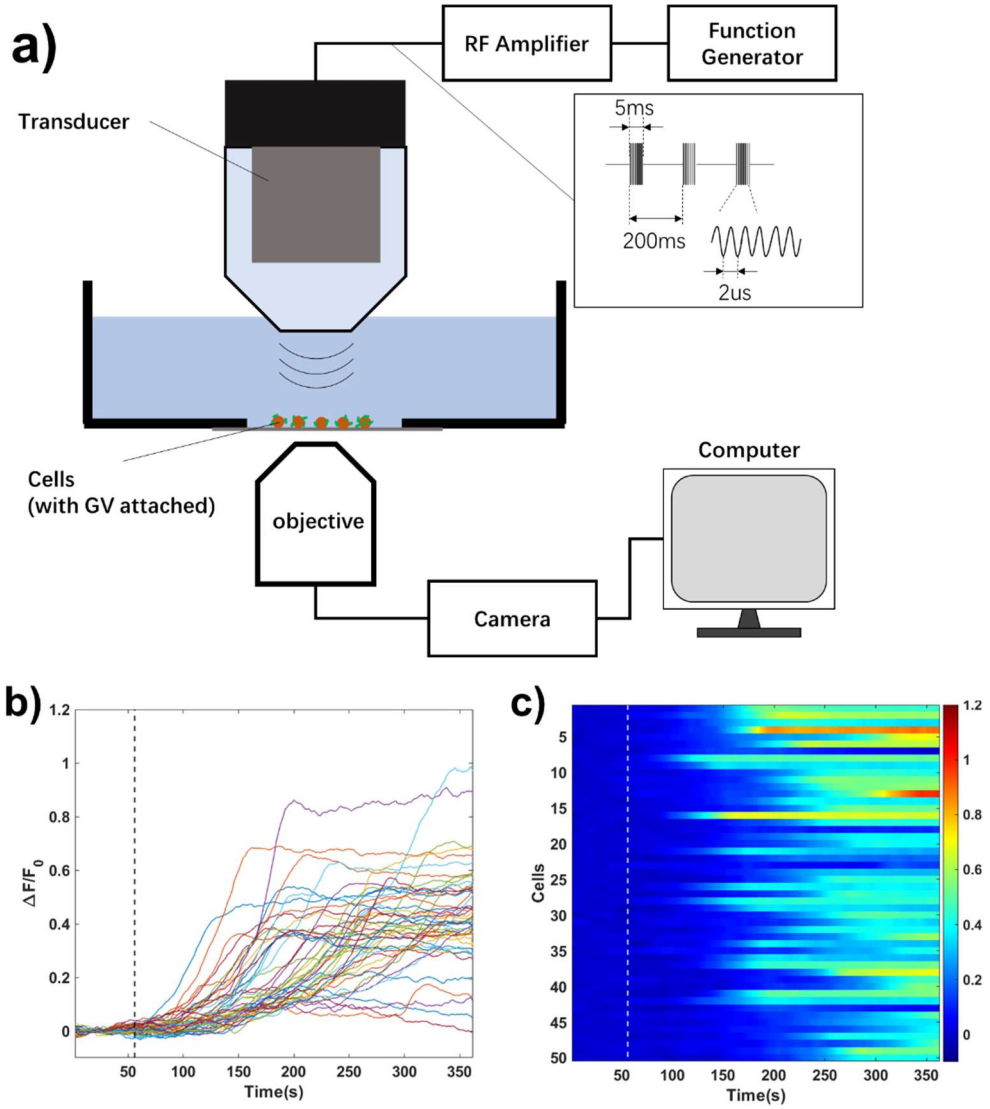

Figure 3.2. In vitro calcium imaging of NK-92 cells treated with mechanosensitive ion channel agonist. **a)** setup of in vitro calcium imaging on NK-92 cells. The cells were seeded on a glass-bottom plate with PDL-assisted adhesion, stained with calcium indicators and imaged with a customized fluorescence

microscopy system for time-lapse fluorescence imaging. **b)** fluorescence changes in of individual NK-92 cells after treatment of Yoda1. Dashed line indicates the time point of Yoda1 addition into the imaging buffer. **c)** heatmap of NK-92 cells calcium responses to Yoda1 stimulation, with pseudo color encoding the fold changes in the calcium indicator fluorescence intensities. White dashed line indicates the time point of Yoda1 addition.

Thus, the functional expression of endogenous mechanosensitive ion channels laying grounds for the implementation of mechanical switching system. However, we shall not be exclusive to Piezo1 as the mediators. Other mechanosensitive components could also be presented in the NK-92 cells, which shall also be advantageous since our goal is to elicit robust calcium events via mechanical stimulation. With the presence of functional mechanosensitive ion channels, we would expect robust calcium responses in the NK-92 cells, upon mechanical ultrasound stimulation with sensitization.

3.3.2 Stimulating NK cells with ultrasound and the sensitizer role of GVs

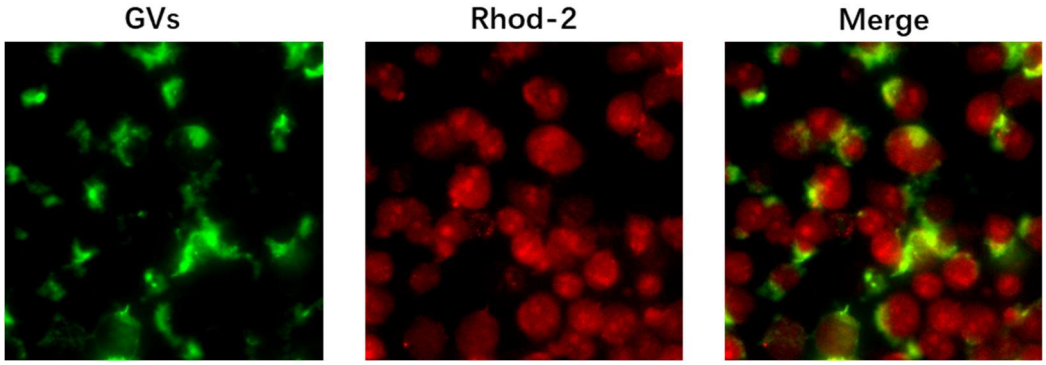

Figure 3.3 Attachment of GVs as actuators on NK-92 cells during calcium imaging. The NK-92 cells were stained with X-Rhod 2 (red), while the GVs were conjugated with Alexa488 (Green) on the surface.

For verifying the GV-sensitized mechanical switching system, we first conducted the *in vitro* calcium imaging experiments on NK-92 cells upon low-intensity ultrasound stimulation, as calcium signaling is central to the activation of nFAT transcription factors. We have adopted the biotin-streptavidin conjugation mechanism for attaching GVs on NK cell surfaces. Indeed,

the GV fluorescence could be observed with a clustered pattern surrounding NK cells (**Figure 3.3**), similar to the labeling outcomes in previous chapter. As the same attachment protocol was used as in previous chapter, we would expect no impact of GV binding on the cellular activities, viability and functionalities of the NK-92 cells during the calcium imaging experiments. Except for the GVs as sensitizers, the broad-spectrum blocker of mechanosensitive ion channels, gadolinium (Gd), was also introduced as a negative control for verifying the role of mechanical signal transduction.

Without sensitization by GVs, the low-intensity ultrasound pulses did not elicit any noticeable calcium events in NK cells, as no calcium indicator fluorescence change was observed in this non-sensitized group. While as expected, robust calcium influx could be induced by the low-intensity ultrasound pulses (0.3MPa) on GV-sensitized NK cells (**Figure 3.4. a&b**). An average peak response of 65±33% rises against baseline was seen in GV-sensitized NK cells, which was followed by a gradual return to baseline, suggesting no obvious compromise to the membrane integrity during the stimulation. By contrast, the addition of blocker, Gd, abolished the calcium responses in the GV-actuated group, with no fluorescence change observed in response to the ultrasound stimuli. The cell viability was further examined at the end of the experiment with Propidium Iodide (PI) staining, with all cells in the stimulated region remained viable after the treatment (**Figure 3.4. c**). This suggests that the proposed actuator scheme provided a robust amplification of ultrasound mechanical effects, enabling on-demand calcium influx induction in a biologically safe manner. Combining the safety examination with the calcium recordings in Gd-treated group, this also suggests mechanosensitive ion channel blocking mechanism behind the abolishment of calcium responses, instead of any potential impact on the cell viability. These results showed that the mechanosensitive ion channel opening was indeed behind the calcium response induction in GV-tethered NK cells, indicating the feasibility of initiating calcium signaling via mechanical ultrasound stimulation in NK-92 cells sensitized with GVs. This shall lay grounds for further manipulation of downstream calcium-responsive transcription factors via the proposed mechanical ultrasound switching system.

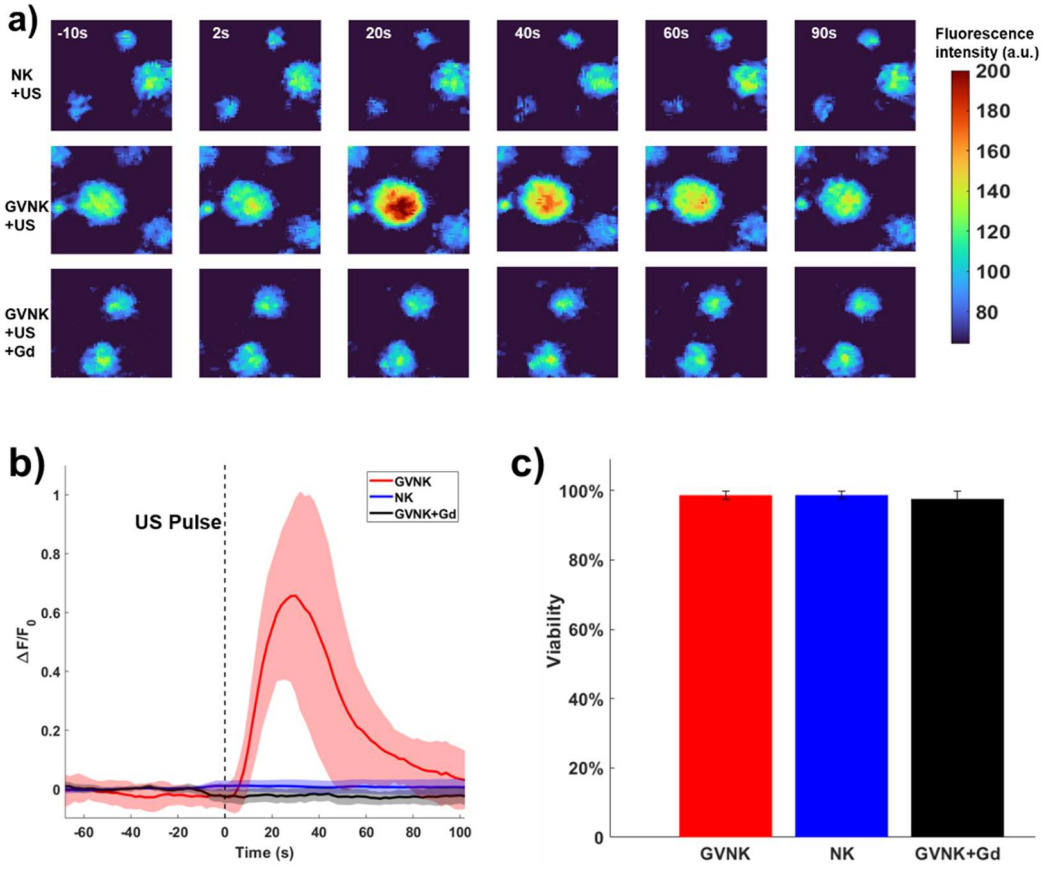

Figure 3.4. Calcium imaging of NK-92 cells stimulated with low-intensity ultrasound *in vitro*. **a)** Representative images calcium indicator fluorescence in NK-92 cells before and at several time points after the ultrasound stimulation, with (GVNK) or without (NK) GVs as actuators. An additional group with blocker (GVNK+Gd) was also included for verifying the mechanical signal transduction. **b)** Averaged changes in calcium indicator fluorescence, normalized to a baseline signal within 30~60s before the stimulation. Data was collected from 3 independent experiments, with solid curves indicating the average responses and shaded areas indicating the standard deviation. **c)** Viability of treated NK-92 cells in each group. Data presented in mean ± SD from 3 independent experiments.

3.3.3 Transduction of calcium influx into transcriptional activities

Downstream to calcium responses, we propose to utilize the nFAT responding components for the switching of GOI. A critical step in calcium-nFAT signaling is the dephosphorylation and translocation of the transcriptional factor into the nucleus, where they shall further regulate

gene expression. To evaluate this key step in the transduction of the ion homeostasis changes into transcriptional activities, we here conducted the immunofluorescence staining of nFAT in NK-92 cells after the mechanical ultrasound stimulation, with colocalization against nucleus and the morphology analyzed with confocal microcopy (**Figure 3.5a**). The level of nFAT translocation was further quantified (**Figure 3.5b**) according to a previously described image-processing algorithm [163], with the colocalization level calculated by the Fisher's z-transform of the Pearson's correlation between nFAT and DAPI staining. Indeed, clear boundaries between the nFAT fluorescence signal (red) and the nucleus (green) could be observed in GVNK, NK, NK+US groups, indicating a cytoplastic distribution of nFAT as expected. In GVNK+US group, a higher level of colocalization between red fluorescence could be seen with the green fluorescence, with the boundaries blurred between two channels. This indicates translocation of the nFAT into the nucleus by visual inspection. Furtherly, the quantification of the translocation profile (**Figure 3.5b**) also suggested a significant increase in nFAT translocation only in GVNK+US group. The attachment of GVs alone led to no noticeable background translocation, neither did the low-intensity ultrasound stimulation elicit any plausible nFAT translocation in NK+US group.

Indeed, the observations were consistent with our calcium imaging results, where the robust calcium influx was only elicited in those cells sensitized with GVs and treated with ultrasound. This suggests that the sensitization strategy itself shall be robust and non-stimulative to the NK-92 cells. This shall be a desirable property for switching system design, as background translocation might lead to certain level of undesired non-specific activation of the downstream genetic circuitry. The significant increase of nFAT translocation in GVNK+US group suggested a robust transduction of calcium influx into transcriptional activities, on the NK-92 cells with GVs as local actuators upon mechanical ultrasound stimulation. The results shall lay grounds for further initiation of nFAT-responding genetic circuitry in the proposed switching system.

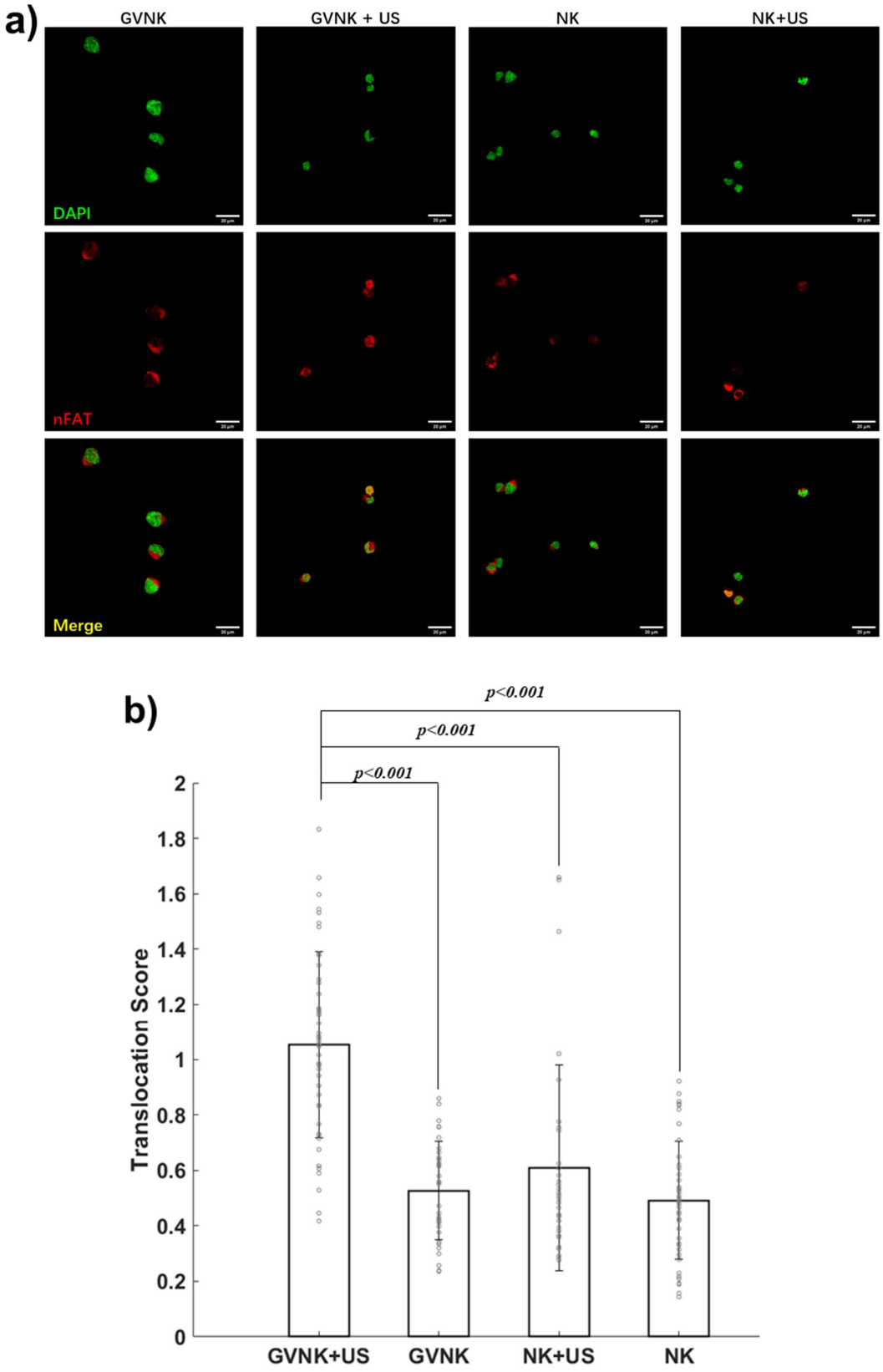

Figure 3.5. Immunofluorescence staining of nFAT translocation in NK-92 cells. **a)** Confocal microscopy images of NK-92 cells, with nFAT (red) and nucleus (green) stained for translocation analysis.

b) Quantification of nFAT translocation according to colocalization and morphology of nFAT staining. Data collected from 3 independent experiments, with statistical significance indicated with *p*-values.

3.3.4 Induction of reporter gene expression in engineered NK cells with GV-sensitized ultrasound switching

After confirming the nFAT translocation in GV-sensitized NK-92 cells upon mechanical ultrasound stimulation, we proceeded to evaluate the efficacy of the proposed switching system in initiating GOI expression *in vitro*. We transfected NK-92 cells with the calcium-responding transduction module, consisting of nFAT-responding element in a tandem design with serum responding element (SRE) and a cyclic adenosine monophosphate response element (CRE), with GOI in cis downstream to a minimal promoter [105]. To demonstrate the efficacy of the proposed mechanical switching system in terms of switching different GOIs in engineered immune cells, which might be of interest according to specific therapeutic designs, we chose two types of different reporter genes as example GOIs for the demonstration on genetic induction. We first used the luciferase as the example GOI to demonstrate the overall induction efficiency. GVs were attached on the transfected NK cells as actuators according to labeling protocols in Chapter 2.

Luciferase expression

The Gd blocker was also introduced in the experiment as negative control, further verifying the role of mechanical signal transduction in the GOI induction. The reporter gene expression was evaluated with the luciferase assay, where the bioluminescence signal was captured via the IVIS imaging system (**Figure 3.6**). As seen in the bioluminescence images (**Figure 3.6a**), minimal background expression was presented in groups without ultrasound treatment, neither in the ultrasound treated groups without GV sensitization. By contrast, clear rise of bioluminescence signal was seen in GV-sensitized NK-92-Luc cells treated with ultrasound, suggesting a successful induction of luciferase expression. Such signal was, however, abolished when mechanosensitive ion channel blocker was introduced in the system. By a further

quantification of signal rise upon ultrasound stimulation, the fold changes in the bioluminescence (**Figure 3.6b**), normalized to the non-stimulated condition, suggested a significant increase of reporter gene expression only in GV-tethered NK-92-Luc cells. By blocking the endogenous mechanosensitive ion channels, the reporter gene expression was abolished to a minimal level, with no significant difference from the non-sensitized control. This indicates that the GOI induction was indeed attributed to the transduction of mechanical stimulation exerted by the low-intensity ultrasound, consistent with what we observed in calcium signaling results. These results suggest that the proposed GV-actuated mechanical switching system is indeed effective in inducing reporter gene expression *in vitro*, with minimal background and high activtion potency.

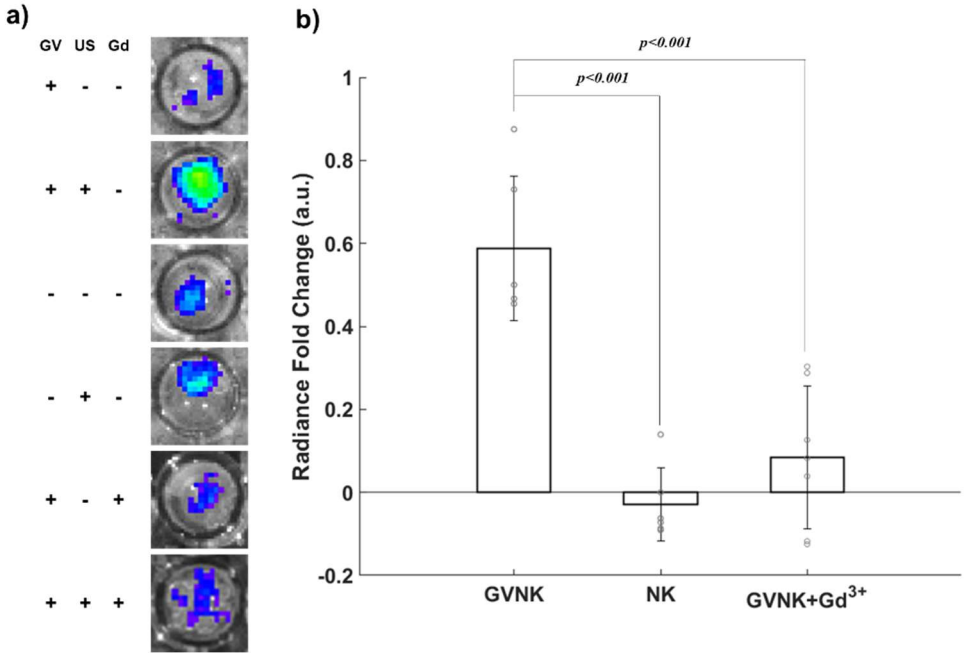

Figure 3.6. Induction of luciferase by the mechanical ultrasound switching system in vitro. **a)** Representative bioluminescence images of stimulated NK-92-Luc cells in 96-well plates. Gadolinium treatment was introduced to confirm the induction was indeed through mechanical signal transduction in the system. **b)** Quantifications of bioluminescence signal changes in ultrasound stimulated NK-92-Luc cells w.r.t. non-stimulated control. Data collected from 5 independent experiments, with statistical significance indicated with *p*-values.

Flow cytometry on tdTomato induction on engineered NK cells

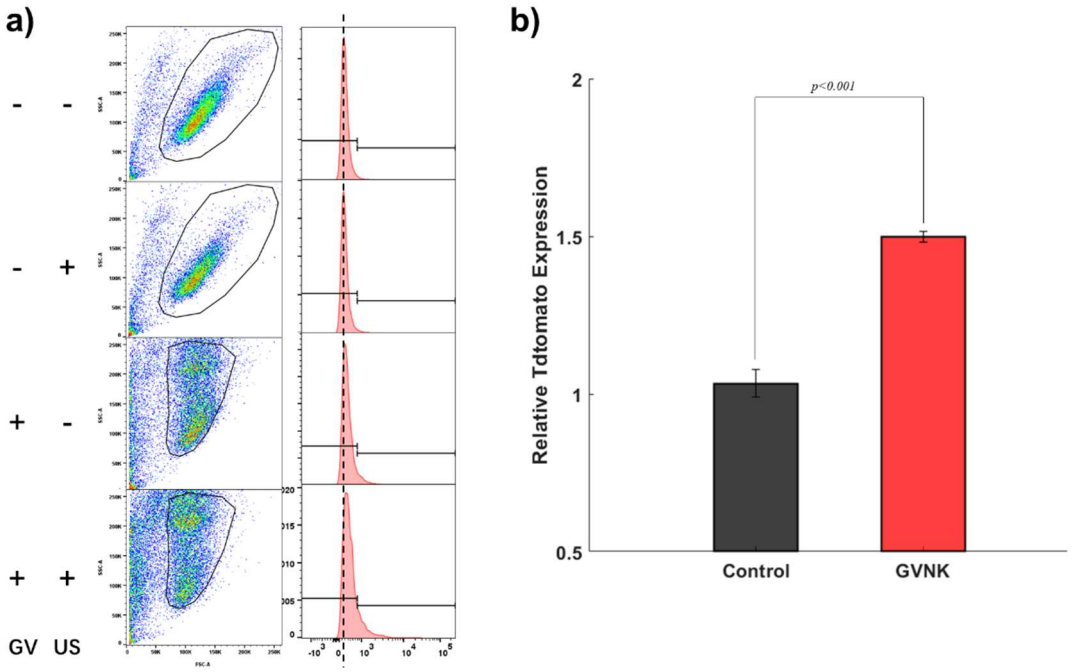

Figure 3.7. Flow cytometry of Tdtomato reporter gene expression *in vitro*. **a)** Representative flow cytometry diagram of NK-92 cells with/without GV attachment, subjected to ultrasound stimulation or sham treatment, with corresponding histograms of reporter gene expression to the right. **b)** Relative reporter gene expression upon ultrasound induction in NK-92-tdTomato cells with/without GV attachment. Data collected from 3 independent experiments, with statistical significance indicated with *p*-values.

We further verified the efficiency of the proposed switching system in population-wise induction of GOI. Similar treatment setup was used for the induction. Instead of reading bioluminescence directly in treated cells, we established the NK-92-tdTomato cell that has tdTomato reporter gene tethered downstream to the transduction module. The GOI induction efficiency in the cell population was then evaluated via flow cytometry (**Figure 3.7**). The results suggested that the stimulated cells in GV-actuated group showed positive expression of tdTomato, with shift of histogram peak towards higher fluorescence intensities (**Figure 3.7a**). While only a minimal number of NK-92-tdTomato cells were showing such expression, either solely upon binding with SA-GVs or receiving ultrasound stimulus without sensitizers. Note that the distribution of GV-bound NK cells was different from that in the control group, with a

shift upwards along SSC axis. This indicated attachment of intact GVs on the cell surface, both with and without ultrasound stimulation, since the opacity of these gas-filled nanostructures was expected to increase the light scattering of cells upon attachment. By quantifying the population with upregulated tdTomato expression, no observable change was seen in control group, while the GOI expression was increased by 1.5-fold in GV-actuated group upon ultrasound stimulation (**Figure 3.7a**). This suggested that the proposed actuation scheme by cell-attached nanobubbles indeed significantly transduced the ultrasound energy into genetic expression, enabling control of GOI expression by mechanical ultrasound stimulation in populations of target cells. These results indicated that the proposed strategy shall enable efficient induction of GOI in a population of stimulated cells, which shall be desirable for controllable initiation of effector genes on adoptive immune cells once they reach tumor sites. At the meantime, the low percentage of background expression further justified the manageability of the switching system, also as a desirable property in developing controlled cellular therapies.

3.4 Discussions

In this chapter, we demonstrated a mechanical switching system for controlling genetic expression in engineered NK cells, with low-intensity ultrasound as external stimulus. We have examined the presence of endogenous mechanosensitive ion channels in NK-92 cells, laying grounds for exploiting the mechanical signal transduction in these cells to implement mechanical switching. We employed GVs as actuators, attaching to surfaces of target cells, to locally amplify the mechanical perturbations from ultrasound, which enabled the calcium influx elicitation by ultrasound stimulation. With confounding membrane disruption effects excluded via channel blocking and PI staining, the transduction of mechanical stimulation into calcium influx was attributed to mechanosensitive ion channel opening. The calcium influx was further shown to elicit nFAT translocation, a critical process linking ion homeostasis changes and transcriptional activities. We then showed that the actuation by GVs enabled the

induction of GOI tethered downstream to nFAT-responding promoters in of NK-92-Luc cells, with the induction efficiency further demonstrated in NK-92-tdTomato cells. Furtherly, we showed that it was feasible to apply the switching system for inducing different types of GOIs in engineered NK-92 cells, using the two reporter genes as proof-of-concept examples. This further indicated the transferability of the mechanical switching system with GV-actuation for induction of other therapeutic genes in specific application designs. Taken together, we demonstrated a plausible mechanical switching strategy for controllable induction of various genes on engineered immune cells. The system exploits the calcium-nFAT signaling pathway for transducing mechanical stimuli into transcriptional behaviors. The surface-attached GVs serve as actuators that amplify the mechanical waves transmitted in forms of ultrasound, exerting cell-perturbating force that cause mechanosensitive ion channel opening and calcium influx. The elevated intracellular calcium level then leads to translocation of nFAT transcriptional factors, inducing expression of genes tethered downstream to nFAT-responding promoters.

We chose the calcium-centered mechanism for the design of switching system with ultrasound, as the ultrasound-inducible calcium activities have been recently demonstrated in various types of cells , with the mechanosensitive ion channels as the mediators [86-94]. This makes it a readily compatible mechanism for exerting ultrasound mechanical modulation on the immune cells, which have been widely shown with mechanosensitivity. Moreover, the calcium-based mechanism has also been widely employed for synthetic biological control on cellular gene expression, leading to plenty of robust transduction modules for the demonstration of ultrasound mechanical switching system [105]. Though the calcium signaling and intracellular calcium levels have been widely reported with significant impact on the activities, viability and fates of immune cells [60, 101], the expression or enhancement of designated genes according to the module design provide the opportunity to shape the phenotype towards desired directions in therapeutic applications. At the meantime, we do not exclude the possibility of employing other potential cellular mechanical sensing mechanisms for genetic manipulation purposes. In fact, we suggest in-depth screening and investigations

for incorporating those pathways with ultrasound-dependent activities, by which a parallel or alternative switching module shall be made available for improving the induction efficiency and/or specificity according to application scenarios.

To achieve manipulation of cellular behaviors by external stimulation, the key is to bring specificity in target cells of interest, either by allowing only these cells to sense the stimuli, or by bringing sensitization specifically to them. For mechanical ultrasound switching system, a localized sensitization specific to target immune cells is desired. On one hand, there is a broad existence of mechanical cues and sensing mechanisms in the biological system, a simple application of high-intensity mechanical agitation might bring up undesired responses non-specifically in surrounding tissues. On the other hand, the immune cells, especially those effectors employed in cellular immunotherapies, are naturally subject to a variety of mechanical cues during their migration and trafficking throughout the system, including shear stress in circulation, stiffness, dynamic contact with antigen-presenting cells or pathogens, etc. A simple application of mechanical agitation through ultrasound waves might not easily surpass thresholds in these cells, built up according to their endogenous mechanical microenvironment. At the meantime, overexpressing mechanosensitive ion channels might also impose complications of background activation by endogenous mechanical cues in the engineered effectors. This naturally suggests a need to introduce localized actuators on the target immune cells, by which the mechanical ultrasound stimuli could be locally amplified for cell-specific agitation.

Indeed, the MB-based sensitization system has been demonstrated in previous study [105]. The mechanical ultrasound stimulus, delivered in low frequency, has been shown insufficient for inducing the signal transduction by its own, even with the presence of mechanosensitive ion channels in the immune cells experimented. By introducing the sensitizers, MBs, the calcium influx was elicited upon ultrasound stimulation, and robust genetic expression was induced. However, the size and stability of MB have been limiting its application for implementing mechanical ultrasound switching *in vivo*.

GVs, with their nanoscale sizes and superior thermodynamical stability, naturally stand out

as an alternative to MBs with prospective applicability to *in vivo* implementations. Essentially, as nanosized bubbles, GVs have been shown to respond to ultrasound agitation, serving similar functions to MBs both in nonlinear ultrasound imaging, as well as membrane perturbation and cellular manipulations [108, 112, 113, 119, 122, 123, 140, 164]. It is thus natural to expect similar amplification of the mechanical effects from ultrasound wave by GVs, which was indeed demonstrated in current chapter. By such, the mechanical signal transduction in the immune cells can then be rewired for desirable genetic expression, with mechanical ultrasound as the external switching mechanism. For the compatibility of GVs for *in vivo* applications, the tracking of GV-tethered NK-92 cells in Chapter 2 has suggested a functional integrity of GVs, in the context of carrier immune cell infiltration in the tumor. The structural integrity, and hence the functional integrity of these gas-filled structures is critical to their capabilities of responding to ultrasound, in terms of scattering and oscillating. The observation of nonlinear ultrasound signal in tumor infiltrating NK-92 cells, labeled by GVs, suggests that these cell-bound GVs remained intact during the infiltration of NK-92 cells to the tumor, which further generated nonlinear ultrasound contrast with their flexible gas-filled structures. Moreover, as strong contrast signal was observed at 24h post-infusion, indicating a superior stability of GVs compared to MBs that have a documented *in vivo* lifespan of minutes. This means that the other factor that hinders the application of MBs as *in vivo* actuators for mechanical switching, i.e., the short lifespan, could be overcome by the use of GVs. Therefore, we believe that the GV shall serve functionally as actuators in the context of cellular immunotherapy for cancers, enabling the remote control of engineered immune cells by the mechanical ultrasound switching system *in vivo*. The combination of the tracking strategy and the switching system further allows image-guided manipulations, where switching stimuli could be delivered with information upon the cell trafficking and accumulation at the tumor site. Moreover, it has been demonstrated that the displacement of GV-bearing bacteria could be manipulated by the acoustic field [122, 123]. This further suggested a potential mechanism for local attraction and infiltration enhancement on adoptive immune cells using the ultrasound, considering the versatility of these nanosized mechanical actuators.

The mechanical effect from ultrasound wave has been shown with superior spatiotemporal precision, standing out as an attractive candidate for the implementation of switching system *in vivo*. It enjoys deep penetration in biological tissues that optical approaches crave for, while it is also free of concerns like heat dissipation and heat sink effects related to hyperthermia-based switching. The GV-actuated mechanical ultrasound switching strategy, demonstrated in this chapter, offers opportunities for designs of remote-controlled cellular immunotherapies with *in vivo* compatibility, exploiting the fine precision of ultrasound modality. Moreover, the proposed mechanical switching system provides an alternative signaling mechanism, different from the heat-responsive elements, for manipulating biological processes in deep tissues. On one hand, it offers a potential way of multiplexing switching input of ultrasound. The mechanical ultrasound stimulation, being the ultrasound wave in nature, should also be compatibly deliverable by operating systems built for hyperthermia ultrasound. By applying different driving parameters, the ultrasound stimulation could be generated in a thermal or non-thermal oriented manner. The initiation of different circuitries, tethered to different responding elements, could then be controlled according to demands by the mechanical or heat signaling transduction. On the other hand, the possibility of controlling multiple genetic circuitries in living cells offers broad prospectives for more sophisticated designs. In a simplest example, the AND logic design could be achieved by conditioning the expressions of components in hyperthermia switching system to mechanical switching, by which a more stringent control of CAR expression could be implemented, further reducing concerns of background expression at undesired sites. Logical control designs shall allow sophisticated programing and directing of cellular behaviors according to our demands, with potentials of attaining droid-mimicking capabilities in engineered cells.

In this chapter, the surface attachment of GVs has been shown to enable ultrasound-controlled induction of genes in engineered NK cells, supporting the rationale of designs with localized actuators. However, considering the contrast signal decay in last chapter, the results suggest the actuator capability could only last for a few days *in vivo* for current stage. In certain scenarios, sensitizers with longer persistence might be desired, with which switching stimuli

could be exerted at later time points according to the needs. Though extra concerns might be raised upon the expression burden, the acoustic reporter gene technology [120, 121] might be a potential solution to bear long-term actuators on the target cells.

3.5 Conclusions

In this chapter, a mechanical switching system for controlling genetic expression in engineered NK cells with low-intensity ultrasound was demonstrated. The surface-attached GVs were shown to enable calcium influx initiation by ultrasound stimulation on NK-92 cells. The calcium events were further shown to induced nuclear translocation of nFAT, establishing grounds for inducing transcriptional activities by mechanical ultrasound stimulation. The nFAT signaling was then exploited for target gene expression, demonstrated on engineered NK-92 cells with reporter gene expression induced by low-intensity ultrasound with the assistance of cell-attached GVs.

The proposed system showed capabilities of controlling genetic expression in engineered immune cells by ultrasound, where GVs were incorporated as cell-specific actuators that amplified the mechanical stimuli with compatibility to *in vivo* applications. The proposed strategy provides solutions to *in vivo* mechanical switching of genetic expression by ultrasound, exploiting fine spatiotemporal precision of the modality in cellular therapies. Furtherly, with the cellular engineering of genetically programed anti-tumor potencies, the proposed system shows substantial potentials in implementing remote control on engineered effectors for both enhanced potencies and safety management. With the versatile ultrasound modality, the proposed strategy shall also provide tremendous opportunities for image-guided manipulation on the engineered living therapeutics.

Chapter 4 Conclusions and future work

In summary, the ultrasound modality has been exploited for applications in cellular immunotherapies. The GVs, protein-shelled nanostructures with gas cores, have been employed as ultrasound-responsive nanobubbles. Exploiting their nonlinear echogenicity, these nanobubbles have been introduced as cell-tethered ultrasound contrast agents, enabling the tracking of adoptive immune cells in cellular immunotherapy with ultrasound imaging. At the meantime, the cavitating effects of these nanobubbles under acoustic field have been utilized as the actuating mechanisms, achieving mechanical switching of genetic circuitry in engineered immune cells by ultrasound stimulation, with prospective compatibility for *in vivo* implementations.

We first established that the ultrasound imaging modality is compatible with the tracking of adoptive immune cells, where cellular viability and functionalities are preserved for their anti-tumor cytotoxicity. We employed nanobubbles for the labeling of NK-92 cells, and we showed that the labeling by nanosized contrast agents impose negligible burden on cellular migration and infiltration, addressing one major issue hindering the application of MBs in cell tracking design. With no observable impact on cell viability or functionalities, we further demonstrated the detectability of GV-labeled NK-92 cells by nonlinear ultrasound imaging *in vitro*. The detection threshold and signal persistence were determined in vitro, with significant contrast arising from labeled NK cells at density of 1×10^6, persisted up to 48h after the labeling procedures. The *in vivo* detection of GV-labeled NK cells by ultrasound imaging was further established in liver imaging, where the presence of systematically infused NK-92 cells was cross-validated with *ex vivo* optical imaging. In tumor-bearing mice, the feasibility of applying ultrasound imaging for immune cell tracking in cellular immunotherapies was further established, with the ultrasound contrast demonstrated to reflect dynamical changes in NK trafficking to tumors. The early-phase trafficking was observed as early as 3h post-transfer, with contrast signal persisted up to 48h after the systematic infusion of NK cells. Altogether, these results suggested the compatibility of ultrasound imaging modality to immune cell

tracking purposes, upon the utilization of contrast agents with desired dimensions and thermodynamical properties. Previous attempts have been made to detect cellular targets *in vivo* by ultrasound imaging [120, 145-147], while the fundamental incompatibility between MBs and immune cell infiltration in tumors was not addressed, or destructive pulses were applied for the one-time detection purposes. In this thesis, we provided a non-destructive ultrasound tracking scheme, with nanosized contrast agents compatible for tumor-infiltrating immune cells. The proposed tracking scheme has been demonstrated suitable for detecting and monitoring the functional effector cells, in the context of systematic infusion for cancer immunotherapy.

The detection of ultrasound contrast signal in the tumor, hours following transferred of GV-tethered NK cells, further suggested the structural integrity of these nanobubbles during the process of immune cell infiltration in tumors. This indicated the compatibility of exploiting these nanobubbles as *in situ* actuators for sensitization of immune cells to ultrasound stimulation. Hence, in this thesis, we further verify the feasibility of inducing gene expression by mechanical ultrasound stimulation in NK cells, with GVs as localized nanosized sensitizers. With the functional mechanosensitive components checked in NK-92 cells, we first showed that the mechanical effect from ultrasound wave could elicit robust calcium influx in nanobubble-sensitized NK-92 cells. We then showed the nFAT nucleus translocation triggered by ultrasound in GV-tethered NK cells, verifying the transduction of calcium influx into transcriptional activities. The GOI induction was then demonstrated in NK-92 cells transfected with luciferase reporter gene, designed downstream to nFAT-responsive promoters. In a model system of NK-92 cells with IFN-γ secretion bypassed to the ultrasound-controlled circuitry, we showed that the proposed sensitization and switching system allowed controlled activation of anti-tumor potencies in engineered immune cells. In this thesis, we verified that by utilizing nanobubbles as sensitizers, the mechanical ultrasound switching is feasible. Comparing to traditional MBs, the nanobubbles features compatibility with implementations in cell immunotherapies. As clear ultrasound contrast was observed from nanobubbles attached to tumor-infiltrating NK-92 cells, nanobubbles are expected to enter tumor tissues with negligible

impact on the target cell functionalities. With stable nanobubbles like GVs employed in this thesis, or with other possible formulations of high thermodynamical stability, the insufficient lifespan of MB actuators could also be overcome. These suggest nanobubbles as plausible *in situ* actuators to sensitize target immune cells for mechanical ultrasound stimuli, while the current thesis has established the basis of inducing gene expression in GV-sensitized immune cells upon mechanical ultrasound stimulation.

By introducing the ultrasound modality into the field of cellular immunotherapies, several benefits shall be provided. By the introduction of nanobubbles, of any possible formulation with desirable physical properties like sizes, flexibility and stability, the clinical application of cellular immunotherapies would enjoy the already-on-board ultrasound systems for both tracking and remote-control purposes. The easy-to-access and cost-effective monitoring and evaluation method could be implemented with the ultrasound imaging modality, with nanobubbles as cell-tethered contrast agents, taking advantage of the ultrasound imaging systems ubiquitous in most clinical settings. At the meantime, informed with the accumulation status of adoptive immune cells in the tumor, decisions could be made on whether employing interventions or in-depth examination by e.g., biopsies, with the opportunities of implementing such procedures under real-time ultrasound imaging guidance. With cell-tethered nanobubbles as sensitizers, we expect potentials in the on-site activation of highly potent engineered cells by mechanical stimulation, enjoying the fine precision in spatial and temporal domains. As ultrasonic waves in essence, the mechanical ultrasound switching shall be readily compatible with the focused ultrasound apparatus, with amplitude and pulsing parameters controlled for delivering agitations in mechanical-only manners. With nanobubbles, the proposed mechanical switching strategy features prospective compatibility with applications in living organisms, providing an alternative deep-tissue switching mechanism apart from hyperthermia. This further paves the avenue for implementing sophisticated switching designs, and hence stringent management strategies on engineered cells, with opportunities to independently control different genetic circuitries with different mechanisms, at depth in biological tissues.

In this thesis, the functional induction of genes in engineered immune cells by ultrasound

was demonstrated *in vitro*, serving as the basis for implementing mechanical remote control in cellular immunotherapy using ultrasound modality. The nanobubbles were used as the cell-attached actuators that exert the modulating mechanical force with specificity on carrier cells, enabling manipulation of transcriptional behaviors in engineered immune cells on demands. With the *in vivo* compatibility of nanobubbles, the implementations of the proposed mechanical switching scheme in animal models shall be first pursuit. Indeed, with the complication in the TME, the switching efficiency shall be determined with more stringent *ex vivo* or *in vivo* scenarios, with genes of therapeutic interests employed over the reporter gene examples. Engineered immune cells, with activatable CAR expression and/or cytokine release shall be incorporated for solid tumor models. The GVs shall be attached on the surface of these activatable effectors, serving both roles of markers for ultrasound-based tracking as well as actuators for mechanical switching of the effector genes. The ultrasound imaging will be applied for the tracking of these cells after adoptive transfer, monitoring the dynamical accumulation of the engineered immune cells in the tumor. The gene-activating ultrasound stimulation shall be applied on the tumor site, within windows with high immune cell recruitment profiles determined by the ultrasound imaging, ensuring effective exertion of triggering stimuli on the engineered immune cells. By such, the on-site remote control of the engineered immune cells shall be achieved, with image guidance for improved spatiotemporal precision. Moreover, the compatibility of the proposed mechanical switching system with the heat-shock responsive systems shall be explored. In a simplest *in vitro* setting, model cell shall be simultaneously transfected with spectrally multiplexed reporter genes, tethered downstream to HSF and nFAT respectively. The switching of either or both reporter genes could be examined, with the mechanical and hyperthermia ultrasound applied in designated orders. By establishing such a multiplexed switching system, more sophisticated control on the cellular genetics shall be made possible, with the opportunity to apply logical control on the cellular behavior.

The surface attachment scheme was employed in this thesis for the tethering of nanobubbles with the target cells, by which the functional roles of nanobubbles as contrast

agents and sensitizers were demonstrated. Limitations, however, exist for such surface-attaching scheme. On one hand, as determined in the previous chapters, the ultrasound contrast signal decayed in GV-tethered cells within 48h after the binding, becoming indistinguishable from non-labeled counterparts at 72h. The signal persistence observed both *in vitro* and *in vivo* was indeed shorter than previously reported GV lifespans [109, 113]. The limited lifespan observed on cell-bound GVs might be attributed to certain cell-cell and/or GV-cell interactions, presented among immune cells that GVs attached to or from resident cells in the TME. On the other hand, presence of these gas-filled entities on cellular surfaces might impose certain level of steric hindrance, introducing potential barriers, if any, between effector cells and their designated targets. Therefore, the introduction of intracellular labeling mechanisms would provide a potential way of reducing the cell-GV interactions in the TME to prolong GV persistence, as well as avoiding potential steric hindrance that might impact execution of effector functions. The GV, as biogenic protein structures, has been demonstrated in recent years as genetically encodable acoustic reporters, serving versatile roles in ultrasound imaging and manipulations of GV-expressing cells [120-123]. With such potentials, future studies shall also pursue the expression of GVs as reporter genes in adoptive immune cells. On one hand, the intracellularly expressed GVs shall be minimally impactful on the cell-cell contact between immune cells and their targets. On the other hand, the stably expressed GVs in the adoptive cells would also allow longer-term tracking by ultrasound imaging, as well as exploiting the acoustic reporter gene for imaging their viability and functionalities.

Apart from GVs, nanobubbles of other possible formulations that exhibit similar echogenicity and stability shall also be explored, with certain properties optimized for either tracking or switching purposes. Specifically, the lipid formulations similar to FDA approved MBs have been exploited for the synthesis of nanobubbles [165], with several demonstrated applications in ultrasound imaging [166-168]. Interestingly, the intracellular trapping of such synthetic nanobubbles has prolonged the contrast enhancement up to 24h [168], a lifespan beyond the known circulation time of traditional MBs. By reducing the sizes, the nanobubble, with similar formulations to MBs, exhibits signal persistence that shall also suffice the need of

early-phase tracking of adoptive immune cells, as well as sensitizing tethered cells for ultrasound stimulation within this time window. Such synthetic formulations shall also be investigated and pursued for the labeling, tracking and stimulation of immune cells, such that an implementation closer to clinical translation might be obtained, also with opportunities for bulk production. At the meantime, with either source or formulation of nanobubbles, the in-depth investigations on the imaging sensitivity and quantification values shall be pursued. With standardized labeling protocols and well-characterized nanobubble-cell binding efficiency, a stringent relation between ultrasound contrast and the number of cells in a voxel shall be established. This shall contribute to the quantitative tracking of adoptive immune cells by ultrasound imaging, featuring greater values in post-treatment evaluations of cellular immunotherapies.

The compatibility of the proposed tracking and switching strategies with other immune cell types shall also be investigated. Although all being immune cells, different cell types would exhibit their unique physiologies, which might impose potential influences on the GVs. For example, the macrophages have been known to internalize and degrade GVs through lysosomal proteolysis [111]. Therefore, a simple surface attachment scheme might not allow labeling macrophages with GVs, which might be easily internalized and degraded by upon contact with the cells. Alternatively, an extended space arm between GVs and cell surfaces might be introduced, by incorporation of polyethylene glycol (PEG) for example, or an employment of silica-based contrast agents, might provide possible solutions to macrophage labeling. Similar attachment protocol shall be applicable for lymphocytes like cytotoxic T lymphocytes, on which the biotin-streptavidin conjugation has been shown valid for labeling with various types of probes for tracking purposes [148]. At the meantime, the optimal ultrasound parameters might also be investigated for effective stimulation on different immune cell types, considering the diversity in their mechanical properties such as compliance.

In all, this thesis lays grounds for the application of ultrasound modality for tracking and switching purposes in cell immunotherapies, with the assistance of nanobubbles. A more wholistic and in-depth investigation on nanobubble-assisted ultrasound modality is worth

pursuing, in terms of nanobubble formulations, alternative labeling mechanisms, quantitative tracking, compatibility with diverse cell types, as well as *in vivo* implementations of mechanical switching, multiplexed switching designs. By a deeper understanding of the mechanisms and the optimized strategy design, it paves way for the systematic post-treatment monitoring and interventions paradigm in the application of cellular therapeutics, taking advantages of the already-on-board ultrasound systems.

References

[1] H. Sung *et al.*, "Global cancer statistics 2020: GLOBOCAN estimates of incidence and mortality worldwide for 36 cancers in 185 countries," *CA: a cancer journal for clinicians,* vol. 71, no. 3, pp. 209-249, 2021.

[2] H. Yildizhan *et al.*, "Treatment strategies in cancer from past to present," in *Drug targeting and stimuli sensitive drug delivery systems*: Elsevier, 2018, pp. 1-37.

[3] D. Hanahan and R. A. Weinberg, "Hallmarks of cancer: the next generation," *cell,* vol. 144, no. 5, pp. 646-674, 2011.

[4] S. C. Kamran, A. Berrington de Gonzalez, A. Ng, D. Haas-Kogan, and A. N. Viswanathan, "Therapeutic radiation and the potential risk of second malignancies," *Cancer,* vol. 122, no. 12, pp. 1809-1821, 2016.

[5] M. Lind, "Principles of systemic anticancer therapy," *Medicine,* vol. 48, no. 2, pp. 90-96, 2020.

[6] H. Gonzalez, C. Hagerling, and Z. Werb, "Roles of the immune system in cancer: from tumor initiation to metastatic progression," *Genes & development,* vol. 32, no. 19-20, pp. 1267-1284, 2018.

[7] M. Binnewies *et al.*, "Understanding the tumor immune microenvironment (TIME) for effective therapy," *Nature medicine,* vol. 24, no. 5, pp. 541-550, 2018.

[8] M. Krekorian *et al.*, "Imaging of T-cells and their responses during anti-cancer immunotherapy," *Theranostics,* vol. 9, no. 25, p. 7924, 2019.

[9] J. Galon and D. Bruni, "Approaches to treat immune hot, altered and cold tumours with combination immunotherapies," *Nature Reviews Drug Discovery,* vol. 18, no. 3, pp. 197-218, 2019.

[10] W. K. Decker and A. Safdar, "Bioimmunoadjuvants for the treatment of neoplastic and infectious disease: Coley's legacy revisited," *Cytokine & growth factor reviews,* vol. 20, no. 4, pp. 271-281, 2009.

[11] K. Kakimi, T. Karasaki, H. Matsushita, and T. Sugie, "Advances in personalized cancer immunotherapy," *Breast Cancer,* vol. 24, pp. 16-24, 2017.

[12] A. D. Waldman, J. M. Fritz, and M. J. Lenardo, "A guide to cancer immunotherapy: from T cell basic science to clinical practice," *Nature Reviews Immunology,* vol. 20, no. 11, pp. 651-668, 2020.

[13] J. N. Brudno and J. N. Kochenderfer, "Chimeric antigen receptor T-cell therapies for lymphoma," *Nature reviews Clinical oncology,* vol. 15, no. 1, pp. 31-46, 2018.

[14] B. T. Fife and J. A. Bluestone, "Control of peripheral T-cell tolerance and autoimmunity via the CTLA-4 and PD-1 pathways," *Immunological reviews,* vol. 224, no. 1, pp. 166-182, 2008.

[15] E. Tran *et al.*, "Immunogenicity of somatic mutations in human gastrointestinal cancers," *Science,* vol. 350, no. 6266, pp. 1387-1390, 2015.

[16] C. M. Southam, A. Brunschwig, A. G. Levin, and Q. S. Dizon, "Effect of leukocytes on

transplantability of human cancer," *Cancer,* vol. 19, no. 11, pp. 1743-1753, 1966.
[17] P. L. Weiden *et al.*, "Antileukemic effect of graft-versus-host disease in human recipients of allogeneic-marrow grafts," *New England Journal of Medicine,* vol. 300, no. 19, pp. 1068-1073, 1979.
[18] S. A. Rosenberg *et al.*, "Durable complete responses in heavily pretreated patients with metastatic melanoma using T-cell transfer immunotherapy," *Clinical cancer research,* vol. 17, no. 13, pp. 4550-4557, 2011.
[19] S. S. Neelapu *et al.*, "Axicabtagene ciloleucel CAR T-cell therapy in refractory large B-cell lymphoma," *New England Journal of Medicine,* vol. 377, no. 26, pp. 2531-2544, 2017.
[20] S. L. Maude *et al.*, "Chimeric antigen receptor T cells for sustained remissions in leukemia," *New England Journal of Medicine,* vol. 371, no. 16, pp. 1507-1517, 2014.
[21] S. A. Grupp *et al.*, "Chimeric antigen receptor–modified T cells for acute lymphoid leukemia," *New England Journal of Medicine,* vol. 368, no. 16, pp. 1509-1518, 2013.
[22] A. Mullard, "FDA approves first CAR T therapy," *Nature reviews Drug discovery,* vol. 16, no. 10, pp. 669-670, 2017.
[23] A. Mullard, "FDA approves first BCMA-targeted CAR-T cell therapy," *Nature reviews. Drug Discovery,* vol. 20, no. 5, pp. 332-332, 2021.
[24] A. Mullard, "FDA approves second BCMA-targeted CAR-T cell therapy," *Nature reviews. Drug Discovery,* 2022.
[25] V. Wang, M. Gauthier, V. Decot, L. Reppel, and D. Bensoussan, "Systematic Review on CAR-T Cell Clinical Trials Up to 2022: Academic Center Input," *Cancers,* vol. 15, no. 4, p. 1003, 2023.
[26] A. Shimabukuro-Vornhagen *et al.*, "Cytokine release syndrome," *Journal for immunotherapy of cancer,* vol. 6, no. 1, pp. 1-14, 2018.
[27] S. S. Neelapu *et al.*, "Chimeric antigen receptor T-cell therapy—assessment and management of toxicities," *Nature reviews Clinical oncology,* vol. 15, no. 1, pp. 47-62, 2018.
[28] C. L. Bonifant, H. J. Jackson, R. J. Brentjens, and K. J. Curran, "Toxicity and management in CAR T-cell therapy," *Molecular Therapy-Oncolytics,* vol. 3, p. 16011, 2016.
[29] A. Volpe, P. S. Adusumilli, H. Schöder, and V. Ponomarev, "Imaging cellular immunotherapies and immune cell biomarkers: from preclinical studies to patients," *Journal for ImmunoTherapy of Cancer,* vol. 10, no. 9, p. e004902, 2022.
[30] B. Breart, F. Lemaître, S. Celli, and P. Bousso, "Two-photon imaging of intratumoral CD8+ T cell cytotoxic activity during adoptive T cell therapy in mice," *The Journal of clinical investigation,* vol. 118, no. 4, pp. 1390-1397, 2008.
[31] T. R. Mempel *et al.*, "Regulatory T cells reversibly suppress cytotoxic T cell function independent of effector differentiation," *Immunity,* vol. 25, no. 1, pp. 129-141, 2006.
[32] S. Tavri *et al.*, "Optical imaging of cellular immunotherapy against prostate cancer," *Molecular Imaging,* vol. 8, no. 1, p. 7290.2009. 00002, 2009.
[33] F. M. Youniss *et al.*, "Near-infrared imaging of adoptive immune cell therapy in breast

cancer model using cell membrane labeling," *PLoS One,* vol. 9, no. 10, p. e109162, 2014.

[34] J. Charo, C. Perez, C. Buschow, A. Jukica, M. Czeh, and T. Blankenstein, "Visualizing the dynamic of adoptively transferred T cells during the rejection of large established tumors," *European journal of immunology,* vol. 41, no. 11, pp. 3187-3197, 2011.

[35] L. Zhu *et al.*, "Natural killer cell (NK-92MI)-based therapy for pulmonary metastasis of anaplastic thyroid cancer in a nude mouse model," *Frontiers in immunology,* vol. 8, p. 816, 2017.

[36] B. Meller *et al.*, "Monitoring of a new approach of immunotherapy with allogenic 111 In-labelled NK cells in patients with renal cell carcinoma," *European journal of nuclear medicine and molecular imaging,* vol. 31, pp. 403-407, 2004.

[37] M. J. Pittet *et al.*, "In vivo imaging of T cell delivery to tumors after adoptive transfer therapy," *Proceedings of the National Academy of Sciences,* vol. 104, no. 30, pp. 12457-12461, 2007.

[38] L. M. Lechermann *et al.*, "Detection limit of 89 Zr-labeled T cells for cellular tracking: an in vitro imaging approach using clinical PET/CT and PET/MRI," *EJNMMI research,* vol. 10, no. 1, pp. 1-12, 2020.

[39] M. R. Weist *et al.*, "PET of adoptively transferred chimeric antigen receptor T cells with 89Zr-oxine," *Journal of Nuclear Medicine,* vol. 59, no. 10, pp. 1531-1537, 2018.

[40] N. Sato, H. Wu, K. O. Asiedu, L. P. Szajek, G. L. Griffiths, and P. L. Choyke, "89Zr-oxine complex PET cell imaging in monitoring cell-based therapies," *Radiology,* vol. 275, no. 2, pp. 490-500, 2015.

[41] P. Dubey *et al.*, "Quantitative imaging of the T cell antitumor response by positron-emission tomography," *Proceedings of the National Academy of Sciences,* vol. 100, no. 3, pp. 1232-1237, 2003.

[42] K. V. Keu *et al.*, "Reporter gene imaging of targeted T cell immunotherapy in recurrent glioma," *Science translational medicine,* vol. 9, no. 373, p. eaag2196, 2017.

[43] S. S. Yaghoubi *et al.*, "Noninvasive detection of therapeutic cytolytic T cells with 18F–FHBG PET in a patient with glioma," *Nature clinical practice Oncology,* vol. 6, no. 1, pp. 53-58, 2009.

[44] P. Walczak *et al.*, "Real-time MRI for precise and predictable intra-arterial stem cell delivery to the central nervous system," *Journal of Cerebral Blood Flow,* vol. 37, no. 7, pp. 2346-2358, 2017.

[45] B. P. Barnett *et al.*, "Magnetic resonance–guided, real-time targeted delivery and imaging of magnetocapsules immunoprotecting pancreatic islet cells," *Nature medicine,* vol. 13, no. 8, pp. 986-991, 2007.

[46] M. F. Kircher *et al.*, "In vivo high resolution three-dimensional imaging of antigen-specific cytotoxic T-lymphocyte trafficking to tumors," *Cancer research,* vol. 63, no. 20, pp. 6838-6846, 2003.

[47] K. Li *et al.*, "Clinically applicable magnetic-labeling of natural killer cells for MRI of transcatheter delivery to liver tumors: preclinical validation for clinical translation," *Nanomedicine,* vol. 10, no. 11, pp. 1761-1774, 2015.

[48] T. Kim *et al.*, "Mesoporous silica-coated hollow manganese oxide nanoparticles as positive T 1 contrast agents for labeling and MRI tracking of adipose-derived mesenchymal stem cells," *Journal of the American Chemical Society,* vol. 133, no. 9, pp. 2955-2961, 2011.

[49] J. W. Bulte and H. E. Daldrup-Link, "Clinical tracking of cell transfer and cell transplantation: trials and tribulations," *Radiology,* vol. 289, no. 3, pp. 604-615, 2018.

[50] G. Dranoff, "Cytokines in cancer pathogenesis and cancer therapy," *Nature Reviews Cancer,* vol. 4, no. 1, pp. 11-22, 2004.

[51] R. W. Childs and M. Carlsten, "Therapeutic approaches to enhance natural killer cell cytotoxicity against cancer: the force awakens," *Nature reviews Drug discovery,* vol. 14, no. 7, pp. 487-498, 2015.

[52] G. Parisi *et al.*, "Persistence of adoptively transferred T cells with a kinetically engineered IL-2 receptor agonist," *Nature communications,* vol. 11, no. 1, p. 660, 2020.

[53] B. Kwong, S. A. Gai, J. Elkhader, K. D. Wittrup, and D. J. Irvine, "Localized immunotherapy via liposome-anchored Anti-CD137+ IL-2 prevents lethal toxicity and elicits local and systemic antitumor immunity," *Cancer research,* vol. 73, no. 5, pp. 1547-1558, 2013.

[54] C. M. van Herpen *et al.*, "Intratumoral rhIL-12 administration in head and neck squamous cell carcinoma patients induces B cell activation," *International journal of cancer,* vol. 123, no. 10, pp. 2354-2361, 2008.

[55] L. Klewer and Y. W. Wu, "Light-induced dimerization approaches to control cellular processes," *Chemistry–A European Journal,* vol. 25, no. 54, pp. 12452-12463, 2019.

[56] T.-H. Lan, L. He, Y. Huang, and Y. Zhou, "Optogenetics for transcriptional programming and genetic engineering," *Trends in Genetics,* 2022.

[57] D. Niopek *et al.*, "Engineering light-inducible nuclear localization signals for precise spatiotemporal control of protein dynamics in living cells," *Nature communications,* vol. 5, no. 1, p. 4404, 2014.

[58] Y. Wu *et al.*, "Engineering CAR T cells for enhanced efficacy and safety," *APL bioengineering,* vol. 6, no. 1, 2022.

[59] Z. Huang *et al.*, "Engineering light-controllable CAR T cells for cancer immunotherapy," *Science advances,* vol. 6, no. 8, p. eaay9209, 2020.

[60] G. P. O'Donoghue, L. J. Bugaj, W. Anderson, K. G. Daniels, D. J. Rawlings, and W. A. Lim, "T cells selectively filter oscillatory signals on the minutes timescale," *Proceedings of the National Academy of Sciences,* vol. 118, no. 9, p. e2019285118, 2021.

[61] L. He *et al.*, "Circularly permuted LOV2 as a modular photoswitch for optogenetic engineering," *Nature Chemical Biology,* vol. 17, no. 8, pp. 915-923, 2021.

[62] A. A. Kaberniuk, A. A. Shemetov, and V. V. Verkhusha, "A bacterial phytochrome-based optogenetic system controllable with near-infrared light," *Nature methods,* vol. 13, no. 7, pp. 591-597, 2016.

[63] K. Müller *et al.*, "A red/far-red light-responsive bi-stable toggle switch to control gene expression in mammalian cells," *Nucleic acids research,* vol. 41, no. 7, pp. e77-e77,

2013.

[64] M. Åkerfelt, R. I. Morimoto, and L. Sistonen, "Heat shock factors: integrators of cell stress, development and lifespan," *Nature reviews Molecular cell biology,* vol. 11, no. 8, pp. 545-555, 2010.

[65] Y. Wang *et al.*, "Photothermal-responsive conjugated polymer nanoparticles for remote control of gene expression in living cells," *Advanced Materials,* vol. 30, no. 8, p. 1705418, 2018.

[66] I. C. Miller, M. Gamboa Castro, J. Maenza, J. P. Weis, and G. A. Kwong, "Remote control of mammalian cells with heat-triggered gene switches and photothermal pulse trains," *ACS synthetic biology,* vol. 7, no. 4, pp. 1167-1173, 2018.

[67] Y. Lyu, D. Cui, H. Sun, Y. Miao, H. Duan, and K. Pu, "Dendronized semiconducting polymer as photothermal nanocarrier for remote activation of gene expression," *Angewandte Chemie International Edition,* vol. 56, no. 31, pp. 9155-9159, 2017.

[68] I. C. Miller *et al.*, "Enhanced intratumoural activity of CAR T cells engineered to produce immunomodulators under photothermal control," *Nature biomedical engineering,* vol. 5, no. 11, pp. 1348-1359, 2021.

[69] R. Chen, G. Romero, M. G. Christiansen, A. Mohr, and P. Anikeeva, "Wireless magnetothermal deep brain stimulation," *Science,* vol. 347, no. 6229, pp. 1477-1480, 2015.

[70] R. Munshi, S. M. Qadri, Q. Zhang, I. Castellanos Rubio, P. Del Pino, and A. Pralle, "Magnetothermal genetic deep brain stimulation of motor behaviors in awake, freely moving mice," *Elife,* vol. 6, p. e27069, 2017.

[71] D. Rosenfeld *et al.*, "Transgene-free remote magnetothermal regulation of adrenal hormones," *Science advances,* vol. 6, no. 15, p. eaaz3734, 2020.

[72] X. Ma *et al.*, "Modular-designed engineered bacteria for precision tumor immunotherapy via spatiotemporal manipulation by magnetic field," *Nature Communications,* vol. 14, no. 1, p. 1606, 2023.

[73] H. Chen *et al.*, "An engineered bacteria-hybrid microrobot with the magnetothermal bioswitch for remotely collective perception and imaging-guided cancer treatment," *ACS nano,* vol. 16, no. 4, pp. 6118-6133, 2022.

[74] R. C. Smith, M. Machluf, P. Bromley, A. Atala, and K. Walsh, "Spatial and temporal control of transgene expression through ultrasound-mediated induction of the heat shock protein 70B promoter in vivo," *Human gene therapy,* vol. 13, no. 6, pp. 697-706, 2002.

[75] C. Plathow *et al.*, "Focal gene induction in the liver of rats by a heat-inducible promoter using focused ultrasound hyperthermia: preliminary results," *Investigative radiology,* vol. 40, no. 11, pp. 729-735, 2005.

[76] R. Deckers, B. Quesson, J. Arsaut, S. Eimer, F. Couillaud, and C. T. Moonen, "Image-guided, noninvasive, spatiotemporal control of gene expression," *Proceedings of the National Academy of Sciences,* vol. 106, no. 4, pp. 1175-1180, 2009.

[77] M. H. Abedi *et al.*, "Ultrasound-controllable engineered bacteria for cancer immunotherapy," *Nature Communications,* vol. 13, no. 1, p. 1585, 2022.

[78] Y. Chen, M. Du, Z. Yuan, Z. Chen, and F. Yan, "Spatiotemporal control of engineered bacteria to express interferon-γ by focused ultrasound for tumor immunotherapy," *Nature Communications,* vol. 13, no. 1, p. 4468, 2022.

[79] Y. Wu *et al.*, "Control of the activity of CAR-T cells within tumours via focused ultrasound," *Nature biomedical engineering,* vol. 5, no. 11, pp. 1336-1347, 2021.

[80] N. A. Whitlock, N. Agarwal, J.-X. Ma, and C. E. Crosson, "Hsp27 upregulation by HIF-1 signaling offers protection against retinal ischemia in rats," *Investigative ophthalmology & visual science,* vol. 46, no. 3, pp. 1092-1098, 2005.

[81] B. J. Wu, R. E. Kingston, and R. I. Morimoto, "Human HSP70 promoter contains at least two distinct regulatory domains," *Proceedings of the National Academy of Sciences,* vol. 83, no. 3, pp. 629-633, 1986.

[82] Q. Xu, G. Schett, C. Li, Y. Hu, and G. Wick, "Mechanical stress–induced heat shock protein 70 expression in vascular smooth muscle cells is regulated by Rac and Ras small G proteins but not mitogen-activated protein kinases," *Circulation research,* vol. 86, no. 11, pp. 1122-1128, 2000.

[83] G. M. Lanza, "Ultrasound Imaging: Something Old or Something New?," *Investigative radiology,* vol. 55, no. 9, p. 573, 2020.

[84] G. Köse, M. Darguzyte, and F. Kiessling, "Molecular ultrasound imaging," *Nanomaterials,* vol. 10, no. 10, p. 1935, 2020.

[85] Y.-F. Zhou, "High intensity focused ultrasound in clinical tumor ablation," *World journal of clinical oncology,* vol. 2, no. 1, p. 8, 2011.

[86] C. Rabut *et al.*, "Ultrasound technologies for imaging and modulating neural activity," *Neuron,* vol. 108, no. 1, pp. 93-110, 2020.

[87] R. Beisteiner, M. Hallett, and A. M. Lozano, "Ultrasound Neuromodulation as a New Brain Therapy," *Advanced Science,* vol. 10, no. 14, p. 2205634, 2023.

[88] C. Sarica *et al.*, "Human Studies of Transcranial Ultrasound neuromodulation: A systematic review of effectiveness and safety," *Brain Stimulation,* vol. 15, no. 3, pp. 737-746, 2022.

[89] Q. Xian *et al.*, "Modulation of deep neural circuits with sonogenetics," *Proceedings of the National Academy of Sciences,* vol. 120, no. 22, p. e2220575120, 2023.

[90] Z. Wang, J. Yan, X. Wang, Y. Yuan, and X. Li, "Transcranial ultrasound stimulation directly influences the cortical excitability of the motor cortex in Parkinsonian mice," *Movement Disorders,* vol. 35, no. 4, pp. 693-698, 2020.

[91] G. Leinenga and J. Götz, "Scanning ultrasound removes amyloid-β and restores memory in an Alzheimer's disease mouse model," *Science translational medicine,* vol. 7, no. 278, pp. 278ra33-278ra33, 2015.

[92] T. Liu *et al.*, "Noninvasive ultrasound stimulation to treat myocarditis through splenic neuro-immune regulation," *Journal of Neuroinflammation,* vol. 20, no. 1, p. 94, 2023.

[93] V. Cotero *et al.*, "Noninvasive sub-organ ultrasound stimulation for targeted neuromodulation," *Nature Communications,* vol. 10, no. 1, p. 952, 2019.

[94] Z. Qiu *et al.*, "Targeted neurostimulation in mouse brains with non-invasive ultrasound," *Cell reports,* vol. 32, no. 7, 2020.

[95] H. Shekhar, N. J. Smith, J. L. Raymond, and C. K. Holland, "Effect of temperature on the size distribution, shell properties, and stability of Definity®," *Ultrasound in medicine & biology,* vol. 44, no. 2, pp. 434-446, 2018.

[96] H. Mulvana, E. Stride, J. V. Hajnal, and R. J. Eckersley, "Temperature dependent behavior of ultrasound contrast agents," *Ultrasound in medicine & biology,* vol. 36, no. 6, pp. 925-934, 2010.

[97] K. Ferrara, R. Pollard, and M. Borden, "Ultrasound microbubble contrast agents: fundamentals and application to gene and drug delivery," *Annu. Rev. Biomed. Eng.,* vol. 9, pp. 415-447, 2007.

[98] H. Maeda, "The enhanced permeability and retention (EPR) effect in tumor vasculature: the key role of tumor-selective macromolecular drug targeting," *Advances in enzyme regulation,* vol. 41, no. 1, pp. 189-207, 2001.

[99] X. Zhang *et al.*, "Unraveling the mechanobiology of immune cells," *Current Opinion in Biotechnology,* vol. 66, pp. 236-245, 2020.

[100] D. C. P. Wong and J. L. Ding, "The mechanobiology of NK cells-'Forcing NK to Sense'target cells," *Biochimica et Biophysica Acta -Reviews on Cancer,* p. 188860, 2023.

[101] X. Zhou *et al.*, "A calcium optimum for cytotoxic T lymphocyte and natural killer cell cytotoxicity," *The Journal of physiology,* vol. 596, no. 14, pp. 2681-2698, 2018.

[102] M. Vukcevic, F. Zorzato, G. Spagnoli, and S. Treves, "Frequent calcium oscillations lead to NFAT activation in human immature dendritic cells," *Biophysical Journal,* vol. 98, no. 3, p. 98a, 2010.

[103] B. Helfield, X. Chen, S. C. Watkins, and F. S. Villanueva, "Biophysical insight into mechanisms of sonoporation," *Proceedings of the National Academy of Sciences,* vol. 113, no. 36, pp. 9983-9988, 2016.

[104] A. Delalande *et al.*, "Cationic gas-filled microbubbles for ultrasound-based nucleic acids delivery," *Bioscience Reports,* vol. 37, no. 6, p. BSR20160619, 2017.

[105] Y. Pan *et al.*, "Mechanogenetics for the remote and noninvasive control of cancer immunotherapy," *Proceedings of the National Academy of Sciences,* vol. 115, no. 5, pp. 992-997, 2018.

[106] M. G. Shapiro *et al.*, "Biogenic gas nanostructures as ultrasonic molecular reporters," *Nature nanotechnology,* vol. 9, no. 4, pp. 311-316, 2014.

[107] F. Pfeifer, "Distribution, formation and regulation of gas vesicles," *Nature Reviews Microbiology,* vol. 10, no. 10, pp. 705-715, 2012.

[108] D. Maresca *et al.*, "Nonlinear ultrasound imaging of nanoscale acoustic biomolecules," *Applied physics letters,* vol. 110, no. 7, p. 073704, 2017.

[109] Y. Yang, Z. Qiu, X. Hou, and L. Sun, "Ultrasonic characteristics and cellular properties of Anabaena gas vesicles," *Ultrasound in medicine & biology,* vol. 43, no. 12, pp. 2862-2870, 2017.

[110] A. Lakshmanan *et al.*, "Molecular engineering of acoustic protein nanostructures," *ACS nano,* vol. 10, no. 8, pp. 7314-7322, 2016.

[111] B. Ling *et al.*, "Biomolecular ultrasound imaging of phagolysosomal function," *ACS*

nano, vol. 14, no. 9, pp. 12210-12221, 2020.
[112] M. Wei, M. Lai, J. Zhang, X. Pei, and F. Yan, "Biosynthetic gas vesicles from halobacteria nrc-1: A potential ultrasound contrast agent for tumor imaging," *Pharmaceutics,* vol. 14, no. 6, p. 1198, 2022.
[113] G. Wang *et al.*, "Surface-modified GVs as nanosized contrast agents for molecular ultrasound imaging of tumor," *Biomaterials,* vol. 236, p. 119803, 2020.
[114] D. Maresca, D. P. Sawyer, G. Renaud, A. Lee-Gosselin, and M. G. Shapiro, "Nonlinear X-wave ultrasound imaging of acoustic biomolecules," *Physical Review X,* vol. 8, no. 4, p. 041002, 2018.
[115] D. P. Sawyer *et al.*, "Ultrasensitive ultrasound imaging of gene expression with signal unmixing," *Nature Methods,* vol. 18, no. 8, pp. 945-952, 2021.
[116] L. Song *et al.*, "Gas-filled protein nanostructures as cavitation nuclei for molecule-specific sonodynamic therapy," *Acta Biomaterialia,* vol. 136, pp. 533-545, 2021.
[117] L. Song *et al.*, "Biogenic nanobubbles for effective oxygen delivery and enhanced photodynamic therapy of cancer," *Acta biomaterialia,* vol. 108, pp. 313-325, 2020.
[118] L. Xie, J. Wang, L. Song, T. Jiang, and F. Yan, "Cell-cycle dependent nuclear gene delivery enhances the effects of E-cadherin against tumor invasion and metastasis," *Signal Transduction and Targeted Therapy,* vol. 8, no. 1, p. 182, 2023.
[119] X. Hou *et al.*, "Precise ultrasound neuromodulation in a deep brain region using nano gas vesicles as actuators," *Advanced Science,* vol. 8, no. 21, p. 2101934, 2021.
[120] R. C. Hurt *et al.*, "Genomically mined acoustic reporter genes for real-time in vivo monitoring of tumors and tumor-homing bacteria," *Nature Biotechnology,* pp. 1-13, 2023.
[121] A. Farhadi, G. H. Ho, D. P. Sawyer, R. W. Bourdeau, and M. G. Shapiro, "Ultrasound imaging of gene expression in mammalian cells," *Science translational medicine,* vol. 365, no. 6460, pp. 1469-1475, 2019.
[122] Y. Yang *et al.*, "In-vivo programmable acoustic manipulation of genetically engineered bacteria," *Nature Communications,* vol. 14, no. 1, p. 3297, 2023.
[123] D. Wu *et al.*, "Biomolecular actuators for genetically selective acoustic manipulation of cells," *Science Advances,* vol. 9, no. 8, p. eadd9186, 2023.
[124] J. S. Miller, "Therapeutic applications: natural killer cells in the clinic," *Hematology , the American Society of Hematology Education Program,* vol. 2013, no. 1, pp. 247-253, 2013.
[125] S. Kakarla and S. Gottschalk, "CAR T cells for solid tumors: armed and ready to go?," *Cancer Journal,* vol. 20, no. 2, p. 151, 2014.
[126] M. Shevtsov and G. Multhoff, "Immunological and translational aspects of NK cell-based antitumor immunotherapies," *Frontiers in immunology,* vol. 7, p. 492, 2016.
[127] S. Krebs, M. M. Dacek, L. M. Carter, D. A. Scheinberg, and S. M. Larson, "CAR Chase: Where do engineered cells go in humans?," *Frontiers in Oncology,* vol. 10, p. 577773, 2020.
[128] M. Gerwing *et al.*, "The beginning of the end for conventional RECIST—novel therapies require novel imaging approaches," *Nature Reviews Clinical Oncology,* vol.

16, no. 7, pp. 442-458, 2019.
[129] M. Shapovalova, S. R. Pyper, B. S. Moriarity, and A. M. LeBeau, "The molecular imaging of natural killer cells," *Molecular imaging,* vol. 17, p. 1536012118794816, 2018.
[130] F. Galli, M. Varani, C. Lauri, G. G. Silveri, L. Onofrio, and A. Signore, "Immune cell labelling and tracking: implications for adoptive cell transfer therapies," *EJNMMI Radiopharmacy and Chemistry,* vol. 6, no. 1, pp. 1-19, 2021.
[131] M. Rashidian *et al.*, "Predicting the response to CTLA-4 blockade by longitudinal noninvasive monitoring of CD8 T cells," *Journal of Experimental Medicine,* vol. 214, no. 8, pp. 2243-2255, 2017.
[132] M. Eisenblaetter *et al.*, "Visualization of tumor-immune interaction-target-specific imaging of S100A8/A9 reveals pre-metastatic niche establishment," *Theranostics,* vol. 7, no. 9, p. 2392, 2017.
[133] N. Pandit-Taskar *et al.*, "First-in-Humans Imaging with 89Zr-Df-IAB22M2C Anti-CD8 Minibody in Patients with Solid Malignancies: Preliminary Pharmacokinetics, Biodistribution, and Lesion Targeting," *Journal of Nuclear Medicine,* vol. 61, no. 4, pp. 512-519, 2020.
[134] K. Seitz and D. Strobel, "A milestone: approval of CEUS for diagnostic liver imaging in adults and children in the USA," *Ultraschall in der Medizin-European Journal of Ultrasound,* vol. 37, no. 03, pp. 229-232, 2016.
[135] M. Varani, S. Auletta, A. Signore, and F. Galli, "State of the art of natural killer cell imaging: A systematic review," *Cancers,* vol. 11, no. 7, p. 967, 2019.
[136] S. Maddineni, J. L. Silberstein, and J. B. Sunwoo, "Emerging NK cell therapies for cancer and the promise of next generation engineering of iPSC-derived NK cells," *Journal for Immunotherapy of Cancer,* vol. 10, no. 5, 2022.
[137] J. A. Myers and J. S. Miller, "Exploring the NK cell platform for cancer immunotherapy," *Nature reviews Clinical oncology,* vol. 18, no. 2, pp. 85-100, 2021.
[138] H. Klingemann, "The NK-92 cell line—30 years later: its impact on natural killer cell research and treatment of cancer," *Cytotherapy,* 2023.
[139] G. Xie, H. Dong, Y. Liang, J. D. Ham, R. Rizwan, and J. Chen, "CAR-NK cells: A promising cellular immunotherapy for cancer," *EBioMedicine,* vol. 59, p. 102975, 2020.
[140] A. Lakshmanan *et al.*, "Preparation of biogenic gas vesicle nanostructures for use as contrast agents for ultrasound and MRI," *Nature protocols,* vol. 12, no. 10, pp. 2050-2080, 2017.
[141] N. Sato *et al.*, "In vivo tracking of adoptively transferred natural killer cells in rhesus macaques using 89Zirconium-oxine cell labeling and PET imaging," *Clinical Cancer Research,* vol. 26, no. 11, pp. 2573-2581, 2020.
[142] M. A. Cheever, J. A. Thompson, D. E. Kern, and P. Greenberg, "Interleukin 2 (IL 2) administered in vivo: influence of IL 2 route and timing on T cell growth," *The Journal of Immunology,* vol. 134, no. 6, pp. 3895-3900, 1985.
[143] J. Le Floc'h *et al.*, "In vivo biodistribution of radiolabeled acoustic protein nanostructures," *Molecular Imaging and Biology,* vol. 20, pp. 230-239, 2018.

[144] J.-H. Gong, G. Maki, and H. G. J. L. Klingemann, "Characterization of a human cell line (NK-92) with phenotypical and functional characteristics of activated natural killer cells," vol. 8, no. 4, pp. 652-658, 1994.
[145] W. Cui *et al.*, "Neural progenitor cells labeling with microbubble contrast agent for ultrasound imaging in vivo," *Biomaterials,* vol. 34, no. 21, pp. 4926-4935, 2013.
[146] H.-W. Song *et al.*, "Sonazoid-Conjugated Natural Killer Cells for Tumor Therapy and Real-Time Visualization by Ultrasound Imaging," *Pharmaceutics,* vol. 13, no. 10, p. 1689, 2021.
[147] Z. Xu, H. Liu, H. Tian, and F. Yan, "Real-Time Imaging Tracking of Engineered Macrophages as Ultrasound-Triggered Cell Bombs for Cancer Treatment," *Advanced Functional Materials,* vol. 30, no. 14, p. 1910304, 2020.
[148] A. Li *et al.*, "Surface biotinylation of cytotoxic T lymphocytes for in vivo tracking of tumor immunotherapy in murine models," *Cancer immunology, immunotherapy,* vol. 65, pp. 1545-1554, 2016.
[149] Y. IBAYASHI *et al.*, "Effect of local administration of lymphokine-activated killer cells and interleukin-2 on malignant brain tumor patients," *Neurologia medico-chirurgica,* vol. 33, no. 7, pp. 448-457, 1993.
[150] I. S. Mauldin *et al.*, "Intratumoral interferon-gamma increases chemokine production but fails to increase T cell infiltration of human melanoma metastases," *Cancer Immunology, Immunotherapy,* vol. 65, pp. 1189-1199, 2016.
[151] S. Ito *et al.*, "Ultra-low dose interleukin-2 promotes immune-modulating function of regulatory T cells and natural killer cells in healthy volunteers," *Molecular Therapy-Oncolytics,* vol. 22, no. 7, pp. 1388-1395, 2014.
[152] J. Zhang *et al.*, "Stimuli-Responsive Nanoparticles for Controlled Drug Delivery in Synergistic Cancer Immunotherapy," *Advanced Science,* vol. 9, no. 5, p. 2103444, 2022.
[153] Z. Xu, T. L. Hall, E. Vlaisavljevich, and F. T. Lee Jr, "Histotripsy: the first noninvasive, non-ionizing, non-thermal ablation technique based on ultrasound," *International Journal of Hyperthermia,* vol. 38, no. 1, pp. 561-575, 2021.
[154] Z. Qiu *et al.*, "The mechanosensitive ion channel Piezo1 significantly mediates in vitro ultrasonic stimulation of neurons," *IScience,* vol. 21, pp. 448-457, 2019.
[155] J. Zhu *et al.*, "The mechanosensitive ion channel Piezo1 contributes to ultrasound neuromodulation," *Proceedings of the National Academy of Sciences,* vol. 120, no. 18, p. e2300291120, 2023.
[156] W. J. Tyler, "Noninvasive neuromodulation with ultrasound? A continuum mechanics hypothesis," *The Neuroscientist,* vol. 17, no. 1, pp. 25-36, 2011.
[157] S.-J. Oh *et al.*, "Ultrasonic neuromodulation via astrocytic TRPA1," *Current Biology,* vol. 29, no. 20, pp. 3386-3401. e8, 2019.
[158] T. Liu *et al.*, "Sonogenetics: Recent advances and future directions," *Brain Stimulation,* 2022.
[159] S. Ibsen, A. Tong, C. Schutt, S. Esener, and S. H. Chalasani, "Sonogenetics is a non-invasive approach to activating neurons in Caenorhabditis elegans," *Nature communications,* vol. 6, no. 1, p. 8264, 2015.

[160] M. R. Müller and A. Rao, "NFAT, immunity and cancer: a transcription factor comes of age," *Nature Reviews Immunology,* vol. 10, no. 9, pp. 645-656, 2010.
[161] Y.-J. Park, S.-A. Yoo, M. Kim, and W.-U. Kim, "The role of calcium–calcineurin–NFAT signaling pathway in health and autoimmune diseases," *Frontiers in immunology,* vol. 11, p. 195, 2020.
[162] N. Yissachar *et al.*, "Dynamic response diversity of NFAT isoforms in individual living cells," *Molecular cell,* vol. 49, no. 2, pp. 322-330, 2013.
[163] O. Maguire, K. M. Tornatore, K. L. O'Loughlin, R. C. Venuto, and H. Minderman, "Nuclear translocation of nuclear factor of activated T cells (NFAT) as a quantitative pharmacodynamic parameter for tacrolimus," *Cytometry Part A,* vol. 83, no. 12, pp. 1096-1104, 2013.
[164] Y. Yang, Z. Qiu, X. Hou, and L. Sun, "Ultrasonic characteristics and cellular properties of Anabaena gas vesicles," *Ultrasound in medicine biology,* vol. 43, no. 12, pp. 2862-2870, 2017.
[165] R. Perera *et al.*, "Contrast enhanced ultrasound imaging by nature-inspired ultrastable echogenic nanobubbles," *Nanoscale,* vol. 11, no. 33, pp. 15647-15658, 2019.
[166] R. H. Perera *et al.*, "Real time ultrasound molecular imaging of prostate cancer with PSMA-targeted nanobubbles," *Nanomedicine: Nanotechnology, Biology and Medicine,* vol. 28, p. 102213, 2020.
[167] D. G. Ramirez *et al.*, "Contrast-enhanced ultrasound with sub-micron sized contrast agents detects insulitis in mouse models of type1 diabetes," *Nature communications,* vol. 11, no. 1, pp. 1-13, 2020.
[168] R. H. Perera *et al.*, "Intracellular vesicle entrapment of nanobubble ultrasound contrast agents targeted to PSMA promotes prolonged enhancement and stability in vivo and in vitro," *Nanotheranostics,* vol. 6, no. 3, p. 270, 2022.